

Saltillo, Coahuila a 4 de marzo de 2022

Coordinación de Posgrado

Presente

Por este conducto nos permitimos informar a esta coordinación que, el documento de Tesis preparado por MELISA TREJO MALDONADO titulado Synthesis of triazole-functionalized porous polymers using click reactions (Síntesis de polímeros porosos funcionalizados con grupos triazol mediante reacciones tipo click), el cual fue presentado el día 28 de febrero de 2022, ha sido modificado de acuerdo a las observaciones, comentarios y sugerencias, realizadas por el Comité Evaluador asignado. Por tal motivo, avalamos que el documento adjunto corresponde a la versión final del documento de Tesis.

Atentamente,

SINODALES



Dra. Odilia Pérez Camacho
Presidente



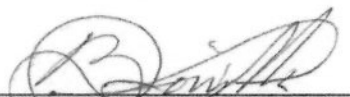
Dra. Diana Morales Acosta
Secretario



Dr. Gregorio Cadenas Pliego
1er. Vocal



Dra. Claudia Verónica Piñón Balderrama
2do. Vocal



Dr. José Bonilla Cruz
3er. Vocal

Vo. Bo. ASESORES



Dr. Luis Ernesto Elizalde Herrera



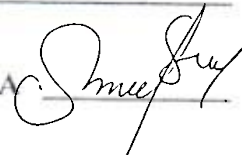
Dr. Carlos A. Guerrero Sánchez

TESIS CON CARACTER ABIERTO

PROGRAMA: DOCTORADO EN TECNOLOGÍA DE POLÍMEROS

AUTOR: MELISA TREJO MALDONADO

FIRMA



TITULO: Synthesis of triazole-functionalized porous polymers using click reactions (Síntesis de polímeros porosos funcionalizados con grupos triazol mediante reacciones tipo click)

ASESORES: Dr. Luis Ernesto Elizalde Herrera

FIRMA



Dr. Carlos A. Guerrero Sánchez

FIRMA



El Centro de Investigación en Química Aplicada clasifica el presente documento de tesis como ABIERTO.

Un documento clasificado como Abierto se expone en los estantes del Centro de Información para su consulta. Dicho documento no puede ser copiado en ninguna modalidad sin autorización por escrito del Titular del Centro de Información o del Director General del CIQA.

Saltillo, Coahuila, a 28 de Febrero de 2022

Sello de la Institución



Dr. Oliverio Santiago Rodríguez Fernández
Director General del CIQA

CENTRO DE INVESTIGACIÓN EN QUÍMICA APLICADA
Programa de Doctorado en Tecnología de Polímeros

TESIS

Synthesis of triazole-functionalized porous polymers using click reactions (Síntesis de polímeros porosos funcionalizados con grupos triazol mediante reacciones tipo click)

Presentada por:

MELISA TREJO MALDONADO

Para obtener el grado de:

Doctor en Tecnología de Polímeros

Asesorada por:

Dr. Luis Ernesto Elizalde Herrera
Dr. Carlos A. Guerrero Sánchez

SINODALES

Dra. Odilia Pérez Camacho
Presidente

Dra. Diana Morales Acosta
Secretario

Dr. Gregorio Cadenas Pliego
Primer Vocal

Dra. Claudia Ivonne Piñón Balderrama
Segundo Vocal

Dr. Jose Bonilla Cruz
Tercer Vocal

DECLARACIÓN

Declaro que la información contenida en la Parte Experimental así como en la Parte de Resultados y Discusiones de este documento y que forman parte de las actividades de investigación y desarrollo realizadas durante el período que se me asignó para llevar a cabo mi trabajo de tesis, será propiedad del Centro de Investigación en Química Aplicada.

Saltillo, Coahuila a 28 de Febrero de 2022



MELISA TREJO MALDONADO

Nombre y Firma



CENTRO DE INVESTIGACIÓN EN QUÍMICA APLICADA
Programa de Doctorado en Tecnología de Polímeros

TESIS

Synthesis of triazole-functionalized porous polymers using click reactions (Síntesis de polímeros porosos funcionalizados con grupos triazol mediante reacciones tipo click)

Presentada por:

MELISA TREJO MALDONADO

Para obtener el grado de:

Doctor en Tecnología de Polímeros

Asesorada por:

Dr. Luis Ernesto Elizalde Herrera
Dr. Carlos A. Guerrero Sánchez

Febrero, 2022



**SYNTHESIS OF TRIAZOLE-FUNCTIONALIZED
POROUS POLYMERS USING CLICK REACTIONS**

By Melisa Trejo Maldonado

Thesis submitted for the degree of
Doctor of Philosophy
in Polymer Technology

February 2022

Supervisors: Dr. Luis E. Elizalde Herrera

Dr. Carlos A. Guerrero Sánchez

Preface

The present work was developed as part of the Doctoral Program in Polymer Technology at the Research Center of Applied Chemistry, (CIQA) in Saltillo, México, and at the Friedrich-Schiller University (FSUJ) in Jena, Germany, as part of an internship.

This project was funded by the National Council of Science and Technology (CONACYT) and congress attendance was supported by project No. 256727. During the internship at FSUJ, the experimental part was kindly supported by the Centre for Excellence “Polytarget” (SFB 1278, projects B02 and Z01) of the Deutsche Forschungsgemeinschaft (DFG, Germany).

Scientific contributions

As part of CONACYT-256727 project the following manuscripts were submitted for publication:

Trejo-Maldonado M., Womiloju A., Stumpf S., Hoepfner S., Schubert U.S., Elizalde L.E., Guerrero-Sanchez C. “*Triazole-functionalized mesoporous materials based on poly(styrene-block-lactic acid): A morphology study of thin films*”. Submitted for publication to [*Polymers*] on [April 2022].

Trejo-Maldonado M., Elizalde L.E., Le Droumaguet B., Grande D. “Synthesis of triazole functionalized diblock copolymers as templates for porous materials” *Reactive and Functional Polymers*, 2021, 164, 104919.

Additional publications

Lechuga-Islas V.D., Trejo-Maldonado M., Stumpf S., Guerrero-Santos R., Elizalde L.E., Schubert U.S., Guerrero-Sánchez C. “Separation of Volatile Compounds from Polymers by Physisorption”, *European Polymer Journal*, 159, 110748.

Lechuga-Islas, V.D. Trejo-Maldonado M., Schubert U.S., and Guerrero-Sanchez C. Separation of Volatile Compounds from Polymers by Physisorption for High Throughput Applications, *Patent Application, German Patent and Trademark Office*, 2021, application number 102021004383.9.

Trejo-Maldonado M., Lechuga-Islas V.D., Anufriev I., Nischang I., Guerrero-Santos R., Elizalde L.E., Schubert U.S., Guerrero-Sánchez C. “All-aqueous, surfactant-free, and pH-driven nanoprecipitation methods to formulate dual-responsive polymer nanoparticle dispersion for drug nanocarrier applications” *Manuscript in progress*

Conferences and courses attended

Poster presentation “Preparation of triazole functionalized mesoporous polystyrene via click chemistry”. at the *Sixth International Symposium Frontiers in Polymer Science*. Budapest, Hungary. May 2019

Attendance to *Symposium on Innovative Polymers for the Nanomedicine of the 21st Century* and workshop “Microwave Assisted Synthesis”. Jena, Germany. July 2019

Automated synthesizers training *Swing XL FORMAX Chemspeed* – FSUJ. Jena, Germany. February 2020

Acknowledgments

Throughout this project I have received generous support and assistance from many people.

First, I would like to thank my supervisors Dr. Luis Elizalde and Dr. Carlos Guerrero, for all their support on the development of this project. Without their guidance and expertise this dissertation would not have been possible. My sincere thanks to Dr. Luis Elizalde, who supported me to undertake the internship in at FSUJ. I would also like to sincerely thank Dr. Carlos Guerrero for his constant feedback and assistance.

I am deeply grateful to Prof. U. Schubert for allowing me to be a part of his investigation team during my internship at FSUJ. I would also like to thank Dr. Juergen Vitz for sharing his continuous help and guidance in the lab. Special thanks to Steffi Stumpf, Aisha Womiloju and Dr. Stephanie Hoepfner for sharing valuable insights on SEM, TEM, and AFM characterization.

I want to thank the Postgraduate Office at CIQA, specially to MS. Aida E. García and Nancy Espinoza for their assistance during this project. I would also like to thank Dr. Odilia Perez, Dr. Diana Morales, and Dr. Gregorio Cadenas for their insightful comments and suggestions on each seminar throughout the PhD. I also want to thank Jorge F. Espinoza and J. Guadalupe Tellez for their assistance in the lab.

I thank friends and colleagues in Lab H2 at CIQA, especially Isis, Juan José, Enrique, Angelica, Asunción, and Gladys. Thank you all for your help and nice company inside and outside the lab. I would also like to thank members in Lab 107 at FSUJ, Alicia, Dulce, Jens, Marco, and Carolina for the pleasant conversations and for the many meals shared.

I am forever grateful for the support of my family. Mom, Dad, Mez and Alex, thank you all for believing in me.

I owe my dearest and deepest gratitude to my loving partner, Victor. I am certain that I could not have come this far without your constant care and encouragement.

Table of Contents

Preface	ii
Acknowledgments	iv
Table of Contents.....	v
List of figures and schemes	ix
List of tables.....	xi
List of abbreviations	xii
Abstract	1
1 Introduction	2
2 Literature review.....	4
2.1 Mesoporous materials	4
2.1.1 Preparation methods.....	4
2.1.2 Block copolymers as templates for mesoporous materials.....	7
2.1.3 Microdomain orientation and selective removal	16
2.1.4 Characterization techniques for mesoporous polymers.....	19
2.1.5 Emerging applications for mesoporous polymers	20
2.2 Block copolymer synthesis	22
2.2.1 Reversible Deactivation Radical Polymerization (RDRP).....	23
2.2.2 Ring opening polymerization (ROP)	28
2.2.3 ATRP and ROP.....	31
2.3 Functionalization and post-polymerization reactions – click approach	39
2.3.1 Cu ^I -catalyzed azide – alkyne 1,3-cycloaddition.....	40
2.3.2 Triazole groups in polymers.....	43
3 Aims and objectives.....	44

3.1	Aim.....	44
3.2	Objectives.....	44
4	Hypotheses.....	45
5	Experimental methods.....	46
5.1	General conditions	46
5.1.1	Solvents	46
5.1.2	Reactants	46
5.1.3	Instrumentation	47
5.2	Initiator synthesis.....	49
5.2.1	Carboxymethylation of 4-bromostyrene (4BS)	49
5.2.2	Bromination of methyl 2-(4-bromophenyl) propanoate (MBP) (I-1)	50
5.2.3	Transesterification of methyl 2-(4-bromophenyl) propanoate (MBP) (I-1)	50
5.2.4	Bromination of 2-hydroxyethyl-2-(4-bromophenylpropanoate) (HEBP) (I-2b).....	51
5.3	Synthesis of polystyrene precursor (PS-N ₃).....	52
5.3.1	Polymerization of styrene with initiator I-2a via ATRP (PS-Br) (A1).....	52
5.3.2	Polymerization of styrene with initiator I-2a via ARGET – ATRP (PS-Br) (A1).....	53
5.3.3	Bromine end-group substitution of PS-Br (PS-N ₃) (A2).....	53
5.4	Synthesis of poly (styrene- <i>block</i> -lactic acid), PS _n - <i>b</i> -PLA _m , copolymers.	54
5.4.1	Route 1 – Click coupling PS-N ₃ and PLA-Ac end groups.....	54
5.4.2	Polymerization of <i>D,L</i> -lactide via ROP (PLA-Ac) (B1/B2).....	54
5.4.3	Synthesis of PS _n - <i>b</i> -PLA _m copolymers (Copper catalyzed azide-alkyne cycloaddition, CuAAC) (C1).....	55
5.4.4	Route 2 – Block copolymer synthesis by ROP of PS-OH macroinitiator.....	56
5.4.5	End-group click reaction of PS-N ₃ (PS-OH) (A3).....	56

5.4.6	Polymerization of <i>D,L</i> -lactide via ROP (PLA-Ac) (C2).....	57
5.5	Preparation of PS- <i>b</i> -PLA based thin films.	58
5.5.1	Substrate preparation.....	58
5.5.2	Annealing experiments.....	58
5.5.3	Hydrolysis experiments.....	59
5.6	Preparation of PS- <i>b</i> -PLA based monoliths.....	59
5.6.1	Method 1.....	59
5.6.2	Method 2.....	60
5.6.3	PLA hydrolysis of monoliths.....	60
5.7	Metal uptake experiments.....	60
6	Results and discussion.....	61
Part A – Synthetic pathway towards the obtention of triazole-embedded PS- <i>b</i> -PLA copolymers.		61
6.1	Synthesis of ATRP active benzylic initiator.....	61
6.1.1	Approach 1: Bromination then transesterification.....	63
6.1.2	Approach 2: Transesterification then bromination.....	66
6.2	Preparation of PS–N ₃ macroinitiator.....	70
6.2.1	Preparation of the PS–Br precursor via ATRP.....	70
6.2.2	Preparation of the PS–Br precursor via ARGET – ATRP.....	73
6.2.3	End bromine group substitution of polystyrene (PS–N ₃ synthesis).....	76
6.3	PLA-Ac synthesis via ROP.....	80
6.4	PS _n - <i>b</i> -PLA _m copolymer synthesis.....	83
6.4.1	Route 1: Block coupling through azide – alkyne 1,3 – cycloaddition.....	84
6.4.2	Route 2: ROP of a PS-OH macroinitiator.....	95

Part B – Self-assembly of PS- <i>b</i> -PLA copolymers on thin films	99
6.5 Annealing experiments of PS- <i>b</i> -PLA thin films	99
6.5.1 SVA experiments.....	99
6.5.2 TA experiments.....	104
6.5.3 Hydrolysis of the as-spun films.....	106
6.6 Binding tests of metal salts using hydrolyzed films	108
6.7 PS- <i>b</i> -PLA semi-bulk and bulk samples as templates for porous membranes	110
7 Conclusions.....	115
8 References	118
9 Appendix.....	133
9.1 Additional characterization of MBBP (I-2a).....	133
9.2 FT-IR spectrum of PS-N ₃	134
9.3 Solvent selection for the polymer casting.....	135
9.4 Atomic Force Microscopy (AFM) of untreated and annealed substrates.	135
9.5 Solvent vapor annealing (SVA) on silylated substrates.	136
9.6 PLA hydrolysis of C1-9 monolith (thicker sample)	137
9.7 Before and after hydrolysis of C1-13 monolith	137

List of figures and schemes

FIGURE 2.1 DIFFERENT MORPHOLOGIES OF BCPs.	5
FIGURE 2.2 SEGREGATION TRANSITIONS OF A SYMMETRIC AB COPOLYMER.....	11
FIGURE 2.3 THEORETICAL PHASE DIAGRAM AND EXPECTED MORPHOLOGIES FOR AN ASYMMETRICAL AB BCP. ²⁴	12
FIGURE 2.4 EXPERIMENTAL PS- <i>B</i> -PLA PHASE DIAGRAM.....	14
FIGURE 2.5 TYPES OF BCPs.	22
FIGURE 2.6 ATRP – ROP BIFUNCTIONAL INITIATOR.	35
FIGURE 2.7 SYNTHESIS OF POLYACRYLATE, POLYMETHACRYLATE AND PS VIA Cu(0)-MEDIATED RDRP. ⁶⁷	37
FIGURE 6.1 COMPARATIVE ¹ H NMR SPECTRA OF I-1 AND I-2A. (600 MHz, CDCl ₃ , R.T.).....	64
FIGURE 6.2 ¹ H NMR SPECTRUM OF I-2B (600 MHz, CDCl ₃ , R.T.)	67
FIGURE 6.3 ¹ H NMR SPECTRUM OF PRODUCT A1-15 (300 MHz, CDCl ₃ , R.T.)	75
FIGURE 6.4 ¹ H NMR SPECTRUM OF PRODUCT A2-11 (600 MHz, CDCl ₃ , R.T.)	77
FIGURE 6.5 SEC TRACES OF B1-1 AND B2-1 PLA-AC PRECURSORS.	81
FIGURE 6.6 ¹ H NMR SPECTRUM OF PRODUCT B2-1 (400 MHz, CDCl ₃ , R.T.).....	82
FIGURE 6.7 ¹ H NMR SPECTRUM OF C1-5 (300 MHz, CDCl ₃ , R.T.)	85
FIGURE 6.8 2D DOSY NMR SPECTRA OF COPOLYMER C1-6.	86
FIGURE 6.9 DSC THERMOGRAMS OF COPOLYMERS C1-3 AND C1-5.	89
FIGURE 6.10 TGA THERMOGRAMS OF COPOLYMERS C1-3 AND C1-5.	89
FIGURE 6.11 SEC TRACES OF PRECURSORS PS-N ₃ (A2-6), PLA-AC (B2-5) AND COPOLYMER PS _N -B-PLA _M (C1-14).	92
FIGURE 6.12 ¹ H NMR SPECTRUM OF PS ₁₁₇ -B-PLA ₁₃₀ (C1-15) COPOLYMER (400 MHz, R.T., CDCl ₃).....	94
FIGURE 6.13 COMPARATIVE ¹ H NMR SPECTRA OF PS-Br, A1-11 (BLUE), PS-N ₃ , A2-7 (PINK), PS-OH, A3-1 (GREEN) AND PS-B-PLA, C2-4 (PURPLE). (ZOOM INTO CHEMICAL SHIFT Δ = 5.2 – 3.0 PPM)	96
FIGURE 6.14 SEM IMAGES OF THE AS-SPUN AND ANNEALED SUBSTRATES AT VARIOUS TIMES: A) AS-SPUN, B) 15 MIN, C) 45 MIN, D) 1H 30 MIN, E) 3H, AND F) 6 H.....	101
FIGURE 6.15 SEM IMAGES OF THE UNTREATED A) AND THE SILYLATED SUBSTRATE B) AFTER 45-MIN SVA WITH O- XYLENE.	103
FIGURE 6.16 SEM IMAGES OF THE THERMALLY ANNEALED THIN FILMS AT 120°C A), AND 150°C, B) IN A 10-MINUTE TA.....	105
FIGURE 6.17 SEM IMAGES OF THE AS-SPUN A) AND THE HYDROLYZED FILM B).	107
FIGURE 6.18 AFM IMAGES AND PROFILES ON THE MORPHOLOGY OF THE AS-SPUN, A), AND THE HYDROLYZED FILM, B), ON PRE-TREATED SUBSTRATES.	108
FIGURE 6.19 SEM-EDX IMAGE OF THE METAL-TREATED PS-FILM A) HYDROLYZED SAMPLE W/CuCl ₂ , AND B) CU- MAPPING IMAGE OF THE SAME SAMPLE.	110
FIGURE 6.20 SEM IMAGES OF COPOLYMER C1-9 ANNEALED AT 110°C FOR 1H, A) AND ANNEALED AT 160°C, B)..	112

FIGURE 6.21 ¹ H NMR SPECTRA OF THE HYDROLYZED SAMPLES AT VARIOUS TIMES (C1-9, METHOD 1).....	113
FIGURE 9.1 HETERONUCLEAR MULTIPLE QUANTUM COHERENCE (GHMQC) ¹ H- ¹³ C OF PRODUCT I-2A.	133
FIGURE 9.2 FT-IR SPECTRUM OF PS-N ₃	134
FIGURE 9.3 AS-SPUN SILICON WAFERS WITH A 2.0% WT. SOLUTION WITH DIFFERENT SOLVENTS: A) THF, B) CH ₂ CL ₂ , C) DIOXANE, AND D) TOLUENE.	135
FIGURE 9.4 AFM OF THE UNTREATED SUBSTRATES AT A) T = 0, B) 15 MIN, C) 30 MIN AND D) 45 MIN OF SVA.....	135
FIGURE 9.5 SVA OF TREATED SUBSTRATES AT LONGER ANNEALING TIMES A) AS-SPUN, B) 45 MIN, C) 2H, D) 4H, E) 8H, AND F) 16 H.	136
FIGURE 9.6 ¹ H NMR SPECTRA OF THE HYDROLYZED SAMPLES AT VARIOUS TIMES (C1-9, THICK SAMPLE, METHOD 1).	137
FIGURE 9.7 SEM IMAGES OF C1-13 MONOLITH A) BEFORE AND B) AFTER HYDROLYSIS (METHOD 2).	137
SCHEME 2.1 ATRP MECHANISM.....	24
SCHEME 2.2 ARGET - ATRP MECHANISM.	26
SCHEME 2.3 SYNTHETIC PATHWAY OF PS- <i>B</i> -PVAC COPOLYMERS. ⁵⁵	27
SCHEME 2.4 GENERAL ROP MECHANISM.	28
SCHEME 2.5 <i>D,L</i> -LACTIDE RING OPENING MECHANISM USING Sn(EH) ₂ AS CATALYST.	29
SCHEME 2.6 SYNTHESIS OF PLLA MACROINITIATORS WITH ACETYLENE END GROUPS. ⁶⁰	30
SCHEME 2.7 PS- <i>B</i> -PLA SYNTHESIS USING A PS-OH MACROINITIATOR.	31
SCHEME 2.8 ATRP - ROP SYNTHETIC ROUTE TO OBTAIN PS- <i>B</i> -PLA COPOLYMERS. ⁶²	32
SCHEME 2.9 SYNTHETIC ROUTE APPLIED FOR THE PREPARATION OF PLA- <i>B</i> -P(S-STAT-4-AMS) AZIDO FUNCTIONALIZED DIBLOCK COPOLYMERS. ⁶³	34
SCHEME 2.10 CARBOXYMETHYLATION OF STYRENE.....	36
SCHEME 2.11 CUAAC REACTION. ⁷³	40
SCHEME 2.12 END-BROMINE GROUP TRANSFORMATION INTO TRIAZOLE-END PS. ⁷⁵	41
SCHEME 2.13 SYNTHESIS OF PCL- <i>B</i> -PS- <i>B</i> -PCL BY PHOTOINDUCED ATRP AND CUAAC. ⁷⁶	42
SCHEME 5.1 SYNTHETIC ROUTE TO OBTAIN I-3 (HEBBP).	49
SCHEME 5.2 SYNTHETIC ROUTE TO OBTAIN PS-N ₃ (A2) PRECURSORS.	52
SCHEME 5.3 ROUTE 1 SYNTHESIS TO OBTAIN PS- <i>B</i> -PLA (C1) COPOLYMERS.....	54
SCHEME 5.4 ROUTE 2 SYNTHETIC PATHWAY TO OBTAIN PS- <i>B</i> -PLA (C2) COPOLYMERS.....	56
SCHEME 6.1 CARBOXYMETHYLATION OF 4BS.....	62
SCHEME 6.2 APPROACH 1: BROMINATION THEN TRANSESTERIFICATION OF I-1.	63
SCHEME 6.3 APPROACH 2: TRANSESTERIFICATION THEN BROMINATION OF I-1.	66
SCHEME 6.4 SUMMARY OF APPROACH 1 AND 2 TO OBTAIN I-3 INITIATOR.....	68
SCHEME 6.5 SYNTHESIS OF PS-BR VIA ATRP WITH I-2A.	70

SCHEME 6.6 SYNTHESIS OF PS-BR VIA ARGET – ATRP WITH I-2A.	73
SCHEME 6.7 SUBSTITUTION REACTION OF PS—BR WITH NAN ₃	76
SCHEME 6.8 PLA-AC SYNTHESIS VIA ROP.	80
SCHEME 6.9 SYNTHETIC ROUTES TOWARDS THE OBTENTION OF PS _N -B-PLA _M COPOLYMERS.	83
SCHEME 6.10 CLICK COUPLING OF PS-N ₃ AND PLA-AC VIA CUAAC REACTION.	84
SCHEME 6.11 CLICK COUPLING OF PS-N ₃ AND PLA-AC VIA CUAAC REACTION.	90
SCHEME 6.12 ROUTE 2 SYNTHETIC PATHWAY TO OBTAIN PS-B-PLA COPOLYMER.	95

List of tables

TABLE 2.1 SUMMARIZED METHODS TO OBTAIN MESOPOROUS MATERIALS.	6
TABLE 6.1 ATRP EXPERIMENTS WITH BENZYLIC INITIATOR I-2A.	71
TABLE 6.2 SUMMARIZED DATA OF PS-BR SYNTHESIS VIA ARGET – ATRP.	74
TABLE 6.3 SUMMARIZED DATA OF PS-N ₃ PRODUCTS.	78
TABLE 6.4 SUMMARIZED DATA OF PLA-AC PRODUCTS.	81
TABLE 6.5 SUMMARIZED DATA OF PS _N -B-PLA _M COPOLYMER SYNTHESIS WITH MBY.	87
TABLE 6.6 DSC AND TGA SUMMARIZED DATA OF THE SYNTHESIZED COPOLYMERS.	88
TABLE 6.7. SUMMARIZED DATA OF PS _N -B-PLA _M COPOLYMER SYNTHESIS WITH EBAC.	91
TABLE 6.8 SUMMARIZED DATA OF PS _N -B-PLA _M COPOLYMER SYNTHESIS WITH ROUTE 2.	97

List of abbreviations

Abbreviations	Description
4BS	4-bromostyrene
EBAc	4-ethynyl benzoic acid
MBY	2-methyl-3-butyn-2-ol
PMDETA	<i>N,N,N,N',N'</i> -pentamethyl diethylenetriamine
Me₆TREN	Tris [2-(dimethylamino) ethyl] amine
<i>D,L</i>-lactide (LA)	3,6-dimethyl-1,4-dioxan-2,5-dione
Sn(EH)₂	Tin (II) 2-ethylhexanoate
HMDS	1,1,1,3,3,3-hexamethyldisilazane
MBP (I-1)	Methyl 2-(4-bromophenyl) propanoate
MBBP (I-2a)	Methyl-2-bromo-2-(4-bromophenylpropanoate)
HEBP (I-2b)	2-hydroxyethyl-2-(4-bromophenylpropanoate)
HEBBP (I-3)	Hydroxyethyl-2-bromo-2-(4-bromophenylpropanoate)
PS-Br (A1)	End-bromine polystyrene
PS-N₃ (A2)	End-azide polystyrene
PS-OH (A3)	End-hydroxy polystyrene
PLA-ac (B1/B2)	End acetylene polylactic acid
PS-<i>b</i>-PLA (C1/C2)	Poly (styrene- <i>block</i> -lactic acid)
BCP	Block copolymer
RDRP	Reversible Deactivation Radical Polymerization
ATRP	Atomic Transfer Radical Polymerization
ARGET	Activators Regenerated by Electron Transfer
ROP	Ring Opening Polymerization
NMP	Nitroxide Mediated Radical Polymerization
RAFT	Reversible Addition – Fragmentation chain Transfer Polymerization
CuAAC	Cu ^I -Catalyzed Azide-Alkyne Cycloaddition

Abbreviations	Description
SVA	Solvent Vapor Annealing
TA	Thermal Annealing
NMR	Nuclear Magnetic Resonance
FT-IR	Fourier-Transform Infrared Spectroscopy
GC-MS	Gas Chromatography-Mass Spectrometry
SEC	Size Exclusion Chromatography
SEM	Scanning Electron Microscopy
EDX	Energy Dispersive X-ray Spectroscopy
TEM	Transmission Electron Microscopy
AFM	Atomic Force Microscopy
DSC	Differential Calorimetric Analysis
TGA	Thermogravimetric Analysis
BET	Brunauer-Emmet-Teller
T_g	Glass transition temperature
T_m	Melting temperature
T_{ODT}	Order-disorder transition temperature
T_D	Degradation temperature
f_A	Volume fraction of degradable block
n, m	Degree of polymerization
χ_{AB}	Flory-Huggins interaction parameter
χ_N	Degree of segregation
M_n	Number average molar mass
Đ	Dispersity
ρ	Density
G'	Dynamic Modulus

Abstract

This dissertation aimed to investigate the synthesis of poly(styrene)-*block*-poly(lactic acid) (PS-*b*-PLA) copolymers with triazole derivatives as a junction between blocks. The synthetic pathway towards the obtention of these copolymers comprised the synthesis of a benzylic initiator that is active in an Atomic Transfer Radical Polymerization (ATRP) to obtain a polystyrene (PS) precursor, a Ring Opening Polymerization (ROP) to obtain a polylactic acid (PLA) precursor, and a 'click' chemistry coupling of their end functional groups, the synthesized copolymers were used as templates for the preparation of thin films. Self-assembly behavior of these films was studied by Solvent Vapor Annealing (SVA), Thermal Annealing (TA) and Hydrolysis of the as-spun substrates and monitored their morphological changes by means of Scanning Electron Microscopy (SEM) and Atomic Force Microscopy (AFM) techniques. Self-assembly via SVA and TA proved to be strongly dependent on the pretreatment of the substrates. The as-spun substrates exhibited the formation of pores on the surface, which is in good agreement with the cylinder morphology that is usually expected for these systems. It was concluded that as-spun films can be a good alternative to form an ordered pattern at a nanoscale to form a triazole functionalized porous polystyrene matrix after selectively removing the PLA microdomains. The newly functionalized porous matrix can be applied as templates for the preparation of nanomaterials or in the energy storage field in electronics.

1 Introduction

Mesoporous materials are versatile compounds that can be applied to specific fields in science, such as energy storage devices, or in the catalysis of certain processes. For these reasons, among others, these materials have attracted considerable interest. In addition, the available preparation methods allow to modify specific features on the final porous matrix like morphology, microdomain dimensions, functional groups, etc. This investigation established a preparation method to obtain mesoporous materials that comprises the synthesis of PS-*b*-PLA copolymers followed by the soft templating of the triazole-embedded copolymers.

The preparation process to obtain these materials was based on a synthetic pathway that allowed the introduction of functional groups into a copolymeric matrix; the first step consisted in the synthesis of an ATRP initiator capable of polymerizing a stable block of PS. A subsequent functionalization of the PS bromine-end group allowed the addition of a degradable block of PLA, previously synthesized by ROP, to finally isolate a PS-*b*-PLA copolymer. The copolymer synthetic pathway also considered the introduction of triazole functional groups as part of the polymeric chain.

The isolated functionalized copolymer acted as a template to prepare thin films; this method enabled to establish experimental conditions towards the aimed morphology. The intrinsic segregation properties of PS-*b*-PLA copolymers allowed the study of their self-assembly behavior to modulate the final morphology of the material toward the obtention of a cylindrical formation of the mesophases. Once the copolymer was properly segregated, the PLA phase was selectively removed to form cavities on a PS-porous material embedded with triazoles.

The results and discussion of the conducted experiments are divided into two sections: Parts A and B; the Part A focuses on the synthetic route results starting from the initiator synthesis to the characterization of the functional block copolymers (BCPs); the obtention of the products was monitored by Nuclear Magnetic

Resonance (NMR), Infrared Spectroscopy (FT-IR), Gas Chromatography-Mass Spectrometry (GC-MS) and Size Exclusion Chromatography (SEC). Part B includes the discussion regarding the results of the self-assembly of the synthesized BCPs and the preparation of the thin films, the morphology of these films was monitored by Scanning Electron Microscopy (SEM) and Atomic Force Microscopy (AFM).

2 Literature review

2.1 Mesoporous materials

The study of mesoporous materials has gained its share of interest more frequently in performing specific tasks, the applications that stand out from these materials range from energy storage devices to heterogeneous catalysis, as well as filtration or sequencing in chromatography.¹ In recent years special attention has been paid to these materials for their potential for water purification by nanofiltration, where the utilized matrices include, mainly polyamide or cellulose membranes², semipermeable polymers³, zeolites⁴, inorganic nanoparticles, graphene⁵, liquid crystals⁶ and BCPs.⁷

In particular, mesoporous materials derived from BCPs can have functional groups on their surface that are capable of capturing specific pollutants present in water. An example of this is the complexation of functional moieties on the porous matrix with metals in order to reduce salinity and/or toxicity in water wastes.²

Mesoporous materials can be classified according to the International Union of Pure and Applied Chemistry (IUPAC) considering their pore size: microporous materials have a pore size of less than 2 nm, mesoporous materials have pore sizes from 2 to 50 nm, and macroporous materials bear a pore size greater than 50nm.⁸ The pore dimension of a porous material usually determines how this material can be applied, thus, mesoporous materials have a wide field of application.

2.1.1 Preparation methods

The preparation methods to obtain a mesoporous material are developed according to a specific final application. Some preparation methods involve the use of well-known organic chemistry reactions at a certain stage in the process, thus, various methods have emerged to assess these materials.⁵

One of the commonly used techniques for this purpose is based on the use of a soft template, which consists of the preparation of a heterogeneous pattern where one of the phases can be removed by extraction, for example.⁹ This technique proposes the use of a solvophilic and a solvophobic species, in such a way that both phases are assembled into a periodic array according to the chemical properties of each phase.¹⁰

In the late 1990s, this procedure was widely used for the formation of porous materials, using silica matrices as templates, aluminosilicates, or carbon, among others. For example, to prepare a carbon mesostructure, for example, amphiphilic molecules such as cetyltrimethylammonium bromide (CTAB) were used as templates in phenolic resins.¹⁰ Although this technique is not the only method to obtain mesopores in a surface, in the following years it was possible to create ordered structures at a nanometric scale using as BCPs raw material. In this case, BCPs act as amphiphiles (surfactants), where the solvophobic part can assemble into a spherical or a cylindrical morphology. Hence, copolymer phases that are capable of aggregating in two and three dimensions to form structures ranging from cubic, hexagonal to lamellae.¹¹

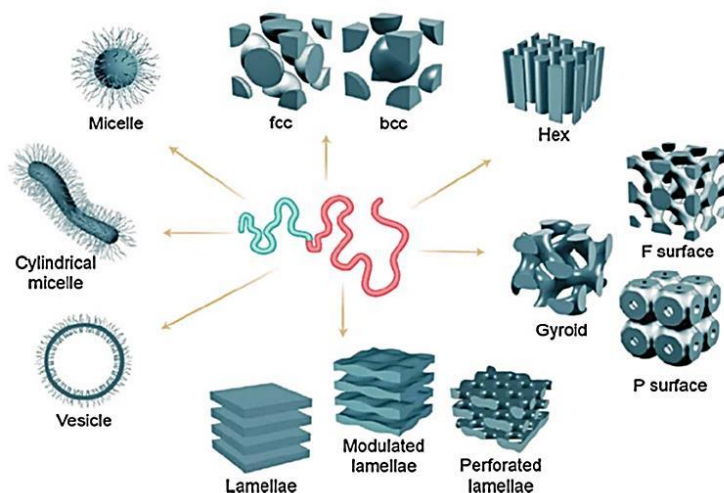
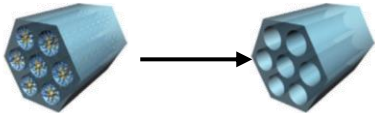
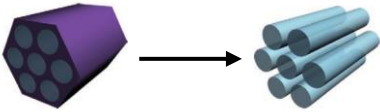
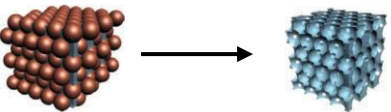
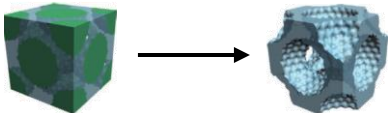
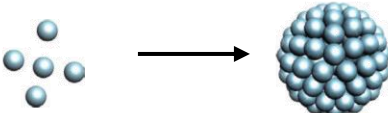
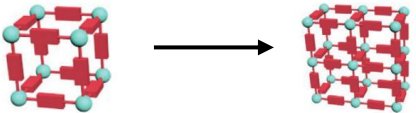


Figure 2.1 Different morphologies of BCPs.

Figure 2.1 shows the possible morphologies that a two-phased copolymer can take up. In addition, there are some physicochemical variables that must be considered to obtain the desired morphology.

Hard templating is another technique used to obtain mesoporous materials where the hard template is primarily made of silica or carbon. Typically, in this process a preformed or predefined shape act as a mold to deposit a certain material. Derived from these techniques, there are further preparation methods as it is summarized in Table 2.1.¹¹ It is worth noting that the preparation methods are closely related with the final applications of the material; in this case soft templates are very useful for the preparation of mesoporous from BCPs.

Table 2.1 Summarized methods to obtain mesoporous materials.

Method	Brief description	Consists of	Selective removal
Soft template	Self-assembly of a surfactant to form ordered mesostructures.	Co-assembly + Surfactant	
Hard template	Mesostructure formation from preformed hard templates like silica.	Preformed template + Filling precursor	
Multiple template	Combination of hard and soft templates.	Multiple template + Precursors infiltration	
In-situ template	In situ formation of a hard template via phase separation.	Phase separation + in-situ template	
No template	Cavity formation as a result of the block segregation at a nanoscale.	Nucleation	
Reticular chemistry	Uses molecular building blocks to create metal-organic frameworks (MOFs).	Nucleation + MOFs	

2.1.2 Block copolymers as templates for mesoporous materials

The synthesis of BCPs has attracted special attention in the preparation of mesoporous materials, particularly to obtain pore sizes in the order of nanometers.^{12,13} One of the first contributions that studied the use of BCPs to form nanopores was reported by Park and collaborators¹⁴ in 1997, their investigation explored the use of polystyrene-polybutadiene copolymers (PS-*b*-PB) and polystyrene-polyisoprene (PS-*b*-PI) as templates to generate an ordered mesostructure. By preparing thin films of these materials, it was possible to obtain hexagonal and spherical geometries of PS-*b*-PB and PS-*b*-PI, respectively. The procedure roughly consisted in the preparation of a thin film by annealing the copolymers at a temperature higher than its T_g (125 ° C) for 24 h, morphologies of this type were obtained with ~20 nm pore dimension. These results not only demonstrated that BCPs can act as precursors to obtain nanoporous materials but also demonstrated that it is possible to obtain specific pore geometries and dimensions because of the intrinsic periodic array that these copolymers can generate.

In the following decades these investigations became popular exploring the use of BCPs where differences in chemical properties between the polymer blocks promote the self-assembly of the final material. There are numerous pairs of blocks that, according to their physicochemical characteristics, are capable of self-assembling and further promoting the phase segregation, which subsequently results in the formation of a porous material. PS was one of the components with the highest demand for the manufacture of these materials, since it has shown great versatility as the majority block in an asymmetric BCP

For example, poly(styrene)-*block*-poly(4-vinylpyridine)), PS-*b*-P4VP, has been studied as a precursor to obtain a mesoporous material through the preparation of thin films.¹⁵ The authors claim to obtain nanoporous materials based on PS-*b*-P4VP starting from the synthesis of this copolymer; its structural properties enable the

phase self-assembly required to form a periodic array. An additional example of a copolymer template is poly(styrene)-*block*-poly(dimethylsiloxane), PS-*b*-PDMS. *Lo et al.* published the use of these copolymers to obtain an ordered mesoporous structure by performing an orientation of the copolymer phases.¹⁶ In general, BCPs have received special attention as precursors of mesoporous materials since the synthetic procedure as well as the preparation methods enable, up to a certain point, to regulate the cavity dimensions. Therefore, there are studies with different pairs or triads of monomers (diblock or triblock) whose physicochemical properties can promote phase self-assembly to further design porous matrices with a specific morphology.^{17,18}

This investigation focused on the evaluation of a PS-*b*-PLA copolymer as a precursor to prepare a mesoporous material. In this system, the degradable block was PLA (hydrophilic part) and the stable block consisted of PS (hydrophobic part). Previously, in our research team, progress was made in this area, using PLA-*b*-PS copolymers containing imidazole functionalities in their structure. These synthesized polymers were used as templates to obtain mesoporous materials.¹⁹ Therefore, the present work enables us to give continuity to the topic by exploring further possibilities when it comes to the functionalization of well-established copolymeric systems like PS-PLA.

The synthesis of BCPs as precursors of mesoporous materials still represents a versatile tool since it allows the introduction of functional groups into the polymeric matrices that can perform highly specific tasks. Additionally, to maintain control over the fabrication process of a mesoporous matrix, the synthetic pathway plays an important role when considering the polymerization method as it is discussed in section 2.2.1.

2.1.2.1 Thermodynamic variables of BCPs

As applied for discrete molecules, polymers have thermodynamic characteristics that rule its behavior defined by specific variables. BCPs behave in a

certain manner when induced into a phase segregation. In this section it is briefly addressed how the thermodynamic parameters influence the molecular morphology of such systems.

In principle, a BCP tends to spontaneously segregate into microphases, in this process each phase is governed by the chemical properties of their respective block, which are, to a certain extent, intrinsically incompatible. This characteristic of a BCP and its behavior have been proven in numerous systems that have two or three blocks.^{20,21}

One of the determining factors in copolymer phase segregation is the covalent bond between the blocks that restricts the macroscopic separation of the chemically dissimilar blocks. Generally, the equilibrium of the polymer-polymer phase depends on the following variables:

- Molecular architecture
- Monomer nature
- Ratio between blocks, volume fraction (f_A)
- Degree of polymerization, repeating unit (n)

The chosen monomers that make up the copolymer determine the stability of the system; such an effect can be estimated by the Flory-Huggins interaction parameter (χ_{AB}) according to Equation 2.1.²²

$$\chi = \frac{1}{\kappa_B T} \left[\epsilon_{AB} - \frac{1}{2}(\epsilon_{AA} + \epsilon_{BB}) \right]$$

Equation 2.1 Flory-Huggins interaction parameter.

Where κ_B is the Boltzmann constant, and ϵ_{AA} is the energy between A and B blocks in the copolymer. A χ negative value indicates a favorable energy of the

copolymer to undergo phase segregation, and the bonding between the *A-B* blocks generates a lower energy value than the sum of the *A-A* and *B-B* interactions.

As the copolymer reaches equilibrium, phase segregation opposes the loss of entropy in the system. This phenomenon is attributed to the covalent unions between segments at the interface and to the stretching strain of the chains to maintain a uniform density. To describe this phenomenon, the degree of segregation (χN) is observed. Where N indicates the volumetric degree of polymerization of the polymer; N , is directly estimated from the number average molar mass (M_n) of the polymer, ρ , is the density of the reference volume ($v_0 = 118 \text{ \AA}$), and Avogadro's constant, N_A , according to Equation 2.2.²³

$$N = \frac{M_n}{\rho v_0 N_A}$$

Equation 2.2 Volume degree of polymerization.

In every biphasic system, there are physical limitations that determine the affinity of a phase with another, which ultimately determines the segregation of the phases. Depending on the degree of segregation χN , three possible scenarios can be predicted:

- $\chi N \ll 10$, Weak segregation: The distribution of the segments in the copolymer is homogeneous, the phases are disordered, hence, entropic factors dominate over energetic.
- $\chi N \approx 10$, Mean segregation: There is a balance between entropy and Gibbs-free energy in the copolymer, and an order-disorder transition occurs (ODT).
- $\chi N \gg 10$, Strong segregation: As the degree of segregation increases, there is a better definition in the domains, where the interfaces are narrower, and the system is in a higher energy state.

By increasing χN , the formation of more defined microdomains is promoted due to less contact between *A-B* blocks.²² This is the case for the strong segregation limit (SSL). In an SSL, one of the phases has weak interactions with the other phase, resulting in a highly segregated material with narrow interphases.

A schematic representation of the segregation of a two-phased symmetric copolymer is illustrated in the upper half of Figure 2.2. From left to right, it can be seen that the degree of segregation increases, hence, as segregation is promoted, polymer segments are increasingly ordered. In the lower half of this figure, the graphs show a constant volume fraction (f_A), with respect to the radius of gyration (r), as the segregation increases.

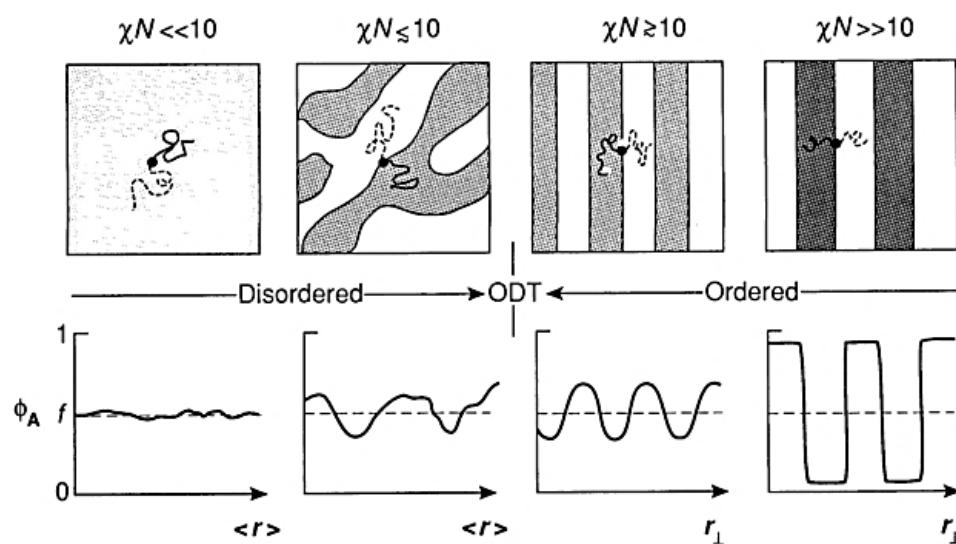


Figure 2.2 Segregation transitions of a symmetric AB copolymer.

The intermediate point between the ODT is critical for knowing the state of the copolymer when segregation occurs. In this regard, the thermal transitions of the copolymer can help to determine a range of values in which it is more likely to find the transition into an ordered state ($\chi N \geq 10$).

Previously, a symmetric composition of the blocks has been considered in the copolymer; however, in many cases the phases are asymmetric, leading to different morphologies of the mesostructures. Therefore, an increase or decrease in the composition or volume fraction (f_A) in the copolymer as well as the χN value, will determine the phase morphology, as illustrated in the phase diagram in Figure 2.3.

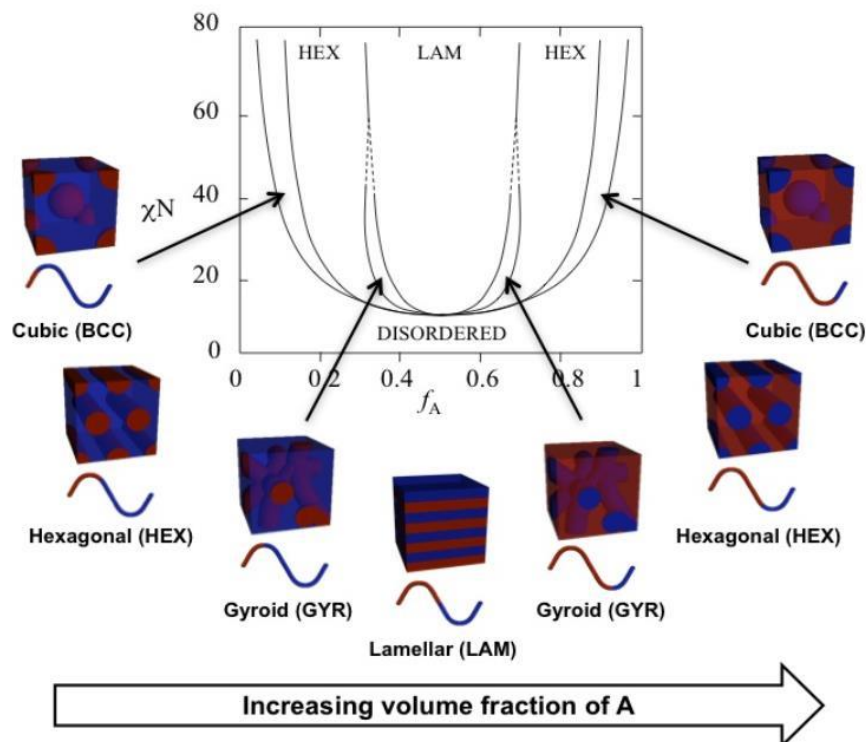


Figure 2.3 Theoretical phase diagram and expected morphologies for an asymmetrical AB BCP.²⁴

Figure 2.3 illustrates the obtained morphology according to the composition of the block. As discussed before, the thermodynamic variable χN determines an ordered or disordered state of the phases, a properly segregated BCP will result in the formation of phases at a nanoscale.²⁴

As suggested above, each block has physicochemical features that, according to the temperature, would allow the system to transition from disordered to ordered

state. In some cases, the differences between transition temperatures of one block and the other allow to promote a certain orientation and geometry in the system. These thermal transitions have been studied by various characterization techniques as discussed in section 2.1.4.

The effect that temperature has on phase segregation has been studied by Leibler²⁵, whose equation (Equation 2.3) considers this variable in the Flory-Huggins parameter for polymeric systems.

$$\chi_{eff} = \alpha T^{-1} + \beta$$

Equation 2.3 Effective Flory-Huggins interaction parameter.

Where χ_{eff} , is the effective Flory-Huggins interaction parameter, $\alpha > 0$ and β are constants for specific volume compositions (f_A) and degree of polymerization (n).²⁶ This equation allowed to presume that a high value of χ_{eff} , will promote a degree of segregation ($\chi_{eff}N$) towards a higher segregation limit, enabling an ordered phase separation. The working temperature value must not reach the degradation temperature (T_D) of the material; moreover, this value should be within the temperature range in which the order-disorder transition (T_{ODT}) of the minority phase occurs. A $T_{ODT} = 150$ ° C value has been used for a wide variety of BCPs, including the PS-PLA pair.²⁷

Considering the afore-mentioned thermodynamic parameters, different studies of copolymeric systems whose properties between blocks differ from each other to promote phase segregation. Wang²⁸ and colleagues studied the possible morphologies that the poly(styrene)-*block*-poly(L-lactic acid)) (PS-*b*-PLLA) copolymer can adopt, specifically targeting a helical geometry. As a result, the PS-*b*-PLLA phase diagram is emphasized, which indicates the different morphologies of the material considering the change in χN in relation to the composition. Authors conclude that within a range of values of f_{PLLA} from 0.20 to 0.30, the preferred

morphology of PLLA if of hexagonal type, this claim agrees with the behavior predicted by Bates²⁴ for BCPs.

Specifically, for PS-*b*-PLA-based systems, various publications include phase segregation studies as well as the synthesis of such copolymers. According to Zaluzky and collaborators²⁹, there are two possible morphologies from which porous materials based on styrene could be obtained: hexagonal or gyroid. After the material was oriented, the PLA minority block was selectively removed, resulting in a hollowed ordered structure. Figure 2.4 displays the experimental phase diagram reported in this investigation where the cylindrical morphology was found in an interval of $f_{\text{PLA}} = 0.20 - 0.45$, and the gyroid morphology in an interval of $f_{\text{PLA}} = 0.38 - 0.45$ approximately. With this precedent, it is possible to predict which block is preferred to obtain a specific morphology on the material.

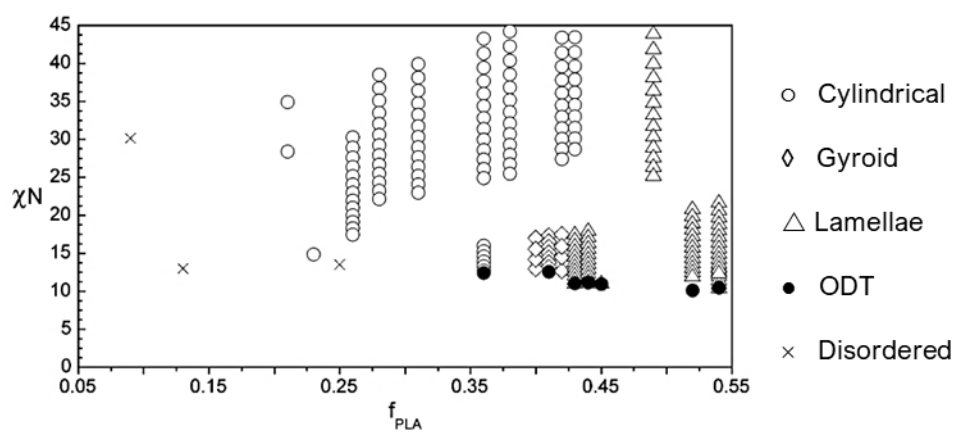


Figure 2.4 Experimental PS-*b*-PLA phase diagram.

Other reports claimed to have obtained similar results when studying the self-assembly of PS-*b*-PLA copolymers; Grande et al.,¹² have successfully verified that $f_{\text{PLA}} = 0.3 - 0.4$ results in a cylindrical hexagonal morphology.

It should be noted that the chain length of the segments is a limiting factor in the mobility of a BCP, and hence the polymer stretchability it also determines its morphology. Therefore, proper control over M_n and dispersity (\mathcal{D}) is required to diminish any variations in the thermodynamic properties of the polymeric material.

2.1.2.2 Thermal transitions of BCPs

An important aspect of the study of BCPs relies on the analysis of thermal transitions, since they indicate at which conditions a transition or structural change occurs. In this case, the synthesized copolymers were the templates for the formation of nanostructured materials, therefore, it is necessary to be familiar with the thermal processes that involve these species. In addition, it is important to understand how these transitions influence the preparation process of a nanostructured material, as well as their impact in the final morphology.

Within the thermodynamic parameters, the relevance of the variable order-disorder transition temperature (T_{ODT}) on segregation-dependent processes has been highlighted. This parameter indicates a temperature value, or a range of values, in which a copolymer undergoes a reversible transition from an ordered state into a homogeneous molten state. As previously mentioned, this transition also depends on the degree of segregation (χN) of the copolymer and it is possible to estimate it by performing a rheological analysis that allows to measure the Dynamic Modulus (G').¹⁷ The obtained data allows to understand the optimal temperature conditions to perform the orientation and therefore obtain an adequate alignment within an ordered state.

Other techniques such as Differential Calorimetric Analysis (DSC) also enable to obtain useful information about the thermal behavior of BCPs, more precisely, it is possible to estimate the glass transition temperature (T_g) as well as the melting temperature (T_m). A BCP with at least one crystalline or semicrystalline component should exhibit a value of T_m , which will depend on the inherent chemical and structural features of the repetitive unit. Therefore, the melting process in a BCP is

directly related to the arrangement of the crystalline block. Regarding the amorphous copolymer, a melting transition is not expected to be observed.³⁰

The glass transition represents an important change in the morphology of the polymer, indicating a state of homogeneous disorder in the system. Within an amorphous or semi-crystalline copolymer, a T_g value is expected for each block. It should be noted that there is a thermal interval in which one of the phases might be above its T_g value, but below the glass transition of the remaining phase. This interval allows to modify the ordering of one of the phases since being in a state of relaxation enhances the orientation.³¹ As reviewed on the following section, some of the orientation methods employ this principle in their technique.

Finally, by knowing the transitions of each block, it is possible to predict a temperature range where the copolymer disordered phases can be shifted. In most polymeric systems, there is no absolute crystalline or amorphous behavior but rather amorphous or crystalline regions within the homopolymer that manifest as thermal transitions. Hence, in a BCP not only physical phenomena is observed between one block and another, furthermore, the interactions within the homopolymer must be considered.

2.1.3 Microdomain orientation and selective removal

It has been established that a defined morphology can be obtained in a nanostructured material considering variables when BCPs are used as templates. This investigation focused on the nanopatterning of PS-*b*-PLA copolymers followed by a selective removal of PLA, also known as the degradable or minority block. In this manner, the PLA phase is susceptible to arrange into cylinders within the PS continuous phase in a periodic and ordered pattern. Once the pattern is defined, the PLA can be removed leading to the formation of a PS-based mesoporous matrix.³²

The applied techniques to remove the minority blocks have been studied along with the development of mesoporous materials. One of the reported methods to form

microdomains from a copolymer, consists in the preparation of a thin film using a hydraulic press. Next, the resulting film is introduced into a narrow channel of a metallic die provided with a fitting counterpart. The die is subjected to a shear stress in the perpendicular direction at a temperature higher than the T_g value of the minority phase, but at a lower value than the T_g value of the continuous phase. As a result, the formation of microdomains in the phase is favored without affecting the thermal stability copolymer. This procedure has been applied to mixtures of ethylene-polypropylene copolymers,³³ where it was demonstrated that the applied stress promotes the crystallization of one of the domains in the material, thus forming an ordered phase within an amorphous matrix. In summary, the mechanical orientation process involves applying pressure on a surface at a certain temperature; choosing the temperature value will depend on the physicochemical properties of each homoblock in the copolymer.

The following studies demonstrated that mechanical orientation is an effective method in the orientation of BCPs; Majdoub³⁴ and collaborators reported obtaining PLA microdomains with a cylindrical morphology in a PS matrix using this technique. Authors claim that their isolated materials have cavities of nanometric dimensions after removing the PLA block by hydrolysis.

Further alternatives to promote the orientation of microdomains in the copolymer have also been explored. These techniques involve the study of the self-assembly of a copolymer in solution; an example of this is discussed below.

2.1.3.1 Solvent vapor annealing (SVA)

Solvent vapor annealing (SVA) is a technique employed to alter the orientation of the phases in a BCP and obtain a defined morphology. In this method, a copolymer film is set in contact with solvent vapor to swell the film and promote the self-assembly of the phases. By definition, annealing is a slow heating and cooling process of a material that allows to modify its ductility.³⁵ Incorporating this concept into the SVA technique, the solvent vapor is considered as the stimuli, and the

annealing allows to modify the morphology of a material towards the orientation of the domains.

Essentially, this technique consists of depositing a small amount of a copolymer solution on a substrate, typically on a silicon wafer. Then, the as-deposited film is placed in contact only with solvent vapor avoiding any direct contact with the liquid solvent or any component that may damage the film surface. The process is let to occur in a closed recipient for a determined amount of time.³⁶

The premise of this technique suggests that at least one of the components of the copolymer should have a value similar to the Hildebrand solubility parameter. In other words, one of the blocks in the copolymer must be 'alike' to the solvent used for annealing so that the solvent vapor is absorbed by the film and swelled. Once the film has swollen, the glass transition of the copolymer drops below room temperature, allowing chains to have greater mobility and promoting the orientation of the domains.³⁷ The choice of the annealing solvent will determine whether the induced orientation is successful; hence, it is important to correlate the affinity of the block to be oriented with the solvent.

An example of the afore-mentioned is observed for PLLA, of which has demonstrated a successful orientation with this technique using 1,1,2-trichloroethane as an annealing solvent, resulting in cylindrical domains within a PS matrix of PS.³⁸ It was also found that highly volatile solvents, i.e. tetrahydrofuran, promote the formation of a disordered microstructure where there is no sharp definition of the segregated microdomains. Therefore, a phase segregation does not necessarily indicate a proper alignment of the microdomains and the choice of solvent, and in this technique, it is of utmost importance.

As in mechanical orientation, selective removal of the minority phase it can be achieved by an alkaline hydrolysis, as seen for PLA phases. Other investigations propose the use of UV radiation to align and etch the degradable block instead of a

chemical procedure, resulting in the formation of nanoscale cavities in ordered patterns.³⁹

2.1.4 Characterization techniques for mesoporous polymers

Observing the formation of oriented regions in a material is crucial to corroborate that the cavities meet the aimed characteristics. For this purpose, there are different characterization methods, among them is the Microscopy of Atomic Force (AFM). This method allows observation of the topography of a surface by placing a mechanical probe in contact with the sample, and as a result it can provide information about the thickness of the film as well as the dimension of a certain domain at a micro- or nanoscale. This characterization technique has proven to be very useful for monitoring phase segregation in PS-*b*-PLA copolymers and other copolymer-based systems. For instance, Vayer *et al.*⁴⁰ observed the orientation of a PS-*b*-PLA copolymer via AFM to determine an optimal array of the domains and proceeded to selectively remove the degradable block.

Naturally, microscopic techniques are also widely used as characterization tools to monitor the morphology of self-assembled materials. Scanning Electron Microscopy (SEM) and Transmission Electron Microscopy (TEM) systems are used almost routinely to monitor the alignment of the domains in a BCP. These characterizations allow to differentiate a gyroid, hexagonal or a lamellar morphology. Specifically by SEM several investigations evidence the formation of a specific geometry for PS-PLA copolymers.⁴¹ To monitor the domain alignment in a polymer matrix is crucial to ensure that phase orientation has properly taken place and to determine optimal experimental conditions which allow to obtain the aimed morphology. Modifying the cavities dimensions and morphology of a material can determine its potential applications; therefore, microscopy techniques are essential, since they provide an actual image of what occurs as a result of the self-assembly.

In addition to these techniques, the gas adsorption capacity of a porous material can also provide useful information about the analyzed sample. Roughly, a characterization method based on gas adsorption can give an estimate of the pore dimensions in a porous sample based on physisorption, which occurs when a gas is in contact with the surface of a solid.

The Brunauer, Emmet, and Teller (BET) method, proposed in 1938,⁴² is based on the physisorption phenomena, and it consists of placing a porous sample in contact with N₂ gas at T = -198 ° C. At these conditions the volume of the adsorbed gas by the sample is calculated by correlating the total surface area with the adsorbed amount, as a result, an average value of the cavities dimension is obtained. It is worth noting that this is a complementary technique, as it can provide partial information about the material, and thus, it should be supported by a technique that can provide information about the morphology such as AFM, SEM, or TEM.

2.1.5 Emerging applications for mesoporous polymers

There is an upgrowing interest towards mesoporous materials derived from BCPs due to the versatility that self-assembly provides to modulate morphology. One example of emerging applications of these materials is energy storage and conversion (ESC). In this regard, mesoporous polymers can provide better mass transport, in this case ions or electrolytes, compared to microporous materials due to their larger pore size.⁴³

Mesoporous polymers have also been employed as heterogeneous electrocatalysts by means of their catalytic sites within the prepared material. Tang *et al.* reported the use of poly(styrene)-*block*-poly(ethylene oxide) (PS-*b*-PEO), in a co-assembly process with dopamine to generate mesoporous carbon spheres that exhibit catalytic properties in oxygen reduction reactions (ORR).⁴⁴

Other studies have focused on the metal capture capacity of mesoporous polymers, where the material is capable of retaining metallic species through coordination bonds between an embedded functional group and a metallic center.^{45,46}

The aforementioned applications are only a few examples of the use of BCP as templates for nanostructured materials; however, the use of these materials is extended to the preparation of nanomaterials in biomedicine⁴⁷ or in the synthesis of specific nanoparticles.⁴⁸ Therefore, self-assembly of BCP remains in the spotlight due to the design that these macromolecules provide as a result of this process.

2.2 Block copolymer synthesis

BCPs are macromolecules that contain at least two polymer blocks of similar or different chemical structure joined through a covalent bond.⁴⁹ Each block consists of a discrete repetitive unit forming a homopolymer that is linked to another block. Some types of BCPs are illustrated in Figure 2.5.

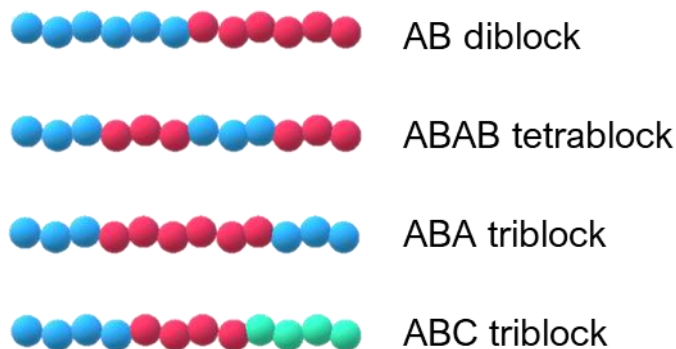


Figure 2.5 Types of BCPs.

Specifically, this project focused on the synthesis of asymmetrical AB diblock copolymers, that is, with different ratios between blocks. The proportion between blocks is commonly observed by the volume molar fraction, f_A , of the minority block. This variable determines a certain behavior of the copolymer phases when induced into a self-assembly process. therefore, it is important to consider the f_A during the synthesis of the BCP since it determines a certain morphology in later stages to prepare mesostructured arrays. The influence of this variable on the self-assembly of BCPs is addressed in Section 2.1.2.

To achieve these specific features in a BCP there have been many studies over the last years within Reversible Deactivation Radical Polymerization (RDRP) processes. There are several types of polymerizations within RDRP, all of them enable to obtain a particular homopolymer or copolymer, maintaining a controlled addition of the monomer during the polymerization reaction.

In addition to RDRP techniques, there are other polymerization processes that enable the obtention of BCPs. ROP involves a polymerization process with a different mechanism but keeping a controlled addition of monomer units. This process can be also used in combination with RDRP to obtain specific macromolecules. Both RDRP and ROP techniques are mentioned in the following sections of this document.

A first stage of our proposal toward the obtention of BCPs considers the use of one of the RDRP processes (ATRP) to obtain a PS block by using a previously synthesized benzylic initiator. A subsequent step is to synthesize the second block of PLA block by using ROP to ultimately obtain a PS-*b*-PLA copolymer.

2.2.1 Reversible Deactivation Radical Polymerization (RDRP)

RDRP techniques consider a mechanism that involves the formation of a radical capable of regulating monomer consumption during a polymerization reaction. The RDRP processes comprise the following: Nitroxide Mediated Radical Polymerization (NMP), Reversible Addition – Fragmentation chain Transfer Polymerization (RAFT) and Atomic Transfer Radical Polymerization (ATRP). In all of these mechanisms, a radical is formed and further controlled by a reactive agent in a reversible activation – deactivation fashion, resulting in a controlled mechanism during the polymerization.

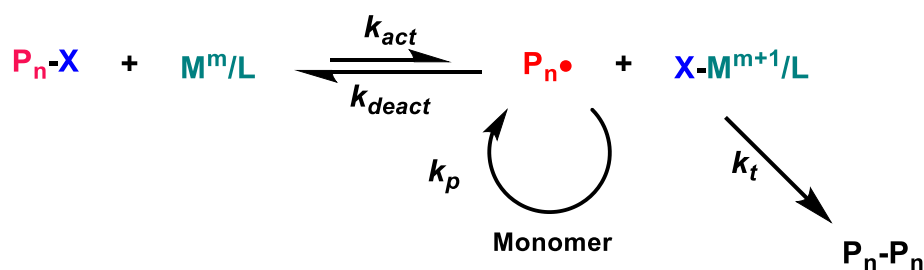
This document focuses on the ATRP process and some of subcategories since it was employed to obtain the starting materials to synthesize the aimed copolymers.

2.2.1.1 Atomic Transfer Radical Polymerization (ATRP)

The ATRP technique has been widely studied on vinylic monomers, from which many other sub techniques have arisen.

The classic ARTP mechanism is based on the activation-deactivation equilibrium that occurs between a growing radical ($P_n\bullet$) and a dormant species (P_nX). The initiator is an alkyl halide, and it can be activated after the reaction with a

transition metal complex which transfers an electron to the halogen atom resulting in the formation of a free radical. This radical reacts with the vinyl group of the monomer molecule, generating a new growing radical. A distinctive feature of this polymerization method is the deactivation of the growing radical through a redox reaction between the free radical and the transition metal complex when the metallic center is at its highest oxidation state. As a result of this reaction, an end-bromine compound is generated, known as dormant species. In this manner, an intermittent activation-deactivation process between the dormant species and the metal complex begins. Thus, the growing radical progressively consumes monomer, resulting in a controlled growth of the polymer chain.⁵⁰



Scheme 2.1 ATRP mechanism.

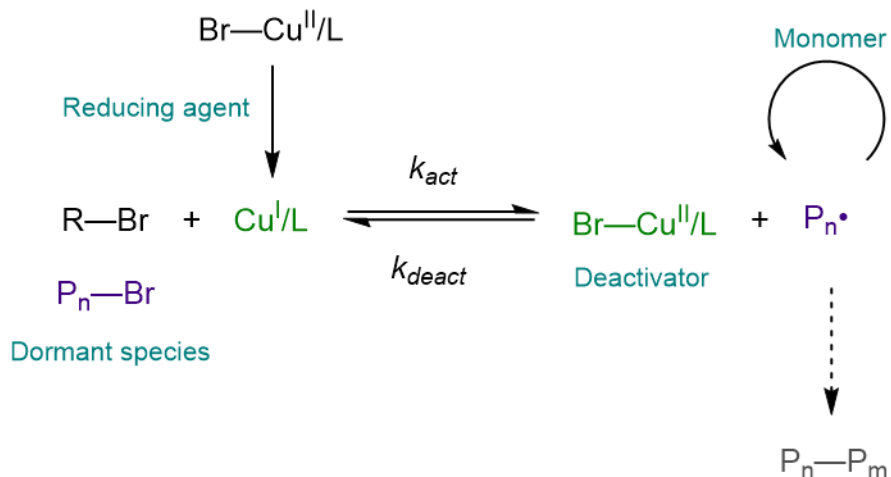
Scheme 2.1 displays the polymerization mechanism. Where k_{act} is the activation constant, k_{deact} is the deactivation constant (inverse process), k_p is the propagation constant, and k_t is the termination constant. The metal complex ($X-M^{m+1}/L$) reacts with the growing radical ($P_n\bullet$) to form the dormant species (P_nX). The most commonly used metal complexes are often those of Cu/Cu^{II} with polydentate nitrogen ligands such as pentamethyldiethylenetriamine (PMDETA), hexamethylenetriamine (HMTA), and tris[2-(dimethylamino)ethyl]amine (Me_6TREN).⁵⁰

There are many ATRP-based mechanisms that arose from this principle, some of these are briefly mentioned in the following section.

2.2.1.2 Emerging ATRP techniques

Derived from this ATRP polymerization mechanism, several sub-categories have developed with significant variations to the classic mechanism. These techniques can be further classified into electrode controlled (eATRP), photoinduced, mechanically controlled (mechanoATRP), thermally controlled, and chemically controlled ATRP.⁵¹ This section addresses the most important techniques within the chemically controlled ATRP techniques as it involves one of the main areas of study in this project.

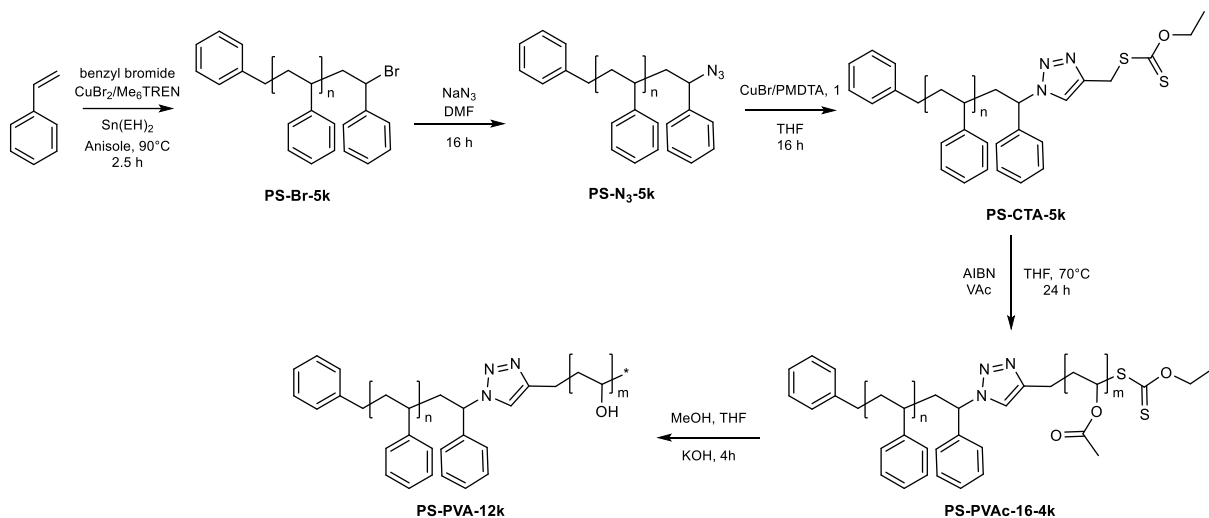
One of the main challenges of the classic ATRP mechanism relies on the experimental limitations when handling a Cu^{I} complex. The oxygen sensitivity of such compounds has driven the focus towards the improvement of this process. In this regard, Activators Regenerated by Electron Transfer (ARGET) presents a suitable option by employing a Cu^{II} salt to form the metal complex, due to the lower reactivity towards oxidant agents like moist and oxygen. This mechanism consists of the formation of a Cu^{II} -complex that is further reduced into the lowest oxidation state, $\text{Cu}^{\text{I-L}}$, by adding a reducing agent.⁵² After the complex has been reduced, the following steps are ruled by the classic ATRP mechanism. This process is summarized in Scheme 2.2.



Scheme 2.2 ARGET - ATRP mechanism.

Another highlight of this technique is the reduced amount of copper salt required to catalyze the reaction, it has been established that a concentration between 10 – 100 ppm is enough to guarantee a controlled process.⁵³ Furthermore, the presence of a reducing agent such as tin (II) 2-ethylhexanoate ($\text{Sn}(\text{EH})_2$) or glucose improves tolerance to air in reaction media.⁵⁴

ARGET ATRP has been widely used to obtain homopolymers or macroinitiators to further copolymerize a second block. Altintas *et al.*,⁵⁵ report the synthesis of poly(styrene)-*block*-poly(vinyl acetate) (PS-*b*-PVAc) copolymers. This approach considers the preparation of a PS macroinitiator ruled by an ARGET ATRP process, followed by the synthesis of the PVAc block using RAFT polymerization.



Scheme 2.3 Synthetic pathway of PS-*b*-PVAc copolymers.⁵⁵

As a result, a PS-Br macroinitiator was obtained by following the reaction proposed on the first step in Scheme 2.3. The isolated product was further functionalized to obtain a suitable transfer agent (step 2 and 3), which is required in the subsequent RAFT polymerization (step 4). This investigation confirms the viability of ARGET ATRP as an initiating step in the synthetic pathway to the obtention of specific BCPs.

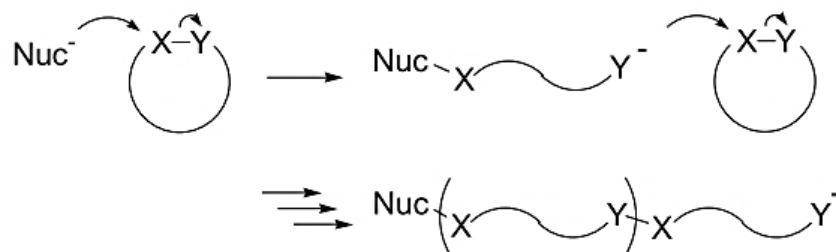
Considering the chemically induced ATRP techniques it is worth to mention the supplemental activator and reducing agent (SARA) process. This procedure modifies the Cu oxidation state by adding Cu⁰, which acts as a supplemental activator of alkyl halides and as a reducing agent for the Cu^{II} salt that is required to form the Cu-complex. A typical reaction involves the presence of a Cu^{II} salt that is being reduced by Cu⁰ following a similar activation-deactivation process as seen in the ARGET initiation step. The following propagation steps occur as the classic ATRP mechanism proposes.⁵⁶

Regardless of the specific utilized technique, ATRP remains a useful tool for synthesizing an end-bromine polymer that is capable of being transformed into a different functional group via a post-polymerization reaction. This topic can lead to a

large number of possibilities within the organic chemistry reactions; this project refers only to the click reactions as described in Section 2.2.3.1.

2.2.2 Ring opening polymerization (ROP)

This polymerization technique allows the synthesis of polymeric structures starting from a cyclic monomer, and according to its chemical nature, it employs a different initiation mechanism. The following types of polymerizations are considered within ROP: Anionic ROP, Cationic ROP and Radical ROP. For instance, ROP processes that use nucleophilic agents as initiators are considered anionic. Scheme 2.4 displays a general mechanism of polymerization, which begins by a nucleophilic attack towards a heteroatom present in the cyclic structure. Subsequently, the ring strain causes the structure to open, and the newly formed nucleophile attacks another monomer unit, repeating the process and ultimately forming the polymer chain.

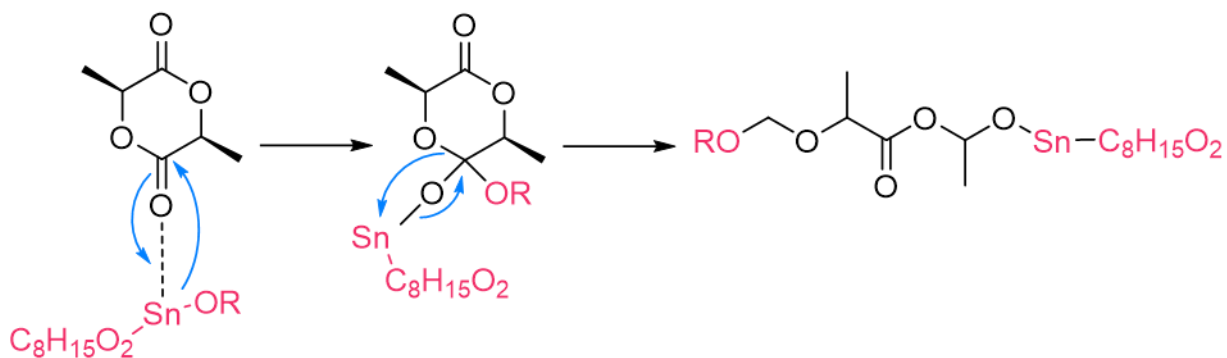


Scheme 2.4 General ROP mechanism.

Some of these nucleophilic species include organometallic compounds, metallic amides, alkoxides, alcohols, phosphines, imines, and water. Regarding the monomers that are susceptible to anionic ROP are esters, carbonates, amides, urethanes, and phosphates.⁵⁷

In general, the thermodynamics of ROP depend on the ring strain of the molecule, therefore a catalyst is necessary to control the addition of monomers and

to inhibit the formation of unwanted by-products.⁵⁸ Specifically, the ROP of lactides enables the synthesis of dimers that are repeated throughout the polymer chain following the mechanism shown in Scheme 2.5.⁵⁹

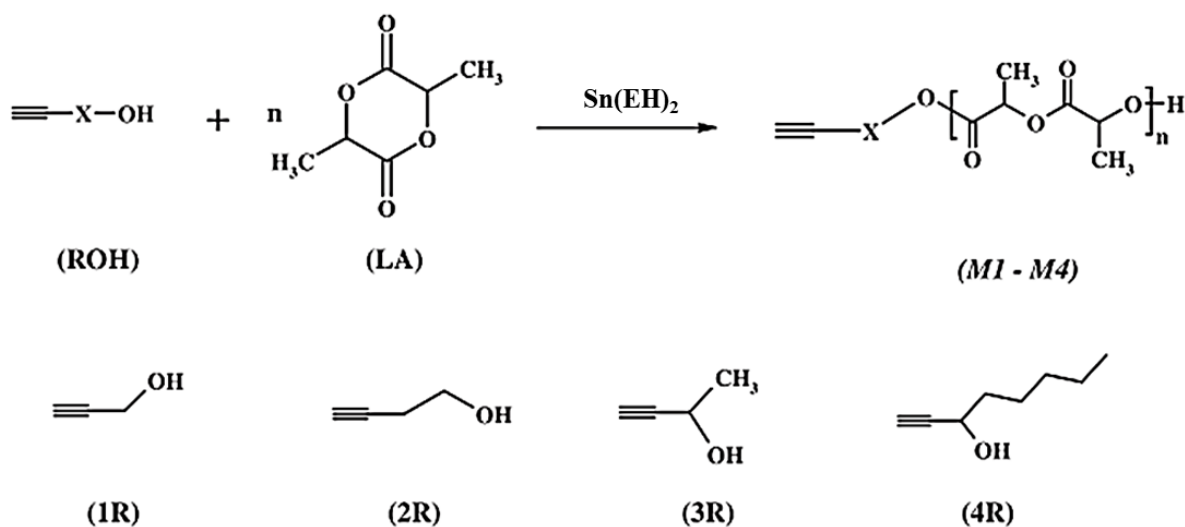


Scheme 2.5 *D,L*-lactide ring opening mechanism using $\text{Sn}(\text{EH})_2$ as catalyst.

Studies regarding this system have established that some organometallic complexes such as tin (II) 2-ethylhexanoate ($\text{Sn}(\text{EH})_2$), act as good catalysts in the ROP of lactides through a coordination-insertion mechanism. This process consists of the monomer coordination towards the catalyst and subsequent insertion of the monomer towards the metal-oxygen bond.⁵⁹

2.2.2.1 ROP of lactides with hydroxy terminated initiators

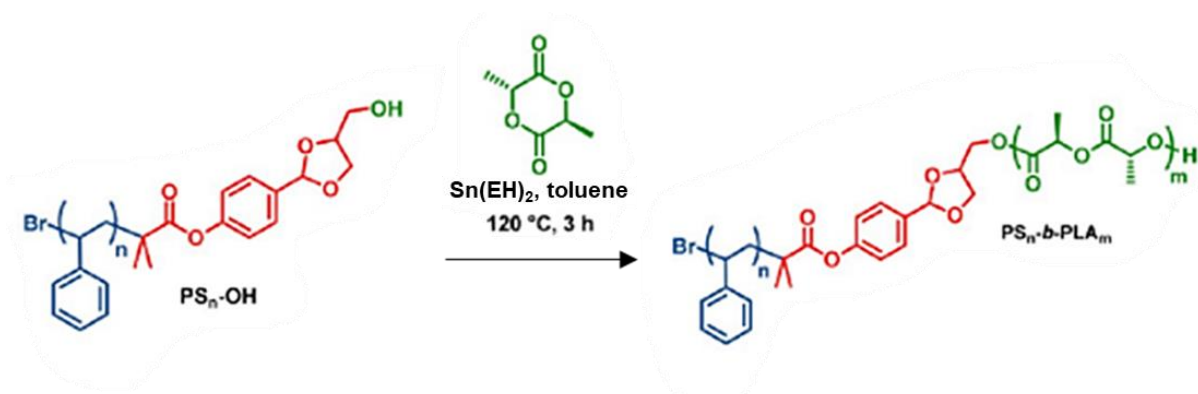
Typically, within ROP processes an initiator with a hydroxy functionality can promote the initiation step following the mechanism as shown in Scheme 2.5. On this subject, Czelusniak *et al.*⁶⁰ reported the synthesis of lactide (LA) based macroinitiators using hydroxy-terminated acetylenes as initiators in the presence of $\text{Sn}(\text{EH})_2$ as catalyst of the reaction.



Scheme 2.6 Synthesis of PLLA macroinitiators with acetylene end groups. ⁶⁰

Scheme 2.6 displays various initiators utilized in the ROP of the LA, in this case, the PLLA macroinitiators have an acetylenic termination to further copolymerize in a subsequent step. Hence, hydroxyacetylenes were efficient initiators in preparing PLA homopolymers.

Further investigations across the literature consider a hydroxy terminated macroinitiator, meaning that a ROP process can be initiated by a previously synthesized homopolymer with a reactive end group. An example of this is the use of a hydroxy terminated PS (PS-OH) as initiator in a typical ROP process. Poupart *et al.*³⁶ reported the synthesis of a PS-*b*-PLA copolymer by copolymerizing the PLA block using a PS-OH macroinitiator as shown in Scheme 2.7.



Scheme 2.7 PS-b-PLA synthesis using a PS-OH macroinitiator.

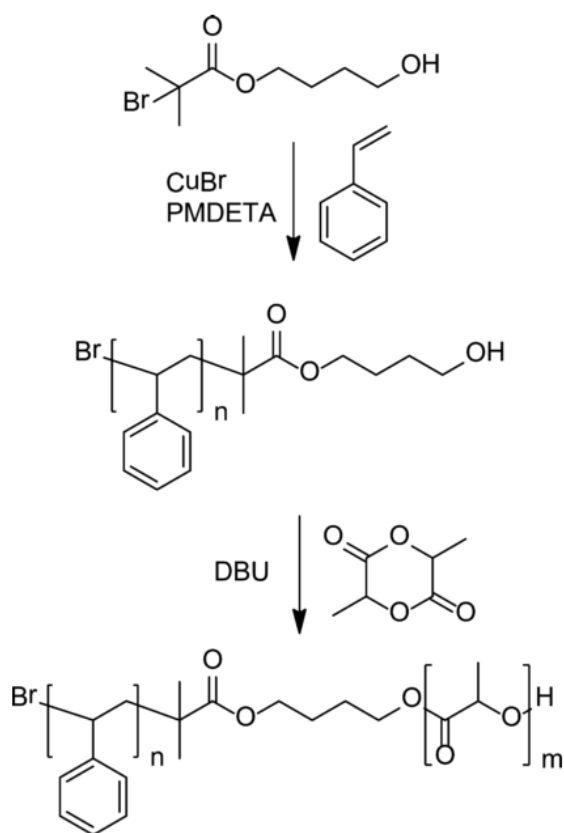
In this investigation, the authors highlight the fact that a post-polymerization reaction allows selective removal of the PLA block and further change the end-functionality of the remaining PS block. Regardless, it is also an example of a ROP copolymerization of PLA using a PS-OH macroinitiator.

There has also been progress regarding the catalytic system in ROP reactions. For instance, a one-pot copolymerization of caprolactone and lactide was achieved by using benzoic acid as the catalyst. In this case, the acidic termination (COOH) enables the polymerization as observed with the hydroxy terminated initiator in a typical ROP process. One of the advantages of this approach is that no organometallic catalyst is needed as opposed to the previous examples.⁶¹ There are new emerging possibilities to explore organocatalyzed processes for this kind of cyclic monomers that may also represent other possible pathways towards the obtention of lactide-based homopolymers and/or copolymers.

2.2.3 ATRP and ROP

It is common to find studies among the literature that combine polymerization techniques to obtain BCPs that have different functionalities in their structure. ATRP and ROP have also been studied to obtain BCP with specific structures and features.

More precisely, the system poly(styrene)-*block*-poly(*D,L*-lactic acid) (PS-*b*-PLA) has been the subject of study using this polymerization technique. A typical route considers the synthesis of a PS macroinitiator following an ATRP-based procedure, the product must have in its structure at least one reactive end-group to continue a second polymerization reaction, ROP in this case. Once this product has been isolated and purified the PLA block is synthesized by ROP according to the mechanism described. Keen *et al.*⁶² reported the use of this synthetic route shown in Scheme 2.8.

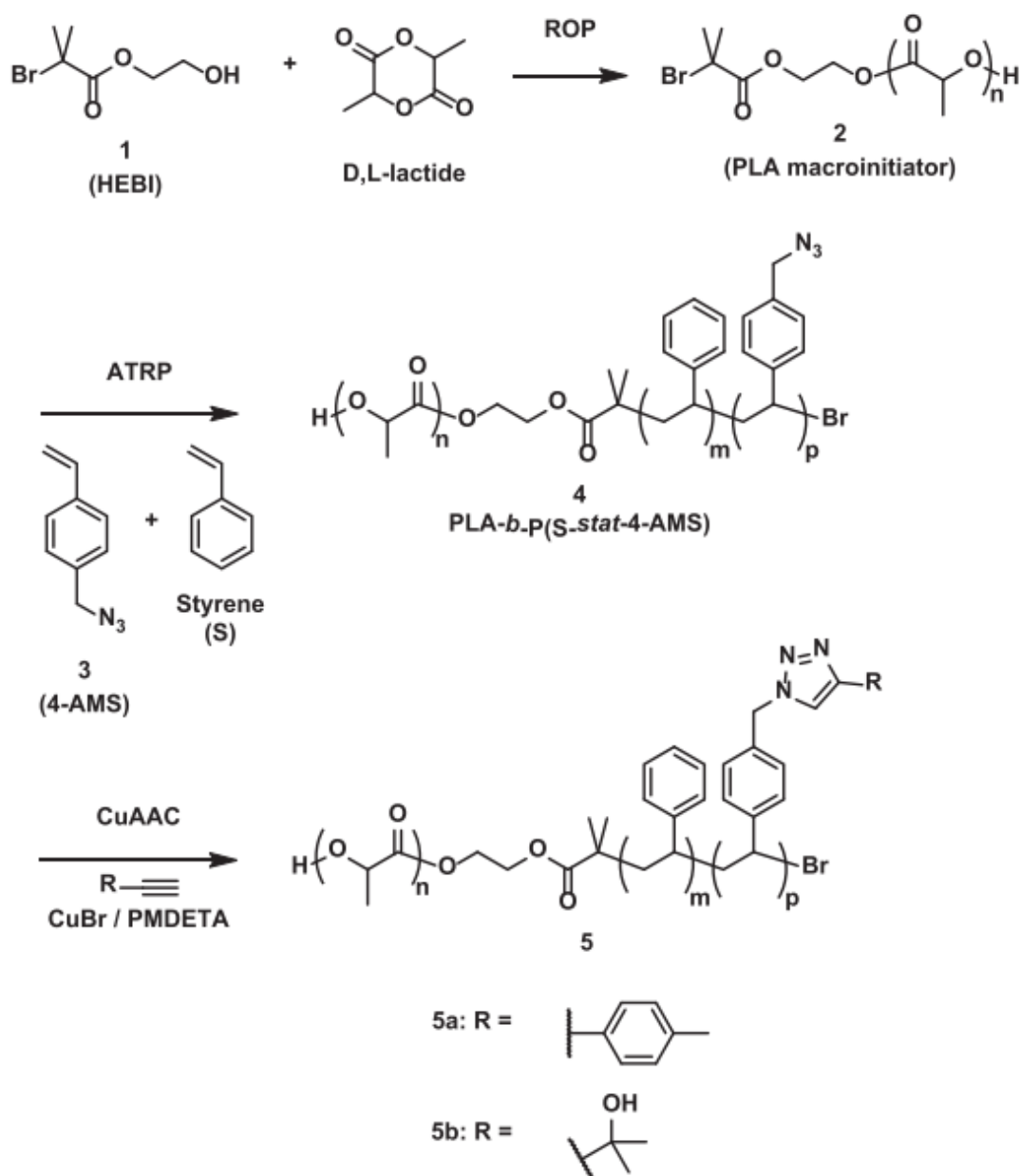


Scheme 2.8 ATRP - ROP synthetic route to obtain PS-*b*-PLA copolymers.⁶²

This combination is useful due to the control it has during the polymerization process, as a result it is possible to isolate polymers and copolymers with a well-defined molar mass (M_n) and narrow dispersity (\mathcal{D}). When these techniques are

combined, one of the possible routes is to synthesize a bifunctional initiator that contains two reactive functional groups toward ATRP and ROP reactions. This would enable the polymerization of both desired blocks following the described mechanisms for each block. Additional details on the bifunctional initiator system are addressed in Section 2.2.3.1.

Further examples in the literature that combine both techniques have proven that it is also possible to synthesize polymers performing ROP prior to the ATRP using a bifunctional initiator as shown in Scheme 2.9.⁶³ In this investigation, the PLA macroinitiator synthesized in the first step enables the copolymerization of a PS block in a subsequent ATRP step. Note that the PS block contains a randomly distributed styrene-based triazole derivative.



Scheme 2.9 Synthetic route applied for the preparation of PLA-*b*-P(S-*stat*-4-AMS) azido functionalized diblock copolymers.⁶³

This confirms the versatility of the combination of ATRP and ROP techniques since it enables the obtention of different blocks containing functional groups.

Other studies have also explored the ARGET ATRP – ROP combination to obtain block copolymers. Yu *et al.*,⁶⁴ reported the synthesis of star shaped poly(ϵ -

caprolactone)-*b*-poly(2-(diethylamino)ethylmethacrylate) (4AS-PCL-*b*-PDMAEMA) via ROP of a caprolactone followed by ARGET ATRP of DMAEMA monomer. In this case, a hydroxy-terminated macroinitiator was transformed into a bromine-terminated caprolactone to enable the polymerization of DMAEMA with this end-group.

Therefore, it is possible to obtain BCPs with specific structures by combining different polymerization techniques. In addition, monomers, initiators, and end-functional groups can be transformed into specific functionality to enable copolymerization and/or a post-polymerization reaction.

2.2.3.1 ATRP – ROP initiator

In order to obtain a PS-*b*-PLA copolymer, the synthesis of a bifunctional initiator was initially proposed. A bifunctional initiator has within its structure at least two different functional groups whose individual chemical characteristics can promote the formation of two different blocks via different polymerization mechanisms. Figure 2.6 displays an ATRP initiator commonly used in the synthesis of block copolymers.⁶⁵

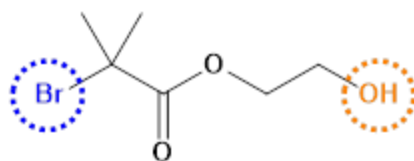
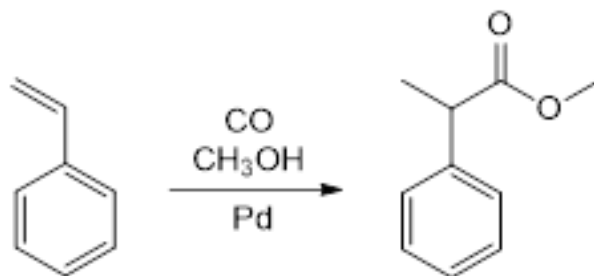


Figure 2.6 ATRP – ROP bifunctional initiator.

The bromide group allows the formation of a radical that is capable of starting the polymerization of a vinylic monomer, in this case styrene. The growing radical is stabilized according to the ATRP mechanism, thoroughly described in Section 2.2.1.1. Regarding the hydroxyl group functionality, a ROP of a lactide occurs in the

presence of a tin-based catalyst (Section 2.2.2). Hence, a bifunctional initiator is useful to obtain diblock copolymers since it enables the presence of two blocks with dissimilar chemical nature stabilized by a covalent bond.

In this fashion, a first stage towards the obtention of a PS-*b*-PLA copolymer could consider the synthesis of bifunctional initiator 2-hydroxyethyl-2-bromo-2-(4-bromophenyl propanoate) (HEBBP). HEBBP can be synthesized by a carboxymethylation reaction of styrene. Pennequin *et al.*⁶⁶ have reported the use of CO and methanol to promote the formation of methyl acetate *in situ* in the presence of a palladium catalyst, resulting in the formation of a carboxymethyl group as shown in Scheme 2.10.



Scheme 2.10 Carboxymethylation of styrene.

Subsequent bromination enables the addition of a bromine group on the alpha carbon atom to the carbonyl. The last step in the initiator synthetic pathway is the transesterification of the hydroxyethyl group for the methoxy group in an excess of ethylene glycol. In this manner, the final initiator contains two of the aimed functionalities to polymerize via ATRP and ROP the PS and PLA block, respectively. Hence, bifunctionality of the initiator converges blocks of different chemical nature to co-exist in a single macromolecule by a covalent bond.

Benzylic initiators have been employed to initiate RDRP processes, Whitfield *et al.*⁶⁷ published a so-called universal method to polymerize styrene, acrylates, and metacrylates by using a benzylic initiator via a Cu(0)-mediated RDRP.

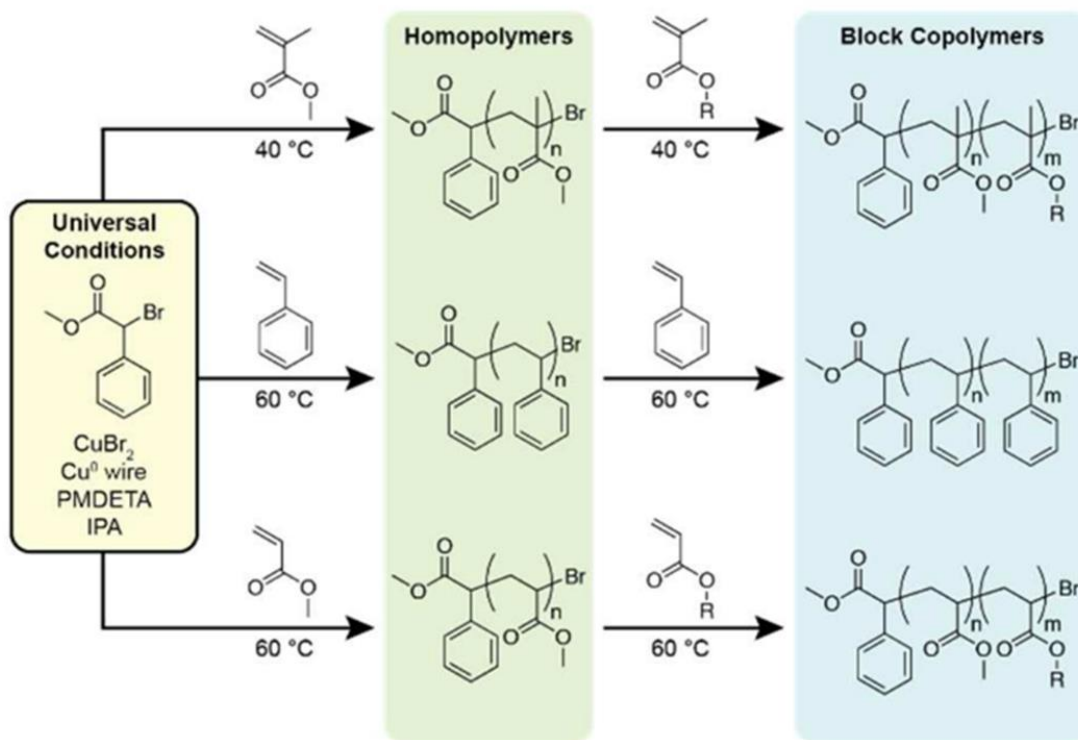


Figure 2.7 Synthesis of polyacrylate, polymethacrylate and PS via Cu(0)-mediated RDRP.⁶⁷

In Figure 2.7 a schematic representation is shown where similar conditions were applied for the synthesis of different BCPs starting from MBPA initiator. In addition, the Cu-PMDETA complex proved to be adequate to control the polymerization at the proposed conditions using this initiator. Previous studies in the same research group have proven that the rate of polymerization of styrene with benzylic initiators is significantly slower than with methacrylates; however, these kind of initiators are active under ATRP based mechanisms controlled by the presence of a Cu^I-catalyst.⁶⁸

Furthermore, there are examples in the literature where more than two functionalities can be found in a single initiator, these functional groups enable the polymerization and determine the architecture of a copolymer, among other features. For instance, the synthesis of a trifunctional initiator was reported that allows the star-

type polymer to grow by combining three polymerization techniques: ATRP, NMP and ROP.⁶⁹

In addition to the above, the bromide termination allows post-polymerization reactions to be carried out to add functional groups. In this regard, reactions of bromine substitution by azido groups have been reported, mainly with the purpose of introducing triazole groups through click cycloadditions (Section 2.3.1).⁷⁰

2.3 Functionalization and post-polymerization reactions – click approach

The introduction of functional groups into BCPs is highly pursued due to the specific features that a certain molecule can provide to the system. There are many possible routes to insert functional groups into a polymer such as the transformation of a reactive end-group. An example of this approach has been studied for end-bromine polymers, commonly synthesized by ATRP based processes. Anastasaki *et al.*⁷¹ reported the synthesis of polymethyl acrylate (PMA) to quantify the transformation of the end-bromine groups into amines, carboxylic acids, phosphonium salts, and azides, among others. The authors claim that the preparation of these end-functional polymers requires mild preparation conditions and that the isolated product can be characterized by different techniques.

As suggested above, a reactive end-functional homopolymer can function as a precursor to further synthesize a BCP. Some functionalities like azides or thiols can undergo transformations via click reactions to form a new reactive site capable of initiating a copolymerization or to add another block into the homopolymer by its own reactive end-group.⁷² In this regard, the use of click chemistry within the synthesis of BCPs is a powerful tool to functionalize macromolecules.

The concept of click chemistry comprises a set of selective reactions through heteroatomic bonds. These reactions are highly efficient and include the following: cycloadditions of unsaturated species (1,3-dipolar and Diels-Alder cycloadditions), nucleophilic substitutions (i.e., epoxide ring opening), non-aldolic reactions (formation of ureas, thioureas, etc.), and carbon-carbon additions (epoxidations, aziridizations, etc.).⁷⁰ Section 2.3.1 addresses one of the most used processes within 1,3-dipolar cycloadditions to obtain triazole groups into a polymeric material.

2.3.1 Cu^I-catalyzed azide – alkyne 1,3-cycloaddition

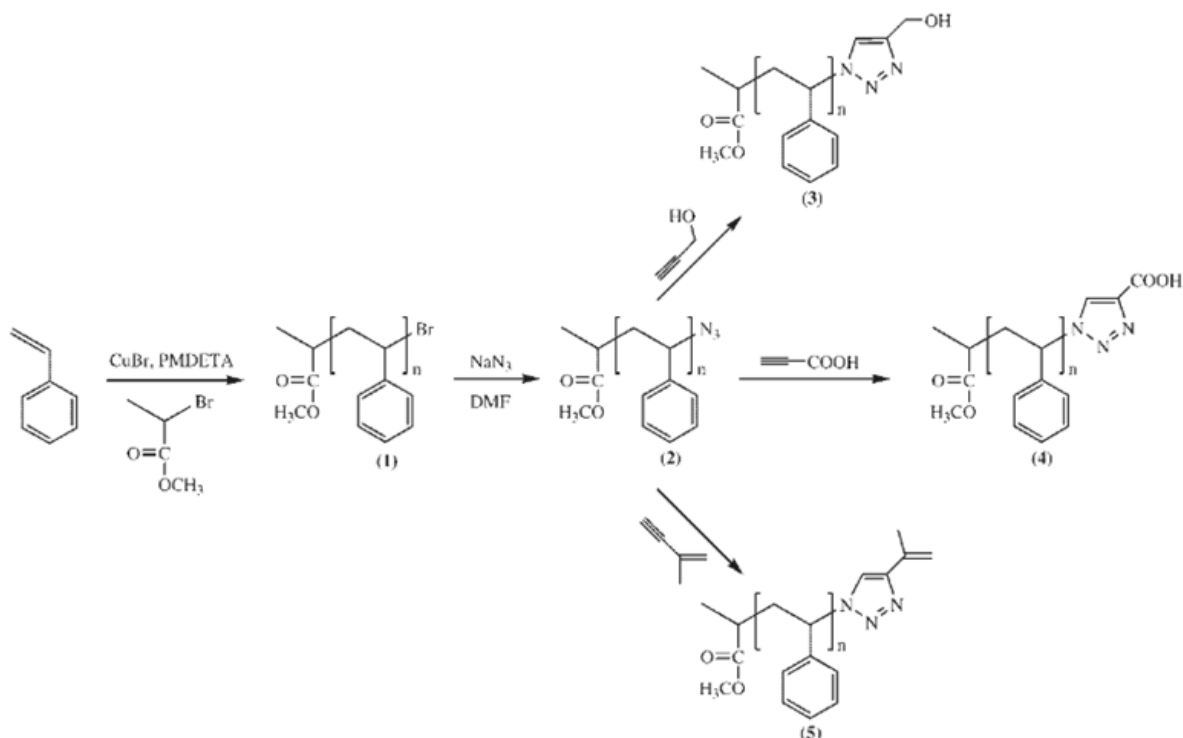
Among the click reactions, the Cu^I-catalyzed azide-alkyne cycloaddition (CuAAC) has been widely used due to the ease of the process. This reaction can be also classified as a Huisgen 1,3-dipolar cycloaddition, that can result in a 1,4-disubstituted,1,2,3-triazole as shown in Scheme 2.11.⁷³



Scheme 2.11 CuAAC reaction.⁷³

One of the main features of this reaction is the Cu-selectivity, which means that via a copper-catalyzed process the formation of a 1,4-triazole is preferred, as opposed to other azide-alkyne cycloadditions where the mechanism is non-selective and may result in a mixture of the 1,4 and 1,5-disubstituted triazoles.⁷⁴

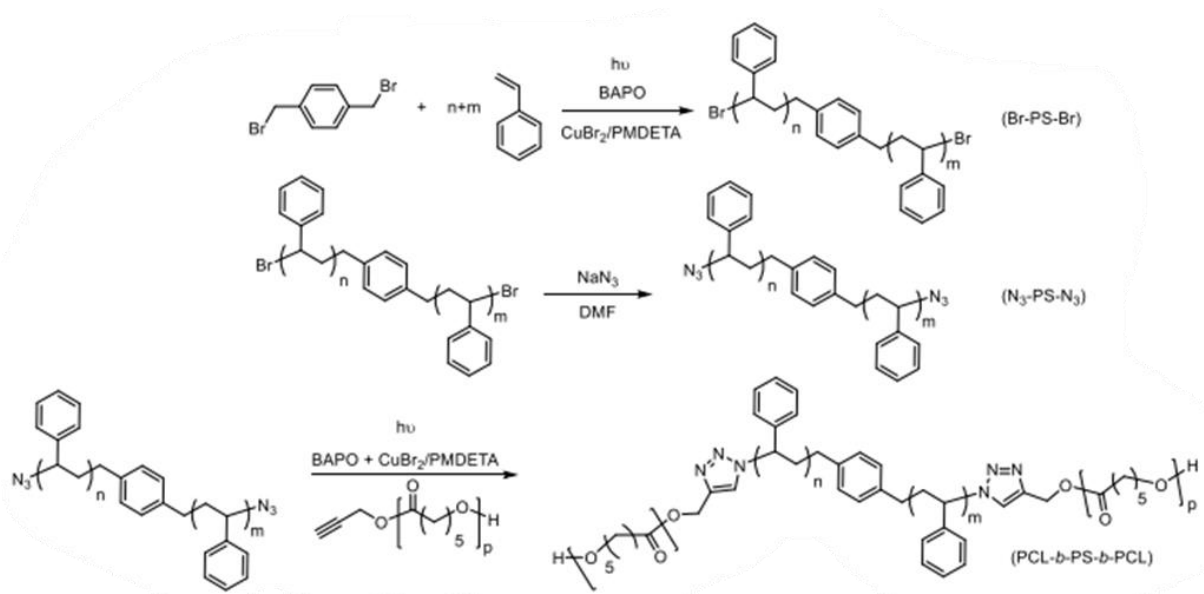
In terms of polymers, the CuAAC process follows the same mechanism for azide groups at the end of a polymer chain. For instance, a PS-Br homopolymer is reactive in the presence of NaN₃ to yield an azide-terminated PS, which can form triazole end-groups after reacting with an acetylenic molecule as reported by Lutz *et al.*⁷⁵ In their investigation PS-based homopolymers (PS-Br) were used to transform their end-bromine terminations. As a result, various derivatives of triazole end groups were obtained following a CuAAC reaction as shown in Scheme 2.12.



Scheme 2.12 End-bromine group transformation into triazole-end PS.⁷⁵

The azide-alkyne addition principle of this reaction is also expanded to the synthesis of copolymers, where the union of the corresponding reactive terminations leads to the formation of two or more blocks.

An example of the synthesis of BCPs via a CuAAC reaction was reported by Yilmaz *et al.*⁷⁶ Their investigation reports the synthesis of poly(caprolactone)-*block*-poly(styrene)-*block*-poly(caprolactone) (PCL-*b*-PS-*b*-PCL) as shown in Scheme 2.13.



Scheme 2.13 Synthesis of PCL-*b*-PS-*b*-PCL by photoinduced ATRP and CuAAC.⁷⁶

In this case, the synthesis of PCL-*b*-PS-*b*-PCL triblock copolymer was achieved by coupling the azide end groups of a symmetrical PS precursor with the alkyne end groups of a caprolactone. The authors highlight the fact that both ATRP and CuAAC processes are photo induced and are suitable to obtain this kind of architecture in BCPs. The aim of achieving a specific architecture in a BCP via CuAAC has also been studied because of the numerous possibilities of addition between the azide and alkyne end-groups. Synthesis of cyclic and/or star-shaped copolymers are examples of architectures in which the triazole groups enable the union of previously synthesized homopolymers.^{77,78}

Further examples on the synthesis of BCPs by click coupling end reactive groups include the synthesis of poly(styrene)-*block*-poly(methyl methacrylate) (HO-P(St-*b*-MMA)-OH) α - ω -functionalized with hydroxy groups.⁷⁹ In this investigation, authors claim to obtain up to 95% of reaction efficiency employing a CuAAC. The isolated PS-*b*-PMMA copolymers have a narrow molecular weight distribution (\bar{D}) as estimated by the SEC measurements, which confirms that CuAAC reactions allow to obtain copolymers with triazole junctions with well-defined molecular features.

An additional study in this type of reactions is the CuI-catalyzed azide-alkyne click polymerization (CuAACP), which is a process based on the CuAAC mechanism to synthesize linear or hyperbranched polytriazoles (PTAs). Hence, a CuAAC reaction is a helpful tool in the insertion of triazole functional groups into a polymer matrix and a CuAACP process is a different kind of polymerization where the triazoles are part of the backbone of the polymer chain.⁸⁰

2.3.2 Triazole groups in polymers

As seen in previous examples, triazole groups can be part of a polymer at the end of the chain, as part of the monomer unit, or as a junction between blocks. In general, the alteration of an end group in a polymer can modify its rheological properties as a result of the aggregation of these terminations. A functional group as a junction can also modify to some extent the microphase segregation of a BCP as a result of the electrostatic interactions between functional groups and polymer chains.⁸¹ Then, it may be expected to observe a slight shift of the physicochemical properties when comparing a triazole-functionalized copolymer with its non-functionalized analogue.

The applications of triazole-derived materials have also been explored due to the electronic properties of these molecules. The triazole complexation towards metallic centers is one the most exploited areas of applications. Triazole binding capacities toward metallic centers have been evaluated in polymer-grafted matrices. A study by Ouerghui and collaborators,⁸² claimed that triazole-grafted PS can extract metals like Cd, Fe, Mg, Ni, and Co from a solution.

Further applications of triazole in polymeric materials include, but are not limited to, the development of electrical memory polymers,⁸³ CO₂ adsorption by triazole porous polymers,⁸⁴ and the study of triazole-Cu^I complexes in polymers as antifouling agents.⁸⁵

3 Aims and objectives.

3.1 Aim

To obtain functionalized mesoporous materials capable of capturing metal cations through complexation bonds between a metallic entity and a functional group embedded on the material surface.

3.2 Objectives

To synthesize a functional ATRP initiator by performing carboxymethylation, bromination, and transesterification reaction of a styrene-based precursor.

To synthesize an end-functional PS macroinitiator via ATRP that enables the post-polymerization functionalization or copolymerization of a second block of PLA ROP.

To incorporate a thiol or a triazole functional group on the synthesized copolymers by performing a click reaction on the chain-end groups.

To characterize the obtained copolymers via Nuclear Magnetic Resonance (NMR), Size Exclusion Chromatography (SEC), and Fourier-Transformed Infrared Spectroscopy (FT-IR).

To prepare functional mesoporous materials using the synthesized copolymers as templates and test their metal-captation capacity.

To characterize the obtained materials via Scanning Electron Microscopy (SEM), Atomic Force Microscopy (AFM) and Transmission Electron Microscopy (TEM).

4 Hypothesis

It has been established that via ATRP-ROP techniques and click reactions it is possible to synthesize functionalized PS-*b*-PLA copolymers with specific molecular features such as molar mass, dispersity, and volume molar fraction of the minority block (PLA). If such PS-*b*-PLA copolymers are intrinsically capable of self-assembling into a specific morphology at determined experimental conditions, then, this phenomenon would trigger the formation of a nanopatterned structure. This nanostructured pattern would act as a template for the generation of a functionalized nanoporous matrix after selectively etching one of the phases.

5 Experimental methods

5.1 General conditions

Most reactions were conducted in an inert atmosphere by previously drying the utilized glassware in a conventional oven ($T = 100^{\circ}\text{C}$). In addition, the glassware was connected to a stream of nitrogen or argon gas to produce an inert atmosphere and minimize the water and/or oxygen interaction with any of the utilized reactants.

The purifications of the synthesized polymers and copolymers were conducted using a chromatographic column using aluminum oxide (neutral, 0.063 – 0.200 mm, Merck) as stationary phase.

5.1.1 Solvents

Tetrahydrofuran (THF), dichloromethane (CH_2Cl_2), methanol (CH_3OH), diethyl ether ($\text{C}_4\text{H}_{10}\text{O}_2$), and *N, N* – dimethylformamide (DMF) were dried using the solvent purification system PureSolv – EN™ (Innovative Technology). Toluene (anhydrous), carbon tetrachloride (CCl_4), ethylene glycol ($\text{C}_2\text{H}_6\text{O}_2$), ethanol ($\text{C}_2\text{H}_5\text{OH}$), acetone ($\text{C}_3\text{H}_6\text{O}$), ethyl acetate ($\text{C}_4\text{H}_8\text{O}_2$), and *n*-hexane (C_6H_{14}) were used without any further purification unless otherwise stated.

5.1.2 Reactants

Copper bromide (I) and copper chloride (I) were purified by stirring an undetermined amount of the powder in glacial acetic acid for several days, acetic acid was replaced every other day to remove Cu (II) moieties. Afterward, the mixture was filtered and thoroughly rinsed with methanol and anhydrous diethyl ether. A white powder was isolated after vacuum drying overnight in a Schlenk flask.⁸⁶

N-bromosuccinimide (NBS, 99%) was recrystallized by dissolving 10 g in 100 mL of pre-heated water ($90 - 95^{\circ}\text{C}$), once it was dissolved, the solution was chilled

in an ice bath for 2 h. White crystals were collected after rinsing with water and vacuum filtration.⁸⁷

Monomer 3,6-dimethyl-1,4-dioxan-2,5-dione (*D,L*-lactide) (LA, 99%) was freeze dried prior to its use. Monomer styrene (C₈H₈, 99%, 4-*tert*-butylcatechol as stabilizer) was stirred with an undetermined amount of inhibitor remover for *tert*-butylcatechol for 30 – 60 minutes. Then, the monomer was filtered to remove the solid remaining and was used for the polymerization.

The following reactants were obtained from *Aldrich* and used as received:

- 4-bromostyrene (4BS, 97%)
- Bis(triphenylphosphine)palladium (II) dichloride (PdCl₂(PPh₃)₂, 98%)
- Lithium chloride (LiCl, 99.98%)
- Calcium oxide (CaO, 99.9%)
- Sodium chloride (NaCl, 99.5%)
- 2,2'-Azobiss(2-methylpropionitrile) (AIBN, 98%)
- *N,N,N,N',N'*-pentamethyldiethylenetriamine (PMDETA, 99%)
- Magnesium sulfate, anhydrous (MgSO₄, 97%)
- Tin (II) 2-ethylhexanoate (Sn(EH)₂, 98%)

The following reactants were obtained from *TCl chemicals* and were used as received:

- Tris [2-(dimethylamino) ethyl] amine (Me₆TREN, 98%)
- 4-ethynyl benzoic acid (EBAc, 98%)
- 2-methyl-3-butyn-2-ol (MBY, 98%)
- Sodium hydroxide (NaOH, 98%)
- Sodium azide (NaN₃, 99.5%)
- 1,1,1,3,3,3-Hexamethyldisilazane (HMDS, 98%)

5.1.3 Instrumentation

¹H Nuclear Magnetic Resonance (NMR) spectra was measured on a 400 MHz Bruker Avance III spectrometer. The obtained copolymers were recorded at 128 scans with

2 s delay between scans using deuterated chloroform (CDCl_3) at room temperature and tetramethylsilane (TMS) as internal standard.

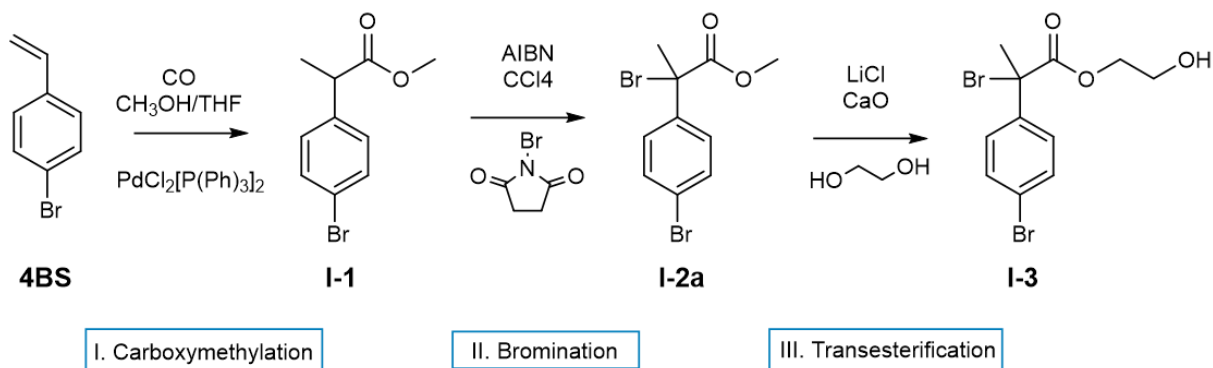
Gas Chromatography-Mass Spectrometry (GC-MS) was measured in an Agilent 5977B GC/MSD spectrometer. A 1 μL sample was injected and thermally treated with a temperature program from 25 to 300°C at a heating rate of 20°C min^{-1} .

The molar mass of the copolymers was determined using a Size Exclusion Chromatography (SEC) Shimadzu system with a mixture of chloroform, triethylamine, and 2-propanol (94:4:2 v/v/v) as eluent at a flow rate of 1 mL min^{-1} . The system is equipped with an CBM-20A controller, a LC-10AD pump, a RID-10A refractive index detector, and a PSS SDV linear S, 5 μm , column (Polymer Standards Service, PSS, Mainz, Germany). The M_n was estimated against a calibration curve built with polystyrene (PS) standards of narrow dispersity (\mathcal{D}).

Scanning electron microscopy (SEM) imaging was performed using a Zeiss Sigma VP Field Emission Scanning Microscope equipped with an Everhart-Thornley SE and InLens detector (Carl Zeiss AG, Germany), using an accelerating voltage of 10kV. The samples were coated with a thin layer of platinum via sputter coating (CCU-010 HV, Safematic, Switzerland) prior the measurement. The films were also investigated under ambient condition by means of atomic force microscopy (AFM) (NTegra Aura (NT-MDT) in tapping mode utilizing cantilevers (NSC35/AIBC, MicroMash) under hard tapping conditions, *i.e.*, high ratio of free amplitude of cantilever oscillation and set point.

5.2 Initiator synthesis

The synthesis of initiator **I-3** (HEBBP) consisted in the carboxymethylation of an styrenic adduct,⁸⁸ the subsequent bromination of the benzylic position,⁸⁹ and the transesterification of the methoxy group as a final step.⁹⁰ Scheme 5.1 summarizes the synthetic route proposed towards the obtention of **I-3**.



Scheme 5.1 Synthetic route to obtain I-3 (HEBBP).

5.2.1 Carboxymethylation of 4-bromostyrene (4BS)

40.0 g (218.5 mmol) of 4-bromostyrene (4BS), 0.7780 g (1.092 mmol) of Bis(triphenylphosphine)palladium (II) dichloride, 88.9 g (1232.8 mmol) of THF, and 35.0 g (1092.5 mmol) of CH₃OH were added into a 250 mL stainless steel reactor vessel. The vessel was attached to a high-pressure reactor (*Parr 4563 Mini reactor*) provided with a moveable head and a mantle heater. Carbon monoxide (CO) and CH₃OH were used to introduce a carboxy group on the vinyl group. Therefore, the reactor was connected to a stream of CO and pressure of the gas was carefully set at 600 psi while constantly stirring for 18 h. During this time, the reactor pressure was periodically monitored and adjusted to 600 – 650 psi to compensate for the pressure loss due to the CO consumption. Afterwards, the mantle heater was placed to cover the vessel and the temperature was set to 80°C for 16 h. At the end of the reaction, the vessel was cooled, and the pressure was released by carefully opening

the valve. Once the vessel was open, the resulting solution was extracted with *n*-hexane and the non-polar phase was further purified with a chromatography column to isolate the product methyl 2-(4-bromophenyl) propanoate (MBP) (**I-1**) (Exp. Yield = 81.1%).

¹H NMR (500 MHz, CDCl₃): δ, ppm 7.47 (2H, d, *J* = 8.2 Hz), 7.20 (2H, d, *J* = 8.2 Hz), 3.75 (4H, m), 1.57 – 1.41 (3H, m).

5.2.2 Bromination of methyl 2-(4-bromophenyl) propanoate (MBP) (**I-1**)

1.0 g (4.1 mmol) of MBP (**I-1**), 0.8785 g (5.0 mmol) of NBS and 0.034 g (0.20 mmol) of AIBN were added into a round bottom flask and dissolved in CCl₄. The solution was refluxed at 65 – 70°C for 8 h. The resulting solution was re-dissolved in a minimum amount of CH₂Cl₂ and extracted with a NaCl saturated solution. The organic phase was dried with MgSO₄ and concentrated using a rotatory evaporator. The product methyl 2-bromo-2-(4-bromophenyl) propanoate (MBBP) (**I-2a**), was isolated by chromatographic column purification using a mixture of hexane: ethyl acetate as eluent. (Exp. Yield = 85.7%).

¹H NMR (500 MHz, CDCl₃): δ, ppm 7.48 – 7.32 (4H, m), 3.70 (3H, s), 2.20 – 2.19 (3H, m).

5.2.3 Transesterification of methyl 2-(4-bromophenyl) propanoate (MBP) (**I-1**)

2.86 g (11.8 mmol) of MBP (**I-1**), 8.0 mg (0.18 mmol) of LiCl, and 0.037 g (0.666 mmol) of CaO were dissolved in 6.0 mL of ethylene glycol in a round bottom flask. The solution was refluxed with constant stirring at 80°C for 14 h. At the end of the reaction, the product was re-dissolved in CH₂Cl₂ and further extracted with a NaCl saturated solution. The organic phase was recovered and dried with MgSO₄. Then,

the product 2-hydroxyethyl-2-(4-bromophenylpropanoate) (HEBP) (**I-2b**) was isolated by placing it in the rotatory evaporator to eliminate the solvent. (Exp. Yield = 95.4%).

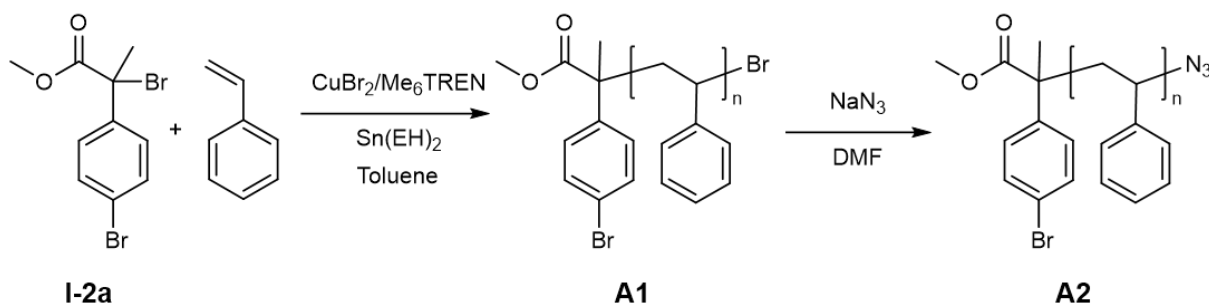
^1H NMR (500 MHz, CDCl_3): δ , ppm 7.37 (2H, d, $J = 8.2$ Hz), 7.10 (2H, d, $J = 8.2$ Hz), 4.21 – 3.99 (2H, m), 3.85 -3.59 (3H, m) 1.43 – 1.17 (3H, m).

5.2.4 Bromination of 2-hydroxyethyl-2-(4-bromophenylpropanoate) (HEBP) (**I-2b**)

0.15 g (0.55 mmol) of HEBP (**I-2b**), 0.1036 g (0.58 mmol) of NBS and 0.004 g (0.0243 mmol) of AIBN were added into a round bottom flask and dissolved in CCl_4 . The solution was refluxed at 65 – 70°C for 8 h. The resulting solution was re-dissolved in a minimum amount of CH_2Cl_2 and extracted with a NaCl saturated solution. The organic phase was dried with MgSO_4 and concentrated using a rotatory evaporator. The product 2-hydroxyethyl-2-bromo-2-(4-bromophenyl propanoate) (HEBBP) (**I-3**), was isolated by chromatographic column purification using a mixture of hexane: ethyl acetate as eluent.

5.3 Synthesis of polystyrene precursor (PS-N₃)

Scheme 5.2 summarizes the general scheme towards the obtention of PS-N₃ by performing an ARGET – ATRP reaction followed by an end-group substitution.⁵⁵



Scheme 5.2 Synthetic route to obtain PS-N₃ (A2) precursors.

5.3.1 Polymerization of styrene with initiator I-2a via ATRP (PS-Br) (A1).

30.0 mg (0.28 mmol) of CuCl and 71.0 mg (0.41 mmol) of PMDETA were added to a 100 mL Schlenk flask and dissolved in 2.0 mL of toluene. This mixture was let to stir to promote the formation of the Cu/Ligand complex. After 10 – 15 min, 5.7 g (54.6 mmol) of styrene and 0.087 g (0.28 mmol) of I-2a were diluted in 4.0 mL of Toluene and added with a degassed syringe to the Schlenk flask. The resulting solution was degassed after three cycles of freeze-pump-thaw and placed into an oil bath at 100°C for 48 h. The reaction was quenched by cooling to room temperature and opening the flask. The copper catalyst was removed by eluting the mixture with CH₂Cl₂ through an alumina column. The concentrate was precipitated by triplicate in an excess of methanol. A white/yellow solid was isolated after vacuum drying at 40°C for 16 h.

5.3.2 Polymerization of styrene with initiator I-2a via ARGET – ATRP (PS-Br) (A1).

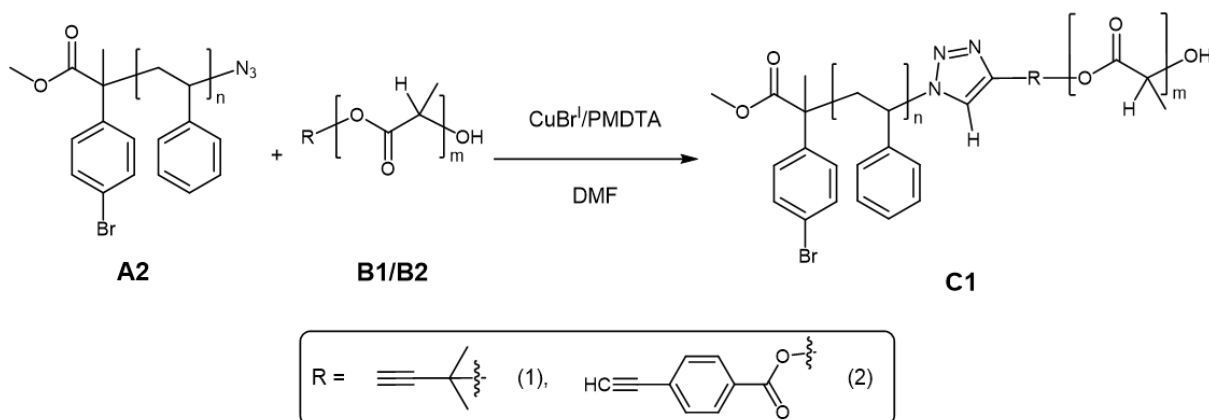
14.0 mg (0.06 mmol) of CuBr_2 were weighed in a 50 mL Schlenk flask and were promptly placed under a N_2 stream to evacuate the oxygen in the atmosphere. 166.0 μL (0.62 mmol) of tris[2-(dimethylamino) ethyl] amine (Me_6TREN), were dissolved in 2.0 mL of toluene, and added with a degassed micropipette to the Schlenk flask. This mixture was let to stir to promote the formation of the Cu/Ligand complex. After 10 – 15 min, 10.2 g (89.4 mmol) of styrene and 105.0 mg (0.31 mmol) of MBBP (I-2a), were diluted in 4.0 mL of Toluene and added with a degassed syringe to the Schlenk flask. Then, 50.3 mg (0.31 mmol) of tin (II) 2-ethynylhexanoate ($\text{Sn}(\text{EH})_2$), were diluted in 2.0 mL of Toluene and added to the mixture. The resulting solution was degassed after three cycles of freeze-pump-thaw and placed into an oil bath at 100°C for 24 – 72 h. The reaction was quenched by placing the Schlenk flask in an ice bath and opening it to air. The copper catalyst was removed by eluting the mixture with CH_2Cl_2 through an alumina column. The concentrate was precipitated by triplicate in an excess of methanol. A white/yellow solid was isolated after vacuum drying at 40°C for 16 h.

5.3.3 Bromine end-group substitution of PS-Br (PS- N_3) (A2).

4.5 g (0.18 mmol) of PS-Br, were dissolved in 7.0 mL of DMF by stirring constantly. Subsequently, 0.587 g (9.04 mmol) of NaN_3 were added to the solution. The resulting mixture was stirred for 4 days at room temperature. After completion, the mixture was precipitated in an excess of distilled water. The solid particles were vacuum filtered and thoroughly rinsed with water to eliminate NaN_3 moieties. White pellets were isolated after freeze-drying for 16 h.

5.4 Synthesis of poly (styrene-*block*-lactic acid), PS_n-*b*-PLA_m, copolymers.5.4.1 Route 1 – Click coupling PS-N₃ and PLA-Ac end groups

Scheme 5.3 summarizes the synthesis of PS-*b*-PLA copolymers via Route 1.



Scheme 5.3 Route 1 synthesis to obtain PS-*b*-PLA (C1) copolymers.

5.4.2 Polymerization of *D,L*-lactide via ROP (PLA-Ac) (B1/B2).

1.0 g (6.95 mmol) of LA and 10.1 mg (6.95 mmol) of the initiator 2-methyl-3-butyn-2-ol (MBY) or 4-ethynyl benzoic acid (EBAc) were weighed in a 0.5 – 2.0 ml *Biotage* vial. A minimum amount of toluene was added to the vial and was later freeze-dried overnight to remove water moieties. In a separate vial, 28.1 mg (6.95 mmol) of Sn(EH)₂ were dissolved in 2.0 mL of anhydrous toluene. The solution was degassed by displacing the air with nitrogen stream for 20 min. After degassing, solution was added to the first vial and the mixture was sealed under nitrogen. Reaction was let to occur in a *Biotage* Microwave reactor by placing the vial under the following parameters: $t = 30 - 90$ min, $T = 120^{\circ}\text{C}$, 600 rpm and 'Normal' absorption set-up. The reaction was quenched by placing the open vial inside an ice bath. The product was re-dissolved in a minimum amount of CH₂Cl₂ and precipitated in an excess of cold methanol. A second precipitation was performed using a mixture

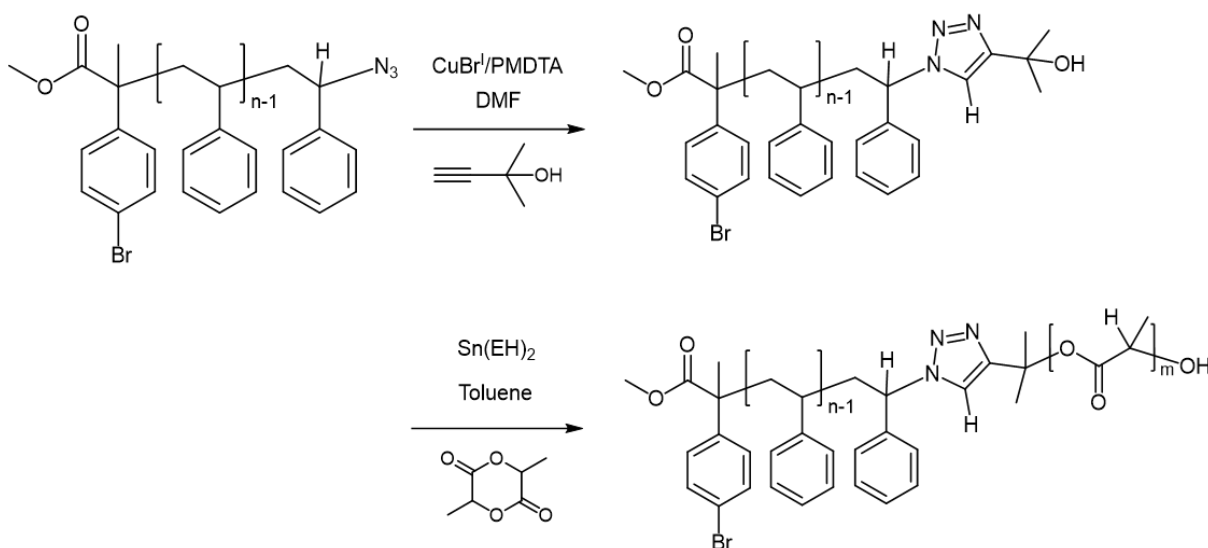
of hexane/ethanol, 8:2. A white powder was isolated after vacuum drying at 40°C overnight.

5.4.3 Synthesis of PS_n-*b*-PLA_m copolymers (Copper catalyzed azide-alkyne cycloaddition, CuAAC) (C1).

2.0 mg (0.0138 mmol) of CuBr^I, 234.0 mg (0.0138 mmol) of PS-N₃ and 287.0 mg (0.0277 mmol) of PLA-Ac were weighed in a round bottom flask and immediately connected to a stream of nitrogen. 5 – 7 ml of DMF were added under stirring until the complete dissolution of both homopolymers. Upon dissolution, 3.0 μL (0.0138 mmol) of PMDETA were added using a degassed micropipette and the system was closed under an inert atmosphere. The mixture was stirred at room temperature for 24 h. Cu^I/PMDETA catalyst was removed using a short column of alumina with CH₂Cl₂ as eluent. The final product was isolated by precipitation in an excess volume of the mixture hexane: ethanol; methanol 6:3:1. A slightly yellow/green-like powder was isolated after vacuum drying overnight at 40°C.

5.4.4 Route 2 – Block copolymer synthesis by ROP of PS-OH macroinitiator.

Scheme 5.4 summarizes the synthesis of PS-*b*-PLA copolymers via Route 1.



Scheme 5.4 Route 2 synthetic pathway to obtain PS-*b*-PLA (C2) copolymers

5.4.5 End-group click reaction of PS-N₃ (PS-OH) (A3).

0.0025 g (0.030 mmol) of CuBr, 0.150 g (0.010 mmol) of PS-N₃, 25.0 μ L (0.030 mmol) of MBY and 2 – 5 mL of DMF were added to a round bottom flask and let to stir at room temperature until full dissolution of the polymer. The mixture was immediately connected to a stream of nitrogen and remained in an inert atmosphere throughout the reaction. Afterwards, 22.3 μ L (0.11 mmol) of PMDETA diluted in 2 mL of DMF were added using a degassed syringe. The resulting solution was degassed after three cycles of freeze-pump-thaw and stirred at room temperature for 16 – 18 h. Cu/PMDETA catalyst was removed using a short column of alumina with CH₂Cl₂ as eluent. The final product was isolated by precipitation in an excess volume of methanol and vacuum drying at 40°C overnight.

5.4.6 Polymerization of *D,L*-lactide via ROP (PLA-Ac) (C2).

0.150 g (0.007 mmol) of PS-OH and 0.100 g (0.070 mmol) of LA were weighed into a 0.5 – 2.0 ml *Biotage* vial. A minimum amount of toluene was added to the vial and was later freeze-dried overnight to remove water moieties. In a separate vial, 0.048 g (1.20 mmol) of Sn(EH)₂ were dissolved in 2.5 mL of anhydrous toluene. The solution was degassed by displacing the air with nitrogen stream for 20 min. After degassing, solution was added to the first vial and the mixture was sealed under nitrogen. Reaction was let to occur in a *Biotage* Microwave reactor by placing the vial under the following parameters: $t = 30 - 90$ min, $T = 120^{\circ}\text{C}$, 600 rpm and 'Normal' absorption set-up. The reaction was quenched by placing the open vial inside an ice bath. The product was re-dissolved in a minimum amount of CH₂Cl₂ and precipitated in an excess of mixture hexane: ethanol (8:2) by triplicate. A white powder was isolated after vacuum drying at 40°C overnight.

5.5 Preparation of PS-*b*-PLA based thin films.

5.5.1 Substrate preparation

Silicon wafers were used as substrates to prepare the copolymer-based thin films. In the indicated experiments, the surface of the silicon wafers was pretreated by a silylation procedure to avoid delamination of the film. The native layer of the silicon substrates was etched by dipping pieces of wafers ($\sim 10 \text{ mm}^2$) into a piranha solution ($\text{H}_2\text{O}_2:\text{H}_2\text{SO}_4$, 1:3, v/v) at 100°C for 60 min. Afterwards, the pieces were extensively rinsed with water and ultrasonicated in an acetone:methanol (1:1, v/v) mixture. After drying under a nitrogen stream, the substrates were dipped in an HMDS:toluene (1:5, v/v) solution overnight. Finally, the substrates were rinsed with toluene and dried in an oven at 80°C prior to use.⁹¹ Substrates not treated with silylation, were simply rinsed with CH_2Cl_2 and ethanol and further cleaned in a plasma oven for 2 min ($160 \text{ cm}^3 \text{ min}^{-1}$ of argon flow rate).

5.5.2 Annealing experiments

A 2.0% w/v PS-*b*-PLA copolymer solution was prepared in THF at room temperature. The copolymer was stirred in the solvent until full dissolution. Once dissolved, the solution was filtered using a $0.2 \mu\text{m}$ polytetrafluoroethylene (PTFE) membrane to diminish the presence of contaminants. Then, $50.0 \mu\text{L}$ of the solution were spin coated onto a silicon wafer. Each substrate was spin coated for 60 s at 2000 RPM and air dried prior annealing.⁹²

For the Solvent Vapor Annealing (SVA) experiments, as-spun substrates were placed inside a closed glass chamber next to an open vial filled with *o*-xylene ($\sim 5.0 \text{ mL}$). On the basis that *o*-xylene and toluene have similar polarity, and added to the affinity between PS and toluene, *o*-xylene was chosen as a selective solvent to promote microphase segregation of the PS domains.⁹³ SVA was performed at

different times. After annealing, the surface was exposed to open air and allowed any remaining solvent to evaporate for a couple of minutes inside a fume hood.

In the case of Thermal Annealing (TA) experiments, as-spun substrates were placed inside an oven at 120 or 150°C for 10 min. Finally, the substrates were carefully removed and cooled to room temperature.⁹⁴

5.5.3 Hydrolysis experiments

To selectively remove the PLA domains of the films, the annealed and/or as-spun substrates were dipped into an alkaline solution (NaOH 0.5 M, H₂O:CH₃OH, 6:4) at different times: 5, 15, 30 and 60 min. Afterwards, each substrate was carefully extracted from the solution and rinsed with an excess of water. The substrates were dried under vacuum overnight prior to SEM analysis.

5.6 Preparation of PS-*b*-PLA based monoliths.

5.6.1 Method 1

A determined amount of a PS_n-*b*-PLA_m copolymer was dissolved in toluene to yield a final concentration of 10.0 wt. %. The copolymer was solubilized for several hours under continuous stirring at room temperature. Afterwards, the solution was filtered with a 0.2 μm Nylon membrane into a new vial to remove any contaminants. When the solution was too viscous, the filtration step was not carried out. Thereafter, the solution was poured into an as-made Teflon mold and let the solvent evaporate for several days in a fume hood. To completely eliminate the solvent, the films were dried in a vacuum oven for 2 h at 40°C. To promote orientation of the domains on the pre-formed film, an annealing procedure was performed by placing the sample in an oven at 160°C for 1h. Finally, sample was cooled down to room temperature and analyzed via SEM.⁹⁵

5.6.2 Method 2

200 – 350 mg of a PS_n - b - PLA_m copolymer were placed inside a PEEK (polyether ether ketone) circular mold ($D = 1.5$ cm). The mold was coated with a thin foil of FEP (fluorinated ethylene propylene) to avoid the copolymer from sticking to the mold and facilitate the collection of the resulting sample. The powder was evenly distributed inside the mold and then, the mold was placed inside an oven at 160 °C. After 1h, the mold was capped with a stainless-steel press of the same diameter of the mold to properly seal it. The mold was carefully placed back inside an oven at 160 °C for 1h. Finally, the sample was allowed to cool down to room temperature and removed from the mold.

5.6.3 PLA hydrolysis of monoliths

A fraction of the prepared film was carefully cut into small pieces ($\sim 2 - 4$ mm), several of these pieces were needed to take samples during the hydrolysis. Then, these pieces were immersed in a large volume of an alkaline solution: NaOH 0.5 M (3:2, H_2O : CH_3OH). The mixture was placed inside an oil bath at 60 °C. The hydrolysis was let to occur for several days, and samples were taken at different times. To monitor the hydrolysis, a sample was taken from the media and extensively rinsed with water and methanol. After briefly drying in the oven the sample was analyzed with 1H NMR and the change in the integral value of PLA repetitive unit was observed (Fig. S5). The final product was freeze-dried prior to SEM characterization.

5.7 Metal uptake experiments

A 1.0 wt. % $CuCl_2$ solution was prepared in a mixture of ethanol:water (1:1, v/v). The hydrolyzed substrates were immersed in 10.0 mL of the prepared solution overnight. Afterwards, substrates were removed from the solution and thoroughly rinsed with water and methanol. Finally, samples were freeze-dried prior to SEM analysis.

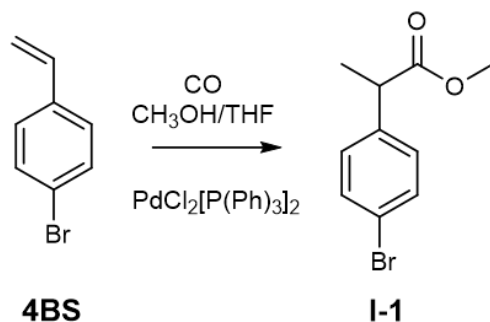
6 Results and discussion

Part A – Synthetic pathway towards the obtention of triazole-embedded PS-*b*-PLA copolymers.

Part A reviews the synthetic pathway towards the obtention of triazole functionalized PS_n-*b*-PLA_m copolymers. The synthesis of such compounds considered three stages: I. Synthesis of a benzylic ATRP Initiator, II. Synthesis of PS and PLA homopolymers with azide and alkyne end-groups, and III. Synthesis of the BCPs via CuAAC click reaction. This section covers the results for all three synthetic stages and discusses the products obtained at each step.

6.1 Synthesis of ATRP active benzylic initiator

The first step toward the obtention of mesoporous materials consisted in the synthesis of an initiator that is active following a classic ATRP mechanism. Initially, the proposal considered the synthesis of a bifunctional initiator capable of polymerizing two monomers of different chemical nature. Specifically, the targeted initiator was the 2-hydroxyethyl-2-bromo-2-(4-bromophenyl) propanoate (HEBBP). At first, the planned scheme towards the obtention of this product considered a three-step synthesis: 1) Carboxymethylation of a styrene adduct, 2) Bromination of the benzylic carbon, and 3) Transesterification of the methoxy group. Scheme 6.1 shows the first step in the synthetic route towards the obtention of HEBBP, following sections address steps 2 and 3.



Scheme 6.1 Carboxymethylation of 4BS.

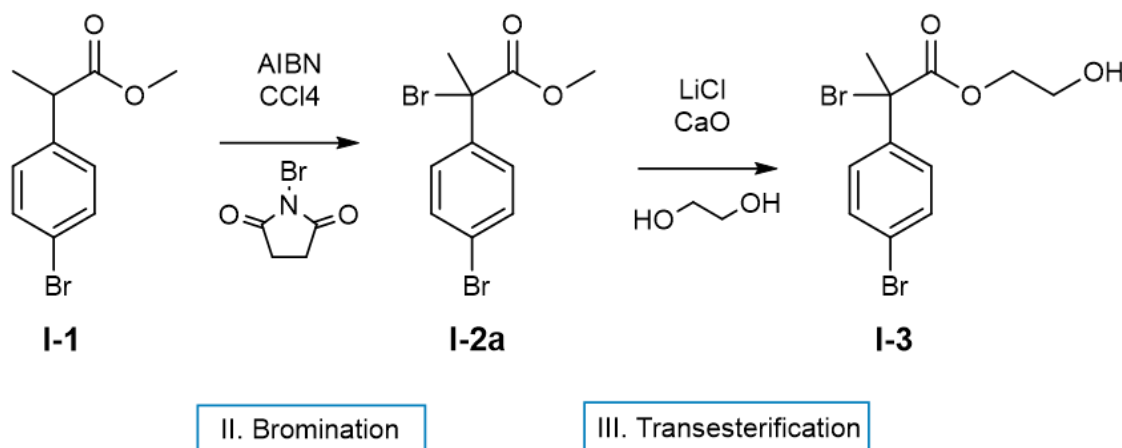
Carboxymethylation (step 1) of 4-bromostyrene was carried out as described in the experimental section. This reaction enabled the formation of a methoxy group in the less saturated vinyl position. During this reaction, the carbon monoxide pressure was adjusted accordingly to maintain a value of 600 – 650 psi. After the reaction was completed, the resulting solution was extracted and further purified by a chromatographic column.

As a result of the liquid chromatography of the raw product, four fractions were isolated according to the retention factor (RF) presented by thin layer chromatography (TLC) of the tubes collected from the column. All four fractions were concentrated using a rotatory evaporator. Fractions 3 and 4 were isolated as a viscous orange-yellow liquid after the solvent was removed. From the ¹H NMR analysis of all fractions, fraction number 3 was the one that contained the desired product MBP (I-1). According to the ¹H spectrum of this product it was possible to confirm the presence of the methoxy group, –OCH₃ at a chemical shift δ = 3.58 ppm. In addition, a quartet signal corresponding to the methine group, –CH, is located at 3.60 ppm and a doublet signal corresponding to the adjacent methyl group –CH₃, is at 1.40 ppm (See Figure 6.1 for more details). A subsequent gas chromatography–mass spectrometry (GC-MS) analysis allowed to determine the charge/mass ratio value of $M^{+} = 242.1$ m/z as well as the isotopic ion with a value of 244.0 m/z (M^{+2}), which confirmed the presence of the aimed product.

The following step in the planned scheme consisted of bromination and transesterification of product **I-1**, as mentioned above. For this purpose, two different approaches were conducted to obtain HEBBP product. The results obtained from this route are discussed in the following sections.

6.1.1 Approach 1: Bromination then transesterification

The first approach considered the bromination of the benzylic carbon of compound MBP (**I-1**) followed by a transesterification of the methoxy group to obtain HEBBP (**I-3**) as shown in Scheme 6.2. In order to add a bromine atom at the benzylic position, bromination of compound **I-1** was carried using NBS under the stated conditions, to add a bromine atom to the benzylic position. As a result, the carbon adjacent to the carbonyl gained a bromine atom yielding product **I-2a**. The solution was purified by chromatographic column in a procedure similar to that described for product **I-1**. The substitution of the proton for the bromine atom was confirmed by observing the chemical shift by ^1H NMR. The methine resonance (quartet) of **I-1**, located at $\delta = 3.60$ ppm is no longer visible on the ^1H spectrum of product **I-2a**.



Scheme 6.2 Approach 1: bromination then transesterification of **I-1**.

Furthermore, the signal of the methyl group shifted from 1.40 to 2.30 ppm due to the vicinity of the bromine. These changes are evidenced in Figure 6.1 where a comparative of both spectra is shown. ^1H NMR of **I-1** displays the chemical shift and the multiplicity of the $-\text{CH}_3$ signal that changed from doublet to singlet after the bromination (product **I-2a**).

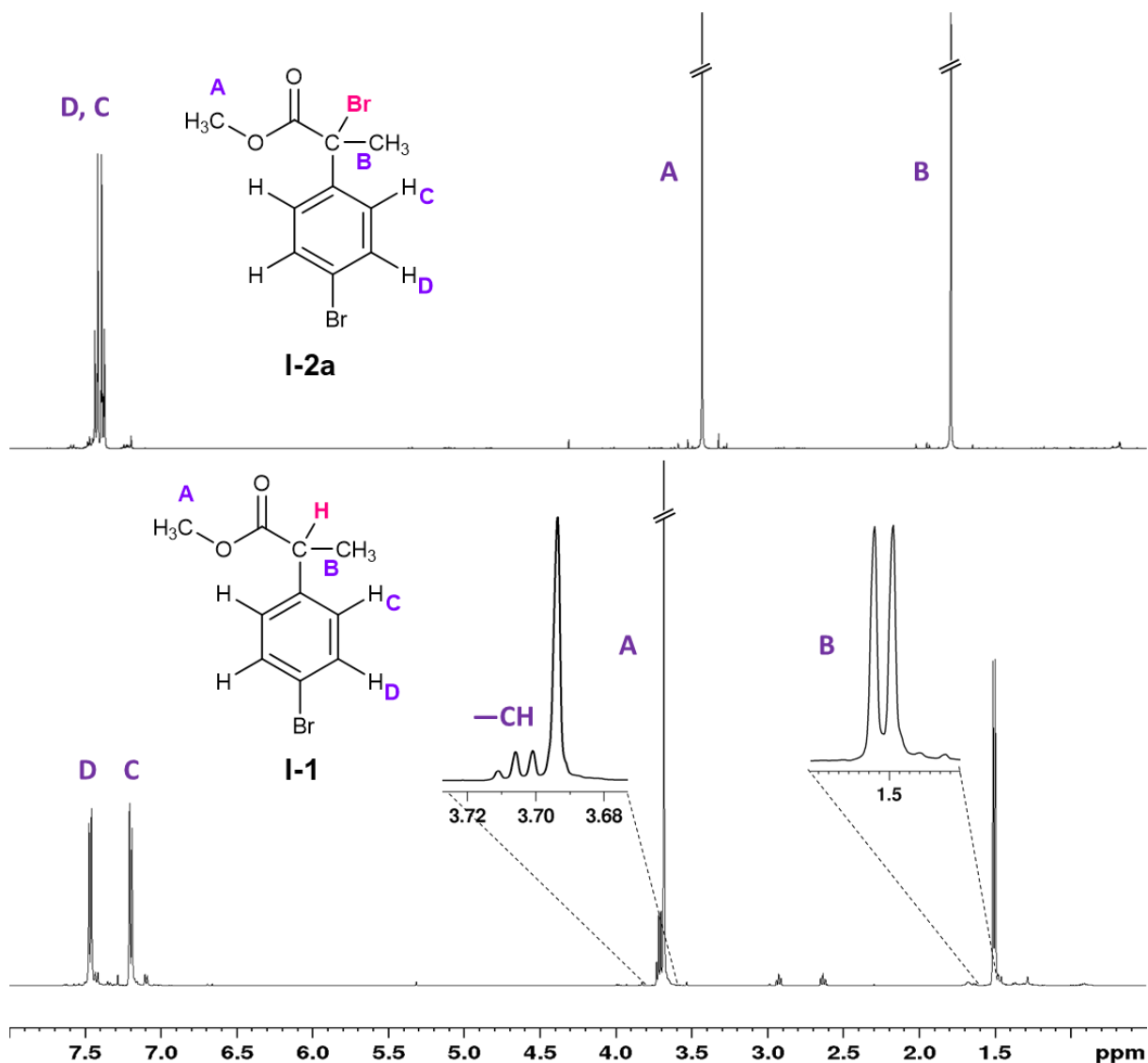


Figure 6.1 Comparative ^1H NMR spectra of **I-1** and **I-2a**. (600 MHz, CDCl_3 , R.T.)

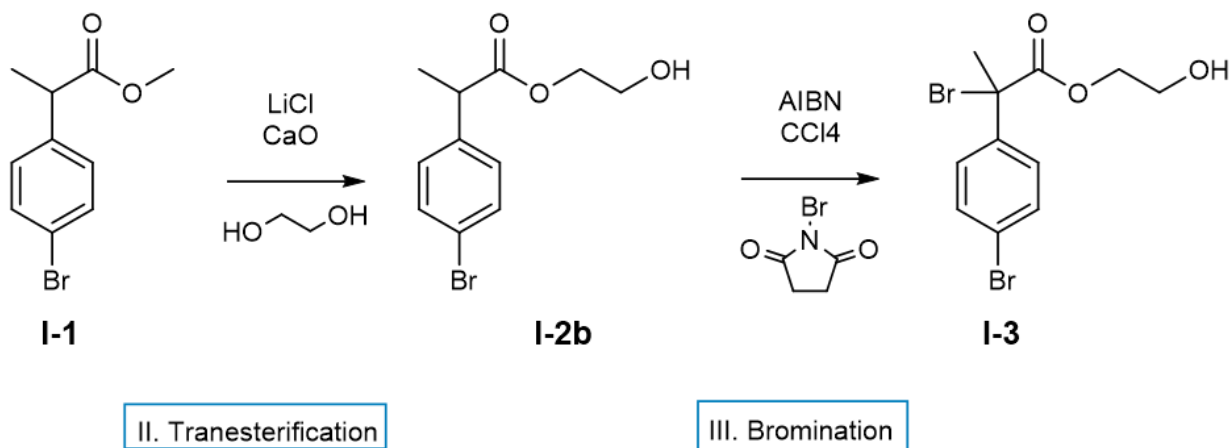
An additional ^{13}C NMR experiment allowed to determine the chemical shift for the $-\text{CH}$ group of **I-1** at $\delta = 44.9$ ppm and compared to the quaternary carbon $-\text{CBr}$ at $\delta = 60.5$ ppm for product **I-2a**. Supplementary 2D-NMR characterization of **I-2a** product can be found in the Appendix (Figure 9.1). To further prove the formation of this molecule, a GC-MS experiment was carried out. As a result, the molecular ion $M^+ = 320.1$ m/z and the isotopic ions with a value of 322.1 (M^{+2}) and 324.0 (M^{+4}) were observed in the spectrometry pattern. It was concluded that the data obtained coincide with the theoretical molar mass of **I-2a**.

Afterwards, the transesterification reaction was performed utilizing the purified **I-2a** product. The instructions were followed as indicated in the experimental section; however, the aimed product, **I-3**, could not be isolated under these conditions. At this last step, a substitution of the methoxy group for the hydroxy ethyl group was targeted and, according to the ^1H NMR spectrum analyzed, the signal pattern does not exhibit formation of the hydroxyethyl group. In addition, the adduct signals (**I-2a**) could not be clearly defined in the afore-mentioned spectrum. It is worth noting that in two frequencies ranges from 8.0 to 7.3 ppm and from 4.7 to 3.2 ppm a cluster of undefined and overlapped signals was visible, which may indicate that the starting materials could be degrading at some point during the reaction.

In summary, the obtention of compound **I-3** was attempted by performing a bromination and a subsequent transesterification of product **I-1**, however, this approach did not allow for the obtention of the bifunctional initiator under the described conditions. A possible explanation to this result could be attributed to the bromine group, acting as a good nucleofuge, in other words it is a good leaving group, and a weaker base than the methoxy group, this fact may hinder the substitution of the hydroxyethyl group.⁹⁶ Considering these results, a second approach was attempted to obtain the bifunctionality on the desired product.

6.1.2 Approach 2: Transesterification then bromination

The second approach considered the transesterification of the methoxy group of **I-1**, and then the bromination of the α -carbon. The synthesis to obtain HEBBP (**I-3**) is summarized in Scheme 6.3.



Scheme 6.3 Approach 2: transesterification then bromination of **I-1**.

For the transesterification reaction, an excess of ethylene glycol was added to promote formation of hydroxyethyl group that would substitute the methoxy. The transesterification reaction followed as expected, and the aimed product 2-hydroxyethyl-2-(4-bromophenyl propanoate), HEBP (**I-2b**) was isolated after purifying. In Figure 6.2 the ¹H NMR spectrum of **I-2b** is shown, in this case the signals that belong to the newly added hydroxy group were located at 4.11 and 3.66 ppm for the nuclei –CH₂OH and –COOCH₂, respectively.

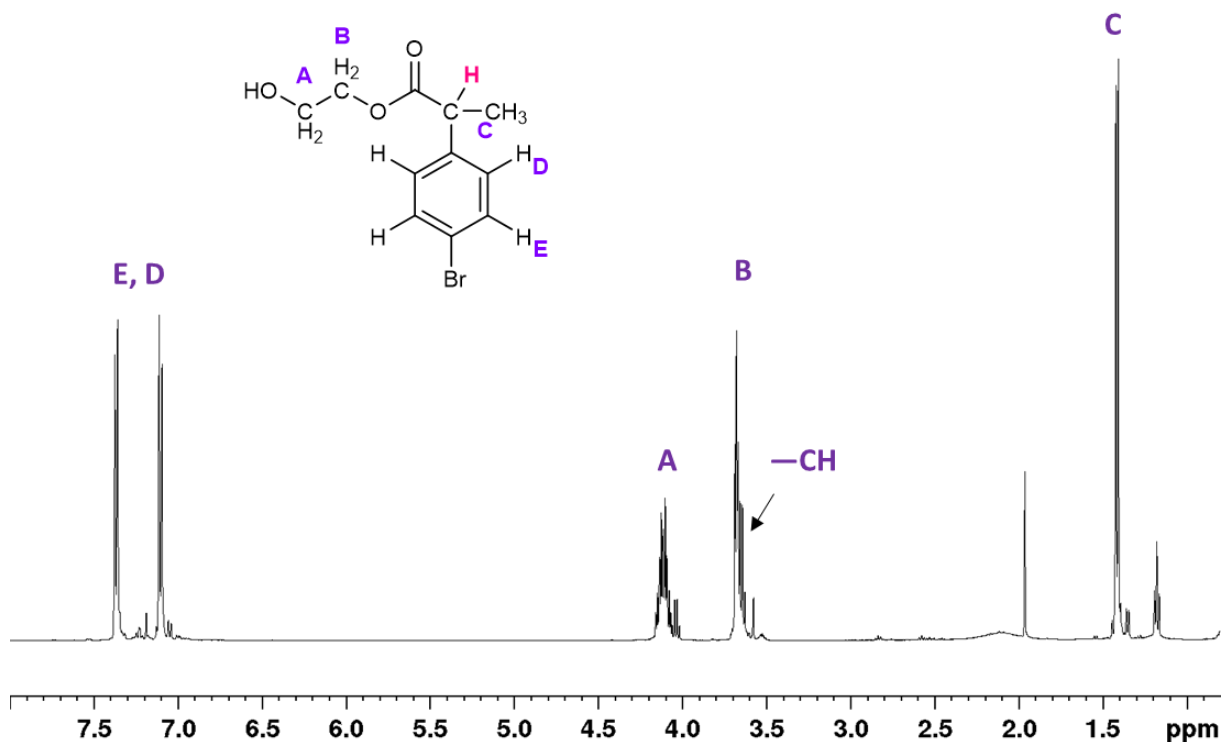


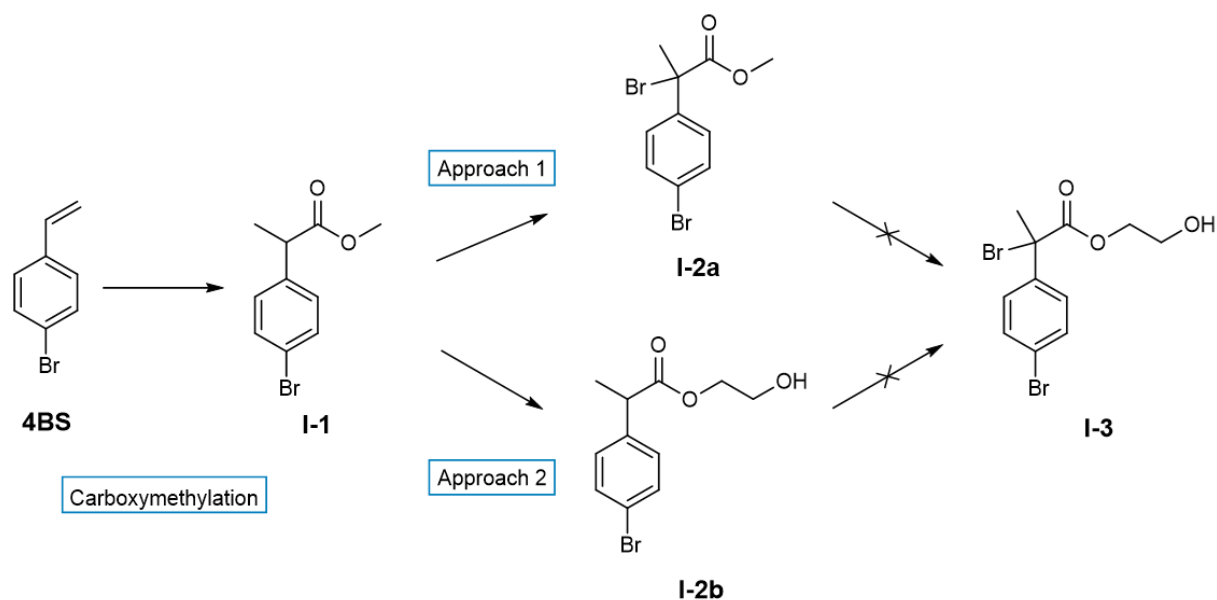
Figure 6.2 ^1H NMR spectrum of I-2b (600 MHz, CDCl_3 , R.T.)

The next step was the bromination of **I-2b** following the reaction conditions described in Section 5.2.4. The isolated product was analyzed by ^1H NMR as well, however, in this case, the product did not exhibit the expected signal pattern for **I-3**. At this point, it was hypothesized that the ethyl hydroxy group may be interfering with the radical formation during the initiation step of the bromination. In such case, the formation of an unwanted or a more stable intermediate would not allow the abstraction of the proton from the benzylic position and in consequence the addition of the α -bromine would not be possible. This hypothetical scenario might explain why it was not possible to isolate product **I-3** at the working conditions.

According to the results of both approaches it was proposed to employ **I-2a** product as an ATRP initiator in the preparation of the PS macroinitiator due to the reactivity that the aliphatic bromine group has in this type of mechanism. The benzylic position containing the bromine, would be stable enough to form a radical in this quaternary carbon. Therefore, a synthesized polymer using this **I-2a** initiator

would contain the carboxy end group (α -functionality) and the bromine end group at the tail (ω -functionality).

Both chain ends are eligible sites to perform a post-polymerization reaction to transform either of these functionalities. A chain-end post polymerization could enable to transform methoxy or bromine group to synthesize the second PLA block and also to introduce a triazolyl group on the polymer chain. Scheme 6.4 summarizes the synthetic routes including both approaches to the synthesis of **I-3**.



Scheme 6.4 Summary of approach 1 and 2 to obtain I-3 initiator.

In light of these results, **I-2a** was employed as an ATRP initiator to synthesize a PS macroinitiator (PS–Br). Then, the end bromide group was transformed into an end-azide PS (PS–N₃), this reactive group was the site to form a triazole group on the polymer chain as discussed in following sections.

It should be noted that the synthetic route of the initiator initially considered the addition of a thiol-imidazole functionality through the aromatic bromine by performing a Heck reaction followed by a click reaction of thiol-ene using the *para* position of product **I-3**. However, due to the difficulties that arouse during the afore-

mentioned synthetic steps the initiator structure was reconsidered to ensure a more feasible route and still include a click-based functionality (triazoles).

Then, it is worth to note that the chemical structure of **I-2a** contains two bromine atoms, where the aromatic bromine was intended for the previously mentioned purpose. However, each one of them is surrounded by a different chemical setting, which provides them with different properties. Among those properties, the redox potential of the benzylic bromide will enable the adjacent carbon to accept electrons more easily in the presence of a Cu^I/L complex (ATRP mechanism). In contrast, the redox potential of the aromatic bromide would not allow to generate a carbon radical at this position,⁹⁷ meaning that the aromatic bromine is inert during the polymerization process. In this fashion, the benzylic radical will promote the initiation step of the polymerization, and the growing radical will consume the monomer regulated by the Cu^I/L complex.

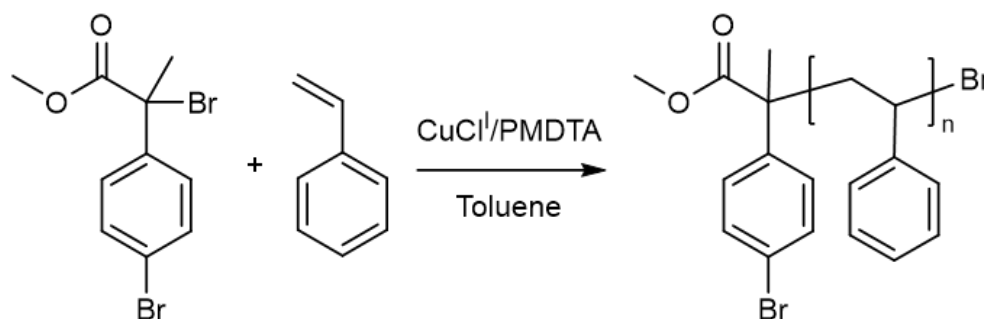
It is also worth to mention that, to the best of our knowledge, there are no reports that use compound I-2a as an initiator in an ATRP-based mechanism to date. However, benzylic compounds with a similar chemical structure have been employed as initiators in Cu-mediated polymerizations.^{67,98}

6.2 Preparation of PS–N₃ macroinitiator.

ATRP is a polymerization technique that requires an alkyl halide initiator to begin the monomer addition in a polymerization reaction, in this case the brominated initiator **I-2a** was used. Hence, this section addresses the experiments that were conducted by following the classic ATRP and ARGET – ATRP mechanism, using **I-2a** as initiator to synthesize a PS macroinitiator. Furthermore, a subsequent functionalization reaction was performed to substitute the bromine end group of the PS adduct with an azide termination.

6.2.1 Preparation of the PS–Br precursor via ATRP.

Initially, a few experiments were set up to prove the efficiency of **I-2a** following a classic ATRP mechanism as shown in Scheme 6.5.



Scheme 6.5 Synthesis of PS-Br via ATRP with **I-2a**.

Table 6.1 summarizes the first polymerization experiments with **I-2a**. As a result of the **A1-1** experiment, it was not possible to isolate the polymer as there was no precipitation of the polymer after the completion of the reaction. It was hypothesized then, that the reaction time may have been insufficient, hence, the reaction time was increased in the following experiment. In this case, the consistency

of the solution was visually monitored considering that an increase in the viscosity of the solution could indicate that polymer formation is occurring.

Table 6.1 ATRP experiments with benzylic initiator I-2a.

ID	Monomer	Cu/L	T (°C)	Time (h)	Conversion (%) ^a	M_n Theo (Kg·mol ⁻¹)	M_n Exp (Kg·mol ⁻¹) ^b	\mathcal{D} ^b
A1-1	styrene	CuCl/ PMDETA	90	20	-	10.7	-	-
A1-2	styrene	CuCl/ PMDETA	100	116	67.0	14.0	19.4	1.20
A1-3	methyl- metacrylate	CuCl/ PMDETA	100	72	80.0	10.7	80.0	1.22
A1-4	styrene	CuBr/ Me ₆ TREN	100	24	31.0	10.7	47.8	1.70

^a Monomer conversion estimated by gravimetry.

^b SEC (THF eluent, PS standard calibration).

After reaction **A1-2** was completed, PS-Br could be isolated under the specified conditions with an estimated molar mass (M_n) and dispersity (\mathcal{D}) within the expected range for a controlled polymerization according to the Size Exclusion Chromatography (SEC) characterization. However, the polymerization occurred at a slower rate than expected, resulting in a final reaction time of 116 hours, which is significantly larger than the reported for a conventional ATRP process.⁹⁹

It is also known that benzylic initiators have higher activation rate constants (k_{act}) than aliphatic initiators in ATRP,¹⁰⁰ then it was hypothesized that this variable could explain the prolonged reaction times. In addition, the fact that styrene also requires a higher activation energy than other vinyl monomers (*i.e.*, methyl methacrylate) might explain the reaction time needed in these polymerizations.

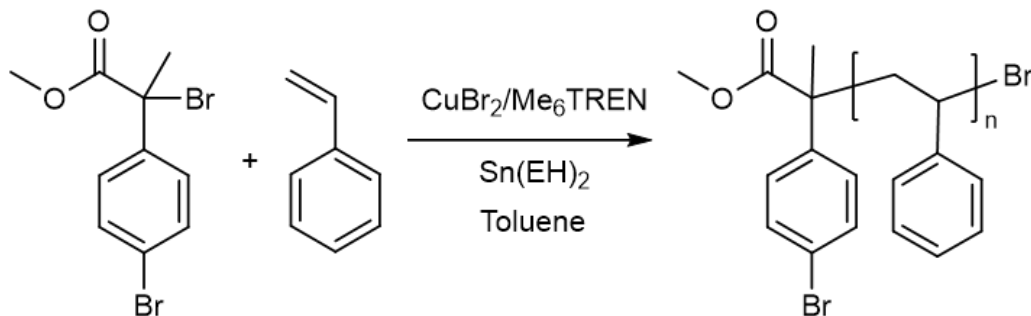
To further prove the initiator activity of **I-2a**, methyl methacrylate (MMA) monomer was used instead of styrene, hypothesizing that this would reduce the reaction time while still being able to polymerize. As a result from **A1-3** reaction, a polymer was isolated following the experimental conditions applied to the styrene polymerization (Section 5.3.1). According to the \bar{D} value of the isolated polymer it appears to have been prepared in a controlled environment even when the calculated M_n by SEC was greater than the expected. In this experiment, the reaction time was less than with PS, but it remained somewhat extended, which might explain the increase in the M_n value. In experiment **A1-4**, a different catalytic system was employed to undergo polymerization, this enabled a controlled polymerization even when the M_n and \bar{D} value increased compared to the previous experiment with styrene monomer.

It is noteworthy that during the preparation of the reaction mixture, right after the addition of the initiator, **I-2a**, there was a slight change in the coloration of the solution. Both CuCl/PMDETA and CuBr/Me₆TREN complexes formed in the first step are green colored, as it is commonly observed for Cu/L complexes. Nonetheless, when adding **I-2a** the reaction mixture changed from green solution into a slight blue color for experiments **A1-1** – **A1-4**. This finding suggested that an oxidative change was occurring on the Cu/L complex, in consequence, if a certain amount of the Cu-catalyst shifted to its highest oxidation state then it may be deactivating prior to the beginning of the reaction. If this were the case, it could be a possible explanation to why there was no polymer formation on the first experiments and the prolonged reaction times on the subsequent experiments.

These results suggested that another approach was necessary to obtain a PS precursor to further synthesize the aimed copolymers. Thus, new experiments were proposed based on the ARGET-ATRP method.

6.2.2 Preparation of the PS–Br precursor via ARGET – ATRP.

In light of previous results, a new ATRP-based technique was considered: Activators Regenerated by Electron Transfer (ARGET). In this process, a Cu-complex is also employed as a catalyst similar to the classic mechanism. However, by following this mechanism the initial oxidation state of the copper salt is higher, Cu^{II} , which is subsequently reduced to Cu^{I} by a reducing agent, in this case $\text{Sn}(\text{EH})_2$. In addition, a new complex was employed by using the Me_6TREN ligand with a lower redox potential than PMDETA.⁹⁷ Scheme 6.6 displays the reaction to obtain a PS-Br precursor via ARGET, following the indicated molar ratio of $[\text{MBBP}]:[\text{styrene}]:[\text{Cu}^{\text{II}}\text{Me}_6\text{TREN}]:[\text{Sn}(\text{EH})_2]:[1]:[150]:[0.2]:[0.5]$.



Scheme 6.6 Synthesis of PS-Br via ARGET – ATRP with I-2a.

Following this method, a series of PS-Br adducts were obtained. Table 6.2 summarizes the obtained data of the ARGET ATRP experiments. M_n was targeted at values of 5 – 40 $\text{Kg}\cdot\text{mol}^{-1}$ and it was estimated by SEC. Initially, a lower M_n value was considered to seek optimal reaction conditions. As a consequence, it was determined that the catalytic system $\text{CuBr}_2/\text{Me}_6\text{TREN}$ adequately controlled the radical formation. This could be confirmed by the dispersity value estimated by SEC resulting in a range of 1.08 – 1.28 (Table 6.2).

Table 6.2 Summarized data of PS-Br synthesis via ARGET – ATRP.

ID	Time (h)	Conversion (%) ^a	F _{Br} (%) ^b	$M_{n\ Theo}$ (Kg·mol ⁻¹)	$M_{n\ Exp}$ (Kg·mol ⁻¹) ^c	\bar{D} ^c
A1-5	36	31.0	98	10.7	5.8	1.28
A1-6	24	59.0	96	10.7	19.6	1.10
A1-7	48	48.0	93	30.4	25.0	1.25
A1-8	68	86.0	83	21.1	31.8	1.19
A1-9	72	70.0	84	28.2	39.4	1.08
A1-10	68	86.0	96	21.1	42.4	1.14
A1-11	48	50.0	93	21.0	19.5	1.20
A1-12	48	45.0	86	21.1	19.9	1.27
A1-13	30	54.0	88	10.0	11.5	1.15
A1-14	54	58.0	90	30.0	31.8	1.18
A1-15	30	48.0	92	15.4	16.3	1.11

^a Monomer conversion estimated by gravimetry.

^b Bromine end functionalization estimated by ¹H NMR (CDCl₃, R.T., 300 MHz)

^c SEC (CHCl₃/LiCl/TEA) RID.

The products **A1-5** – **A1-15** were also analyzed by ¹H NMR, from their spectra it is worth to highlight the presence of the following signals: at $\delta = 7.5 - 6.2$ ppm an aromatic repetitive unit of PS, and at 4.3 ppm a broad signal corresponding to –CHBr end group. The terminal group assignment is consistent with the reported for analogue systems.¹⁰¹ An example of the studied ¹H NMR spectrum is shown in Figure 6.3 where the corresponding signals of the synthesized PS–Br are assigned.

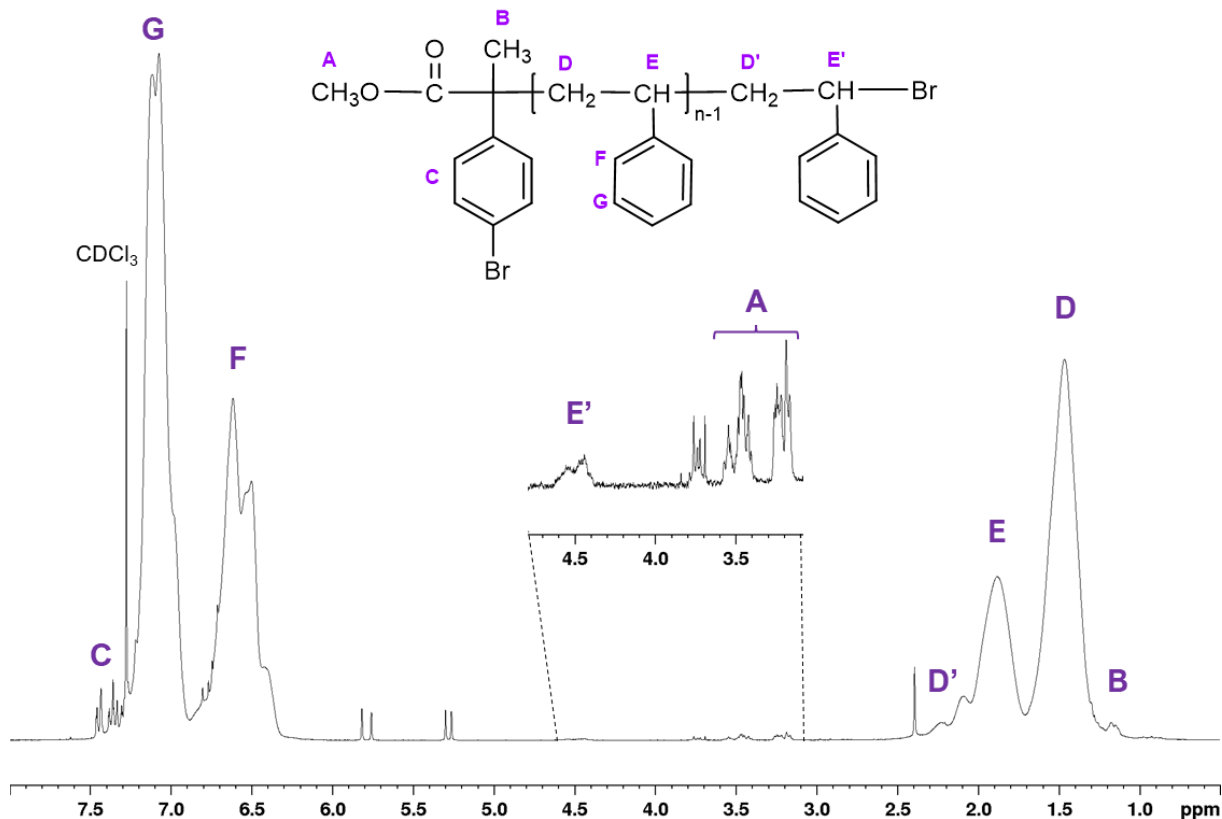


Figure 6.3 ^1H NMR spectrum of product A1-15 (300 MHz, CDCl_3 , R.T.)

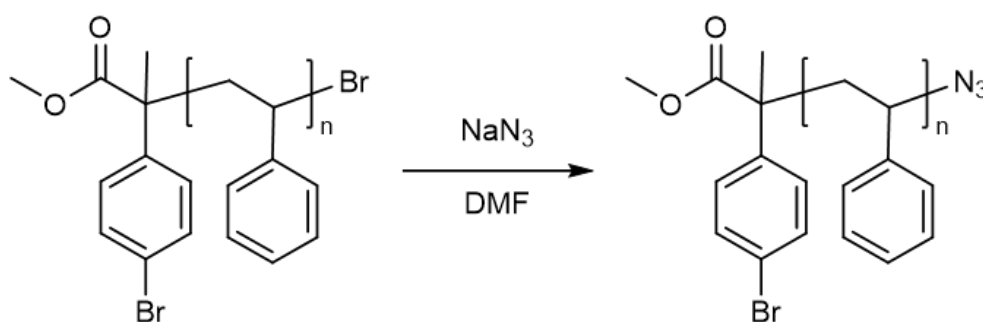
In contrast with the PS–Br adducts obtained by classic ATRP reactions, with ARGET polymerization the correlation between reaction time and conversion improved. For example, product **A1-6** reached a 60% conversion in 24 hours, whereas polymers with a larger M_n , such as **A1-9** a 70% conversion was reached after 72 h while keeping a narrow dispersity for both cases (Table 6.2).

It was possible to synthesize PS–Br homopolymers via ARGET ATRP using the catalyst $\text{CuBr}^{\text{II}}/\text{Me}_6\text{TREN}$ and the previously synthesized initiator **I-2a**, these conditions enabled polymerization of precursors **A1-5** – **A1-15** unlike the experimental conditions with ATRP in experiments **A1-1** – **A1-4**. This effect might be due to the presence of $\text{Sn}(\text{EH})_2$ as a reducing agent in the reaction; this reactant was able to control the reduction of the catalyst from Cu^{II} to Cu^{I} .

It was theorized that an oxidation of the Cu-catalyst occurred after the initiator addition for experiments A1-1 – A1-4 (classic ATRP); by comparing with A1-5 – A1-15 experiments (ARGET) the presence of the reducing agent may inhibit this oxidation.

6.2.3 End bromine group substitution of polystyrene (PS–N₃ synthesis)

As stated before, the end bromine functionalization of the synthesized PS was further substituted with an azide termination, this end reactive site was used to generate a triazole group as a junction between blocks as described in the following sections of this document. Scheme 6.7 displays the utilized substitution reaction.



Scheme 6.7 Substitution reaction of PS–Br with NaN₃.

A proportional amount of PS–Br was dissolved in DMF until complete dissolution, afterwards, NaN₃ was added to the reaction media, and it was let to react. After reaction completion, the PS–N₃ product was precipitated and freeze-dried prior to characterization by Fourier Transform Infrared spectroscopy (FT-IR). The obtained spectrum (Figure 9.2, Appendix) exhibited a small broad band at 2085 cm⁻¹, which was assigned to correspond to the azide end group. ¹H NMR spectrum of the PS–N₃ was also measured (Figure 6.4), it was determined that the terminal proton of the PS chain, –CHN₃, shifted from 4.5 to 4.05 – 3.84 ppm after the

substitution. This evidence proves that the substitution was successfully completed. Table 6.3 summarizes the ^1H NMR and SEC data obtained from the PS– N_3 adducts.

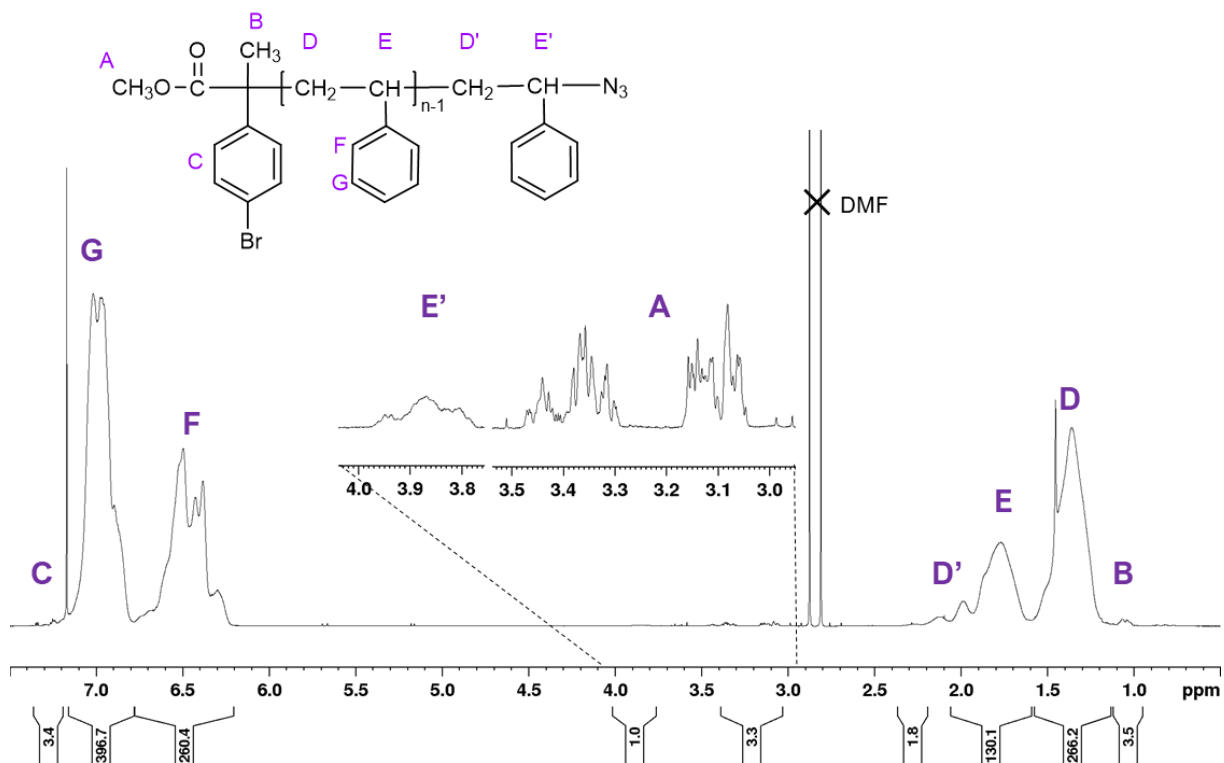


Figure 6.4 ^1H NMR spectrum of product A2-11 (600 MHz, CDCl_3 , R.T.)

Table 6.3 Summarized data of PS-N₃ products.

ID	F _{N₃} (%) ^a	Yield (%) ^b	M _{n Exp} (Kg·mol ⁻¹) ^c	Đ ^c
A2-1	92.0	91.0	5.9	1.28
A2-2	94.0	96.5	20.0	1.28
A2-3	98.0	94.0	21.9	1.17
A2-4	98.0	98.6	25.0	1.20
A2-5	95.0	93.9	25.0	1.27
A2-6	86.0	96.0	38.9	1.12
A2-7	97.0	87.0	19.6	1.18
A2-8	98.0	89.3	18.3	1.16
A2-9	87.0	90.6	11.7	1.14
A2-10	84.0	84.2	32.5	1.19
A2-11	91.0	98.0	17.0	1.11

^a Azide end functionalization estimated by ¹H NMR (CDCl₃, R.T., 300 MHz)

^b Yield estimated by gravimetry.

^c SEC (CHCl₃/LiCl/TEA) RID.

The azide end group functionalization (F_{N₃}) was estimated by comparing the integral values of the signals corresponding to –CHN₃ and –CH₃O terminal groups (**E'** and **A** respectively) shown in Figure 6.4. In theory, the F_{N₃} value indicates a ratio of the α,ω-functionalization in the polymer chain. In order to compare the integral values of the chain end groups, the value per proton was calculated as shown in

Equation 6.1, where the integral value of signal **A** is 3.3 and its corresponding number of protons is 3.

$$\text{value per proton} = \frac{\text{Integral value}}{\text{No. of protons}} = \frac{3.3}{3\text{H}} = 1.1$$

Equation 6.1 Value per proton estimation.

Then, the F_{N_3} ratio was estimated using Equation 6.2 substituting the value obtained from the previous equation. This result indicated a percentage of the functionalized end groups after the azide substitution.

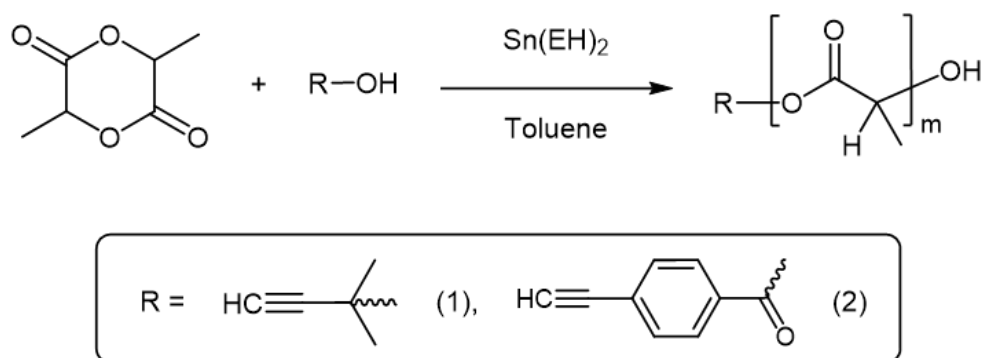
$$\% F_{N_3} = \frac{1H}{\text{value per proton}} \times 100 = 90.9 \%$$

Equation 6.2 Estimation of F_{N_3} end-functionalization.

Overall, the obtained PS–N₃ precursors presented acceptable F_{N_3} values, which indicates that a majority of the bromine end terminations were substituted by azide groups. The isolated products of these reactions were used as precursors in the synthesis of PS-*b*-PLA copolymers with triazole junctions between blocks.

6.3 PLA-Ac synthesis via ROP

As indicated in the experimental section (5.4.2), the PLA-Ac precursor was synthesized and purified prior to its characterization by ^1H NMR and SEC. Following this process, it was possible to obtain a reactive alkyne termination. Scheme 6.8 displays the ROP reaction of the D,L-lactide using two different initiators.



Scheme 6.8 PLA-Ac synthesis via ROP.

As indicated in Scheme 6.8, two different sets of PLA-Ac precursors were synthesized, **B1** corresponds to the aliphatic-alkynyl terminations and **B2** to the aromatic-alkynyl end-groups of PLA homopolymers. Table 6.4 summarizes the obtained data for the synthesized PLA precursors. In general, estimated \bar{D} values are considered within the controlled polymerization scheme. In order to achieve a certain f_{PLA} value in the final PS-*b*-PLA copolymer, various M_n values were targeted. Table 6.4 summarizes some of the most relevant precursors employed in the subsequent coupling step. In addition, SEC traces of **B1-1** and **B2-1** products are displayed in Figure 6.5.

Table 6.4 Summarized data of PLA-Ac products.

ID	Time (min)	Conversion (%) ^a	M_n Theo (Kg·mol ⁻¹)	M_n PLA-Ac (Kg·mol ⁻¹) ^b	\bar{D} ^b
B1-1	35	36.0	9.0	10.4	1.09
B1-2	40	55.0	10.0	16.9	1.16
B1-3	60	73.0	18.0	28.3	1.26
B1-4	30	90.0	27.6	23.3	1.11
B1-5	60	35.0	13.0	14.0	1.23
B1-6	120	64.0	19.6	15.7	1.15
B2-1	60	43.0	5.2	8.8	1.12
B2-2	60	50.0	15.5	16.8	1.16
B2-3	40	24.0	12.5	12.0	1.11
B2-4	30	36.0	9.0	10.4	1.15
B2-5	40	62.0	25.6	22.7	1.22
B2-6	30	34.0	15.0	17.9	1.14
B2-7	80	85.0	30.0	33.8	1.30

^a Monomer conversion estimated by gravimetry.

^b SEC (CHCl₃/LiCl/TEA) RID.

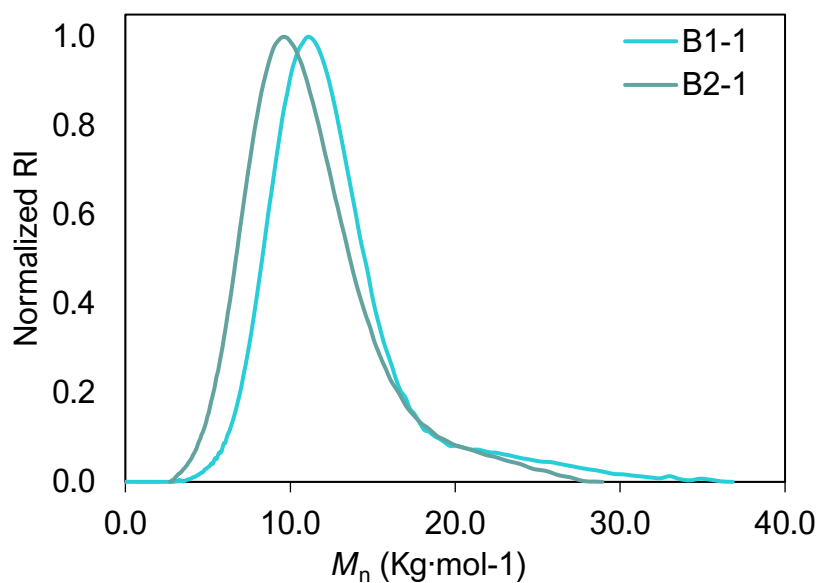


Figure 6.5 SEC traces of B1-1 and B2-1 PLA-Ac precursors.

PLA-Ac precursors were also characterized by ^1H NMR, one example of this is shown in Figure 6.6, where it is worth to highlight the signals corresponding to the PLA repetitive unit, proton **E**, $\delta = 5.30 - 5.07$ ppm, as well as the end-group unit, **E'**, $\delta = 5.05$ ppm. In addition, signal **A**, representative of the acetylenic end group, was assigned at $\delta = 3.77$ ppm, which confirms that the alkyne group is available to react in the next copolymerization step.

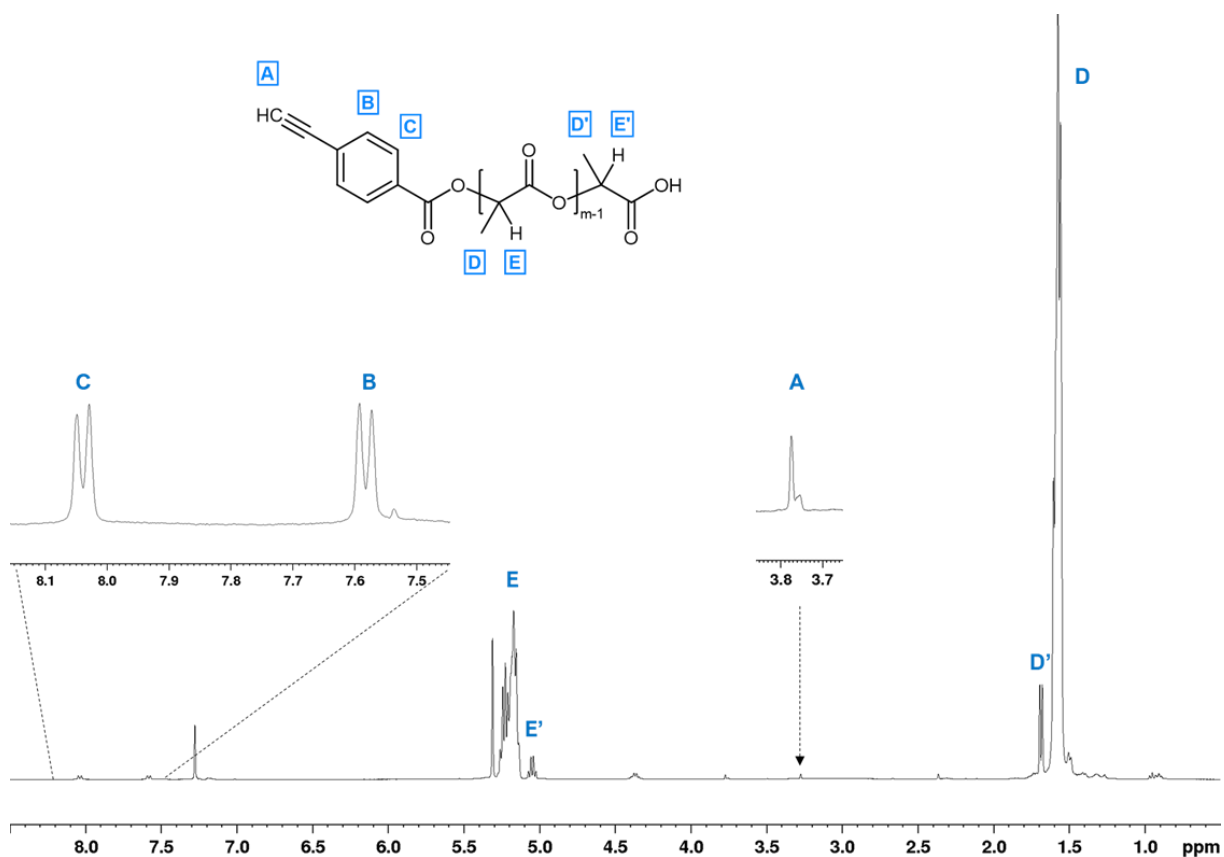
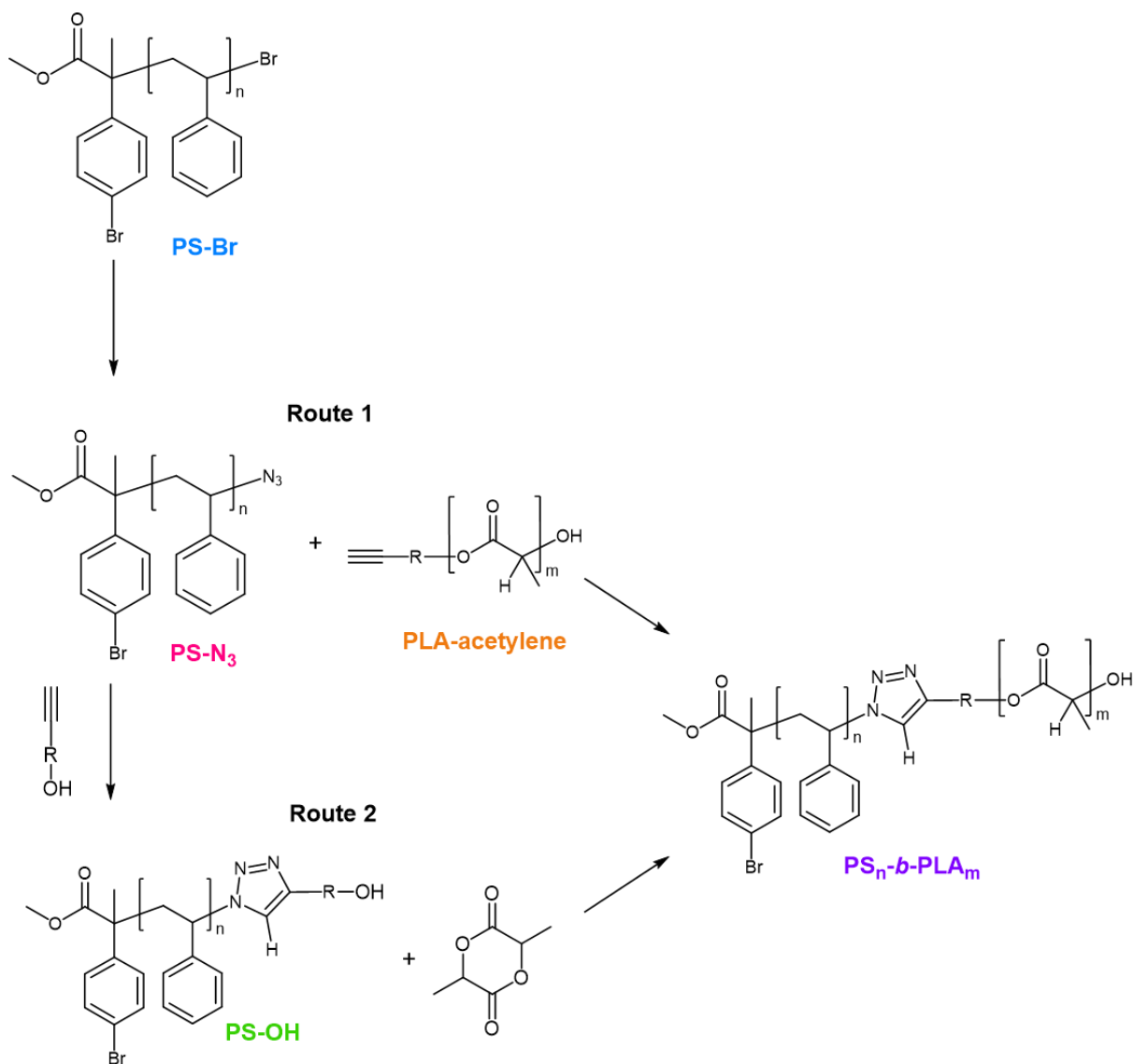


Figure 6.6 ^1H NMR spectrum of product B2-1 (400 MHz, CDCl_3 , R.T.)

This method allowed to obtain the aimed acetylenic terminations on the PLA precursors as evidenced by ^1H NMR. This functional end-group enabled the click coupling of PS- N_3 and PLA-Ac homopolymers as described in the following section.

6.4 PS_n-b-PLA_m copolymer synthesis

As stated in the hypothesis, one of the main premises of the project is to obtain a triazole-embedded BCP through a specific synthetic route. After the synthetic route results of the initiator and the polymeric precursors were analyzed, it was decided to include a triazole derivative as the functional group embedded to the PS-*b*-PLA copolymer. Scheme 6.9 summarizes the possible synthetic routes to obtain the aimed copolymers.



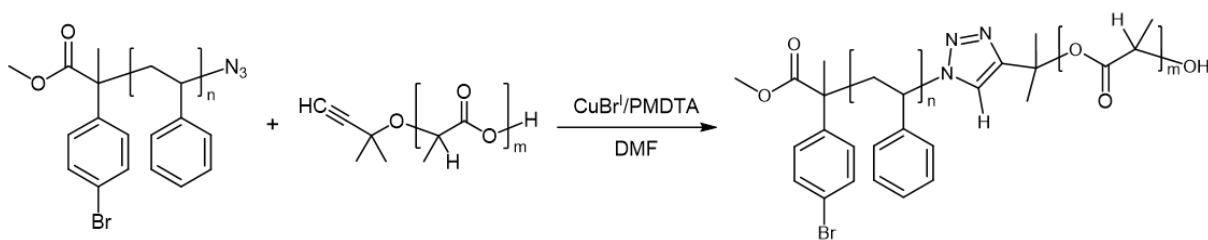
Scheme 6.9 Synthetic routes towards the obtention of PS_n-*b*-PLA_m copolymers.

Hence, two routes were proposed where the functional group would be added by transforming the bromine-end unit of the PS into a triazol group. Route 1 considers the click coupling of the azide and acetylene end groups of PS-N₃ and PLA-Ac, respectively. Route 2 considers the polymerization of the second block by using a PS-OH macroinitiator. In the following sections both methodologies are described.

6.4.1 Route 1: Block coupling through azide – alkyne 1,3 – cycloaddition

Click coupling of the terminal groups was carried out by following the copper catalyzed azide – alkyne cycloaddition (CuAAC) mechanism. The 1,3 – cycloaddition occurs at the azide and alkyne end groups of PS-N₃ and PLA-Ac. Both polymers were synthesized separately as described in the experimental section.

First, the PS-N₃ precursor was obtained and characterized as described in previous section (6.2.3). Then, PLA-Ac adduct was synthesized by ROP using the aliphatic initiator 2-methyl-3-butyn-2-ol (MBY) identified as **B1** in section 6.3. Scheme 6.10 displays the reaction used to prepare PS-*b*-PLA copolymers.



Scheme 6.10 Click coupling of PS-N₃ and PLA-Ac via CuAAC reaction.

By performing this reaction at the stated conditions, various PS-*b*-PLA copolymers were isolated after precipitation. It is worth noting that a mixture of solvents was necessary to precipitate the copolymer sample as a result of the change in polarity of the synthesized product. After purification, the copolymer was

characterized by ^1H NMR spectroscopy; the obtained spectrum is shown in Figure 6.7.

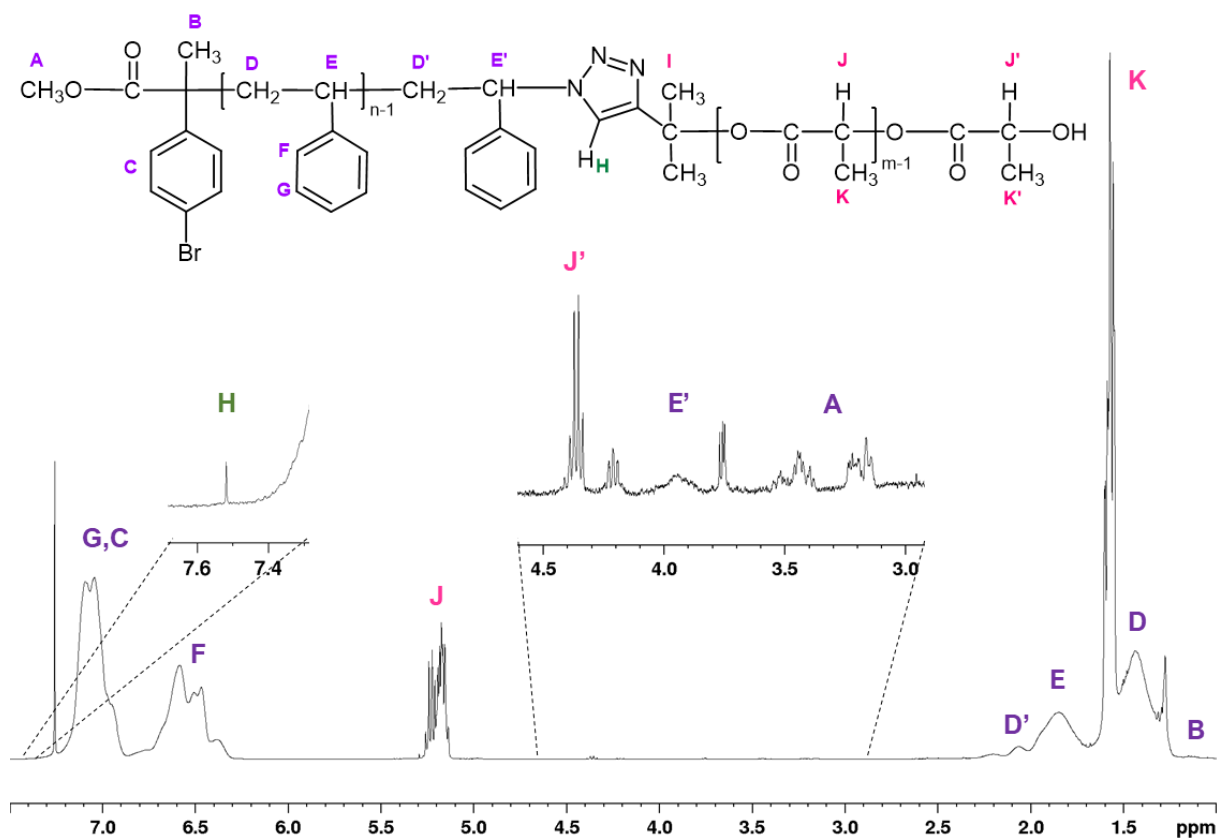


Figure 6.7 ^1H NMR spectrum of C1-5 (300 MHz, CDCl_3 , R.T.)

The aromatic repetitive unit signals for PS block, signals **G** and **F**, were located at $\delta = 7.32 - 6.27$ ppm, while the respective signal for PLA block, **J**, was assigned at $\delta = 5.32 - 5.10$ ppm. Signal **E'** corresponding to $-\text{CH}$ end group of PS block was assigned at $4.06 - 3.82$ ppm and signal **J** assigned to the terminal proton of the PLA block is located at $4.43 - 4.32$ ppm. In addition, the aliphatic signals of the PS repetitive unit were assigned at $2.30 - 1.70$ ppm for signal **E** and at $1.52 - 1.32$ ppm for signal **D**. Regarding the PLA block the signals corresponding to groups $-\text{CH}_3$ and terminal $-\text{CH}_3$, identified as **K** and **K'** respectively, are both overlapped at $1.68 - 1.52$ ppm.

Figure 6.8 displays a Diffusion-ordered spectroscopy (DOSY) NMR experiment of copolymer C1-6. The measurement further confirmed that the copolymer was obtained as evidenced by the presence of a single diffusion coefficient signal as expected for BCPs.

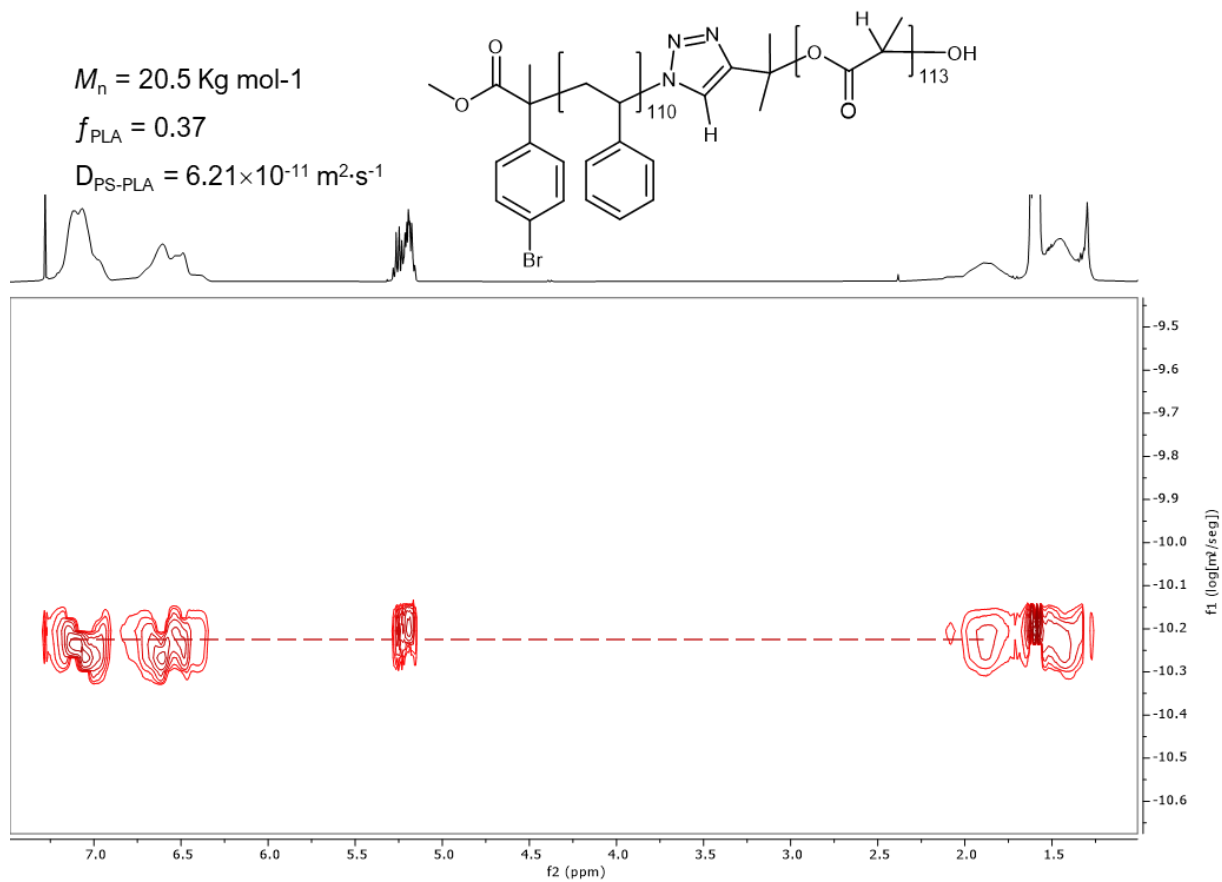


Figure 6.8 2D DOSY NMR spectra of copolymer C1-6.

Table 6.5 Summarized data of PS_n-*b*-PLA_m copolymer synthesis with MBY.

ID	PS _n - <i>b</i> -PLA _m ^a	M _n PS (Kg·mol ⁻¹) ^a	<i>f</i> _{PLA Theo}	<i>f</i> _{PLA Exp} ^a	M _n PS- <i>b</i> -PLA (Kg·mol ⁻¹) ^a	M _n PS- <i>b</i> -PLA (Kg·mol ⁻¹) ^b	Đ ^b	Yield (%) ^c
C1-1	PS ₈₉ - <i>b</i> -PLA ₁₄₀	9.6	0.45	0.47	19.8	20.0	1.65	89.0
C1-2	PS ₁₅₀ - <i>b</i> -PLA ₁₀₉	16.0	0.44	0.30	23.9	21.9	1.23	92.0
C1-3	PS ₁₈₆ - <i>b</i> -PLA ₈₀	19.7	0.30	0.20	25.7	19.6	1.28	93.0
C1-4	PS ₁₄₅ - <i>b</i> -PLA ₁₀₇	15.4	0.50	0.30	23.2	21.0	1.27	81.0
C1-5	PS ₁₂₈ - <i>b</i> -PLA ₁₁₀	13.6	0.40	0.33	21.7	25.6	1.24	87.0
C1-6	PS ₁₁₀ - <i>b</i> -PLA ₁₁₃	11.8	0.36	0.37	20.0	20.5	1.24	89.0
C1-7	PS ₁₇₆ - <i>b</i> -PLA ₉₇	18.7	0.37	0.24	25.7	19.8	1.24	88.0
C1-8	PS ₂₀₁ - <i>b</i> -PLA ₅₄	21.3	0.39	0.14	25.2	23.8	1.36	85.0
C1-9	PS ₁₄₄ - <i>b</i> -PLA ₁₂₉	15.3	0.34	0.34	24.7	24.8	1.24	82.0

^a *n*, *m*: number-average polymerization degree and number-average molar mass, *M_n*, determined by ¹H NMR (CDCl₃, R.T., 300 MHz).

$f_{PLA} = M_{n,PLA}/\rho_{PLA} / (M_{n,PLA}/\rho_{PLA} + M_{n,PS}/\rho_{PS})$, assuming densities of 1.02 and 1.25 g·mL⁻¹, for PS and PLA, respectively.

^b SEC (CHCl₃/LiCl/TEA) RID.

^c Yield estimated by gravimetry.

In Table 6.5 ¹H NMR and SEC characterization results of these experiments are summarized. An important variable in these systems is the PLA volume molar fraction, *f*_{PLA}, of the copolymers. In theory, a *f*_{PLA} = 0.3 – 0.4 value will promote a self-assembly of the phases into a cylindrical morphology.¹⁰² Considering *f*_{PLA} and *M_n*, polymer **C1-5** was used to carry out self-assembly trials as described in section 6.5.

To complement the characterization of the obtained copolymers a Differential Calorimetry Scanning (DSC) analysis was performed. Table 6.6 summarizes the thermal transitions of some of the synthesized copolymers. In principle, PS-*b*-PLA copolymers exhibit two glass transition temperatures (*T_g*), for each block. The *T_g* values reported for the corresponding homopolymers are *T_g*_{PLA} = 50°C and *T_g*_{PS} = 100°C.¹⁰³ Hence, the experimental data is in accordance with the reported values for *T_g*, there can be seen some minor variations on the values that are considered within

the expected experimental error. It is also hypothesized that the SEC-estimated M_n value of the copolymers may influence the T_g transition of both blocks in the copolymer. For instance, sample **C1-3** with a $M_n = 19.6 \text{ Kg mol}^{-1}$, a lower T_g value is observed for both PS and PLA compared to the respective values for sample **C1-9** with a $M_n = 24.8 \text{ Kg mol}^{-1}$.

Table 6.6 DSC and TGA summarized data of the synthesized copolymers.

ID	$T_{g\text{PLA}}^a$ (°C)	$T_{g\text{PS}}^a$ (°C)	$T_{D\text{PLA}}^b$ (°C)	PLA mass loss ^b (%)	$T_{D\text{PS}}^b$ (°C)
C1-1	47.5	99.3	282.1	37.3	322.9
C1-3	42.2	96.7	280.6	16.4	419.0
C1-4	50.8	103.0	273.5	40.0	399.6
C1-5	48.4	95.4	217.5	30.0	385.1
C1-6	47.1	98.5	279.8	27.2	386.4
C1-9	54.9	101.8	291.3	35.2	391.3

^a T_g (°C) = average glass transition temperature measured by DSC (-50°C – 150°C, 10.0 K/min, N₂, 20 mL/min)

^b T_D (°C) = onset decomposition transition measured by TGA (25 – 600°C, 10.0 K/min, N₂ atm)

Figure 6.9 displays the DSC thermograms of samples **C1-3** and **C1-5**, it can be seen that both transitions are within the expected range as compared with the exact values shown in Table 6.6.

In addition, thermogravimetric analysis (TGA) of the indicated copolymers was conducted to observe the thermal degradation of each block also shown in Table 6.6. The mass loss of the PLA block on the copolymer samples was compared to the f_{PLA} estimated by ¹H NMR. The mass loss values are proportional to the calculated volume fraction for the PLA block, which also confirms the ratio between blocks estimated by ¹H NMR (Table 6.5). Figure 6.10 displays the TGA thermograms of samples **C1-3** and **C1-5**, in which each sample has a different mass loss after degradation. For instance, sample C1-3 presented a PLA mass loss of 16.4% at $T_D = 280.6^\circ\text{C}$, which is consistent with the estimated f_{PLA} value at around 0.20 (Table 6.5).

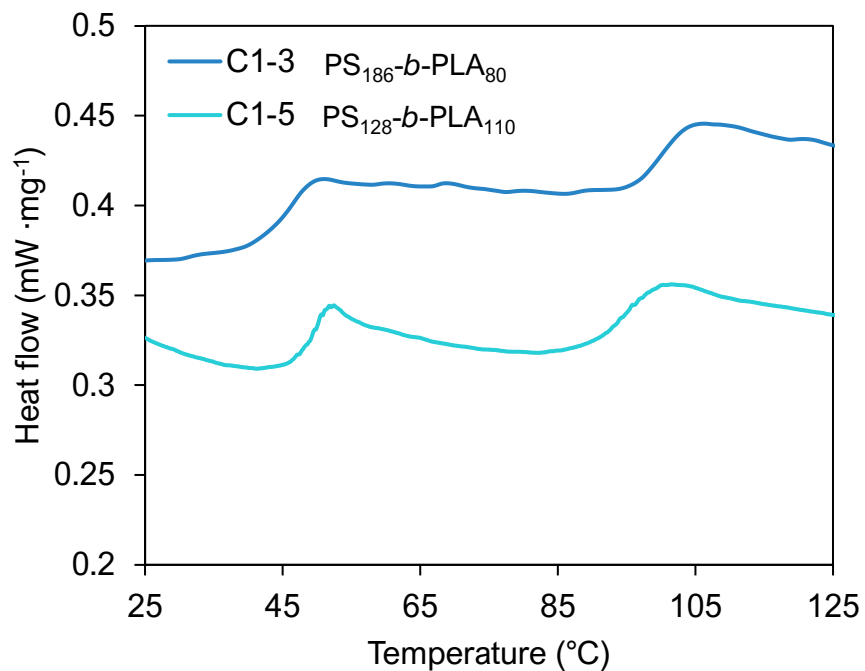


Figure 6.9 DSC thermograms of copolymers C1-3 and C1-5.

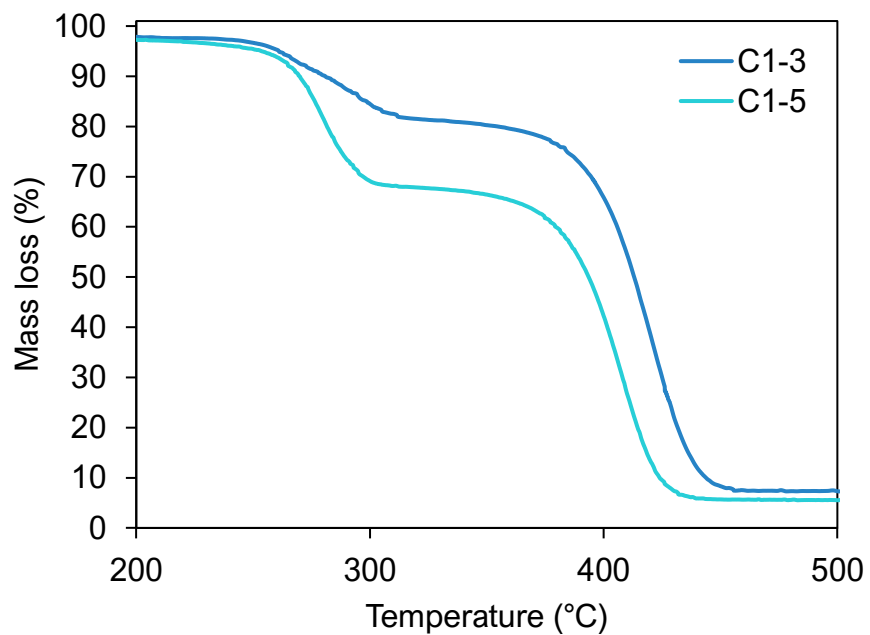
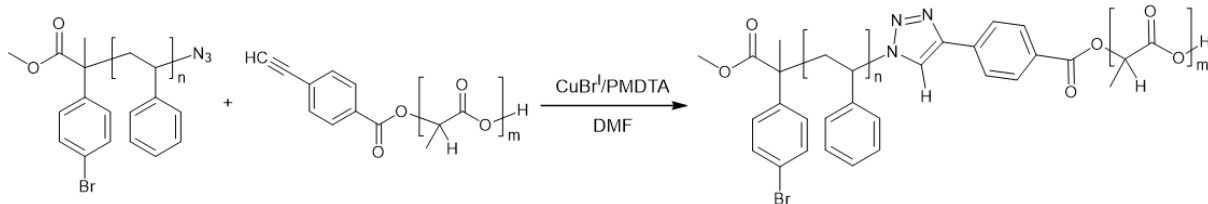


Figure 6.10 TGA thermograms of copolymers C1-3 and C1-5.

Route 1 enabled the synthesis of aliphatic-triazole embedded PS-*b*-PLA copolymers. This approach allowed to obtain the copolymers by coupling the functional end groups and qualitatively demonstrated by spectroscopy.

Consequently, a new series of copolymers was synthesized using this approach. These coupling reactions consider the synthesis of an acetylene-terminated PLA as well. However, an aromatic acetylene (4-ethynyl benzoic acid) (EBAc) was used as an initiator in the polymerization of the PLA instead of the aliphatic analogue used previously. In principle, an aromatic triazole will not largely affect the segregation of the copolymer, compared with the aliphatic junction. However, it may contribute to the complexation with the metallic center on the porous matrix due to electronic delocalization of the aromatic rings.¹⁰⁴ The synthesis of these new copolymers is displayed in Scheme 6.11.



Scheme 6.11 Click coupling of PS-N₃ and PLA-Ac via CuAAC reaction.

Following the described procedure, a new set of copolymers was synthesized. It is also worth to mention that a 1:2 PS: PLA molar ratio allowed to obtain a f_{PLA} experimental value closer to the theoretical one. Table 6.7 summarizes the molecular features of the isolated copolymers **C1-10** – **C1-14**.

Table 6.7. Summarized data of PS_n-*b*-PLA_m copolymer synthesis with EBAC.

ID	PS _n - <i>b</i> -PLA _m ^a	M_n PS (Kg·mol ⁻¹) ^a	f_{PLA} Theo	f_{PLA} Exp ^a	M_n PS- <i>b</i> -PLA (Kg·mol ⁻¹) ^a	M_n PS- <i>b</i> -PLA (Kg·mol ⁻¹) ^b	\bar{D} ^b	Yield (%) ^c
C1-10	PS ₂₀₃ - <i>b</i> -PLA ₁₃₉	21.5	0.41	0.28	31.6	28.0	1.16	90.0
C1-11	PS ₁₈₆ - <i>b</i> -PLA ₇₉	19.7	0.32	0.20	25.5	28.2	1.26	82.0
C1-12	PS ₉₄ - <i>b</i> -PLA ₁₁₀	10.1	0.38	0.40	18.2	16.7	1.11	92.0
C1-13	PS ₁₇₁ - <i>b</i> -PLA ₁₈₁	18.1	0.32	0.38	31.3	26.6	1.34	90.0
C1-14	PS ₁₄₄ - <i>b</i> -PLA ₁₉₆	15.3	0.34	0.44	29.6	34.8	1.21	86.0
C1-15	PS ₇₇ - <i>b</i> -PLA ₈₁	12.5	0.38	0.39	14.3	12.4	1.12	82.0

^a n , m : number-average polymerization degree and number-average molar mass, M_n , determined by ¹H NMR (CDCl₃, R.T., 300 MHz).

$f_{PLA} = M_n^{PLA}/\rho_{PLA} / (M_n^{PLA}/\rho_{PLA} + M_n^{PS}/\rho_{PS})$, assuming densities of 1.02 and 1.25 g·mL⁻¹, for PS and PLA, respectively.

^b SEC (CHCl₃/LiCl/TEA) RID.

^c Yield estimated by gravimetry.

As mentioned before, f_{PLA} parameter is important to determine self-assembly behavior of the copolymer on later stages. Overall, the f_{PLA} value of the synthesized copolymers is considered within the expected range. Copolymers **C1-12** and **C1-14** values are closer to a $f_{PLA} \sim 0.5$, which could direct into a gyroid or lamellar morphology. The click coupling reaction at these conditions enabled to modulate the PS:PLA ratio that is required on the isolated copolymer.

By observing the M_n values reported in Table 6.7, it should be noted that these estimated values present variations when comparing between ¹H NMR and SEC characterization techniques. This effect could be attributed to the size of the copolymer in solution as compared to the size of the PS standard calibration used to estimate M_n values of the copolymer. Hence, variations in the M_n values of the copolymers are expected when observing SEC results due to the chemical difference between the analyte and the standard reference.¹⁰⁵

It is worth mentioning that higher molar masses ($M_n > 20$ Kg mol⁻¹) promote the phase segregation in BCPs. At lower values, the incompatibility between the

blocks is weaker, which inhibits microphase segregation.¹⁰⁶ Thus, we aimed to obtain BCPs with a M_n value between 20 – 30 Kg mol⁻¹ in order to promote phase segregation in the later stages of this investigation.

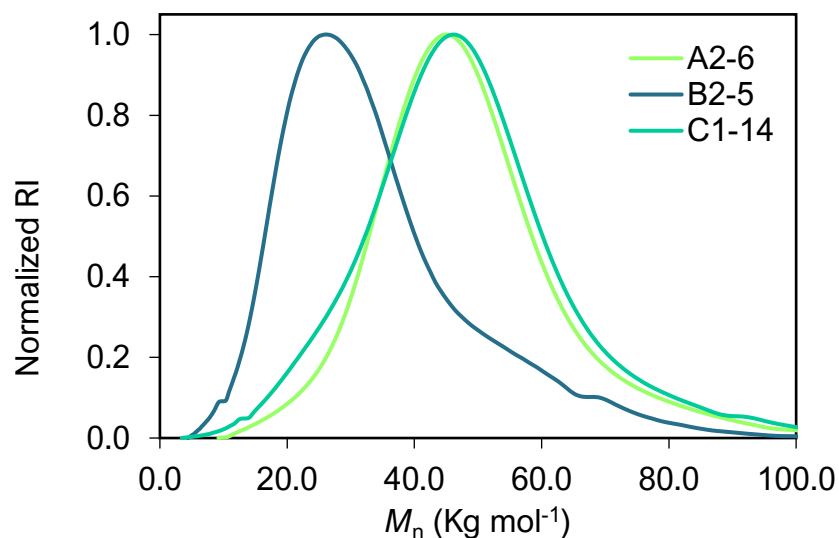


Figure 6.11 SEC traces of precursors PS-N₃ (A2-6), PLA-Ac (B2-5) and copolymer PS_n-b-PLA_m (C1-14).

SEC traces of copolymer **C1-14** are shown in

Figure 6.11, as the corresponding to the PS-N₃ and PLA-Ac homopolymers that were employed in the click coupling reaction. The copolymer peak (**C1-14**) is slightly shifted towards higher molar mass values compared with the PS-N₃ precursor. Regarding the PLA -Ac, the change in the molar mass is more evident when compared to the copolymer curve. Even though the curve shift between precursor and copolymer is not so obvious at a first sight, the increase in the dispersity values: $\mathcal{D} = 1.12$ for PS-N₃ and $\mathcal{D} = 1.21$ for PS-b-PLA (**C1-14**) is an additional indicator that the PS-b-PLA copolymer was successfully obtained. In

addition, a Differential Scanning Calorimetry (DSC) study of the isolated copolymers, exhibited the presence of both blocks within the expected ranges

Further NMR analysis confirmed the successful outcome of the click reaction. Figure 6.12 displays the ^1H NMR spectrum of $\text{PS}_{77}\text{-}b\text{-PLA}_{81}$, **C1-15**, where the most representative signals have been assigned. Copolymer **C1-15**, of a lower molar mass, was used to better observe the end group units of the copolymer. The broad signal within the chemical shift (δ) range from 7.24 to 6.25 ppm was assigned to the aromatic protons of the PS repetitive unit. Similarly, a broad signal at $\delta = 5.47 - 4.90$ ppm was assigned to the $-\text{CH}$ group of the PLA repetitive unit. To further confirm the presence of the triazole derivative, we proposed the following assignments to the phenyl-triazolyl junction group: $\delta = 8.21 - 8.05$ ppm and $7.91 - 7.73$ ppm corresponding to protons **F** and **G** as indicated in Figure 6.12. The triazolyl $-\text{CH}$ group (proton **E**, Figure 6.12) was ascribed to the signal at $\delta = 8.03$ ppm that is slightly overlapped with the aromatic protons assigned to **F**. The assigned proton signals are in good agreement with the previous reports investigating similar systems. For instance, Terzic *et al.* reported the synthesis of poly(vinylidene fluoride) (PVDF) triblock copolymers via CuAAC,¹⁰⁷ where the triazole proton was assigned at $\delta = 8.09$ ppm being in good agreement with our results considering the similarity of the chemical vicinity.

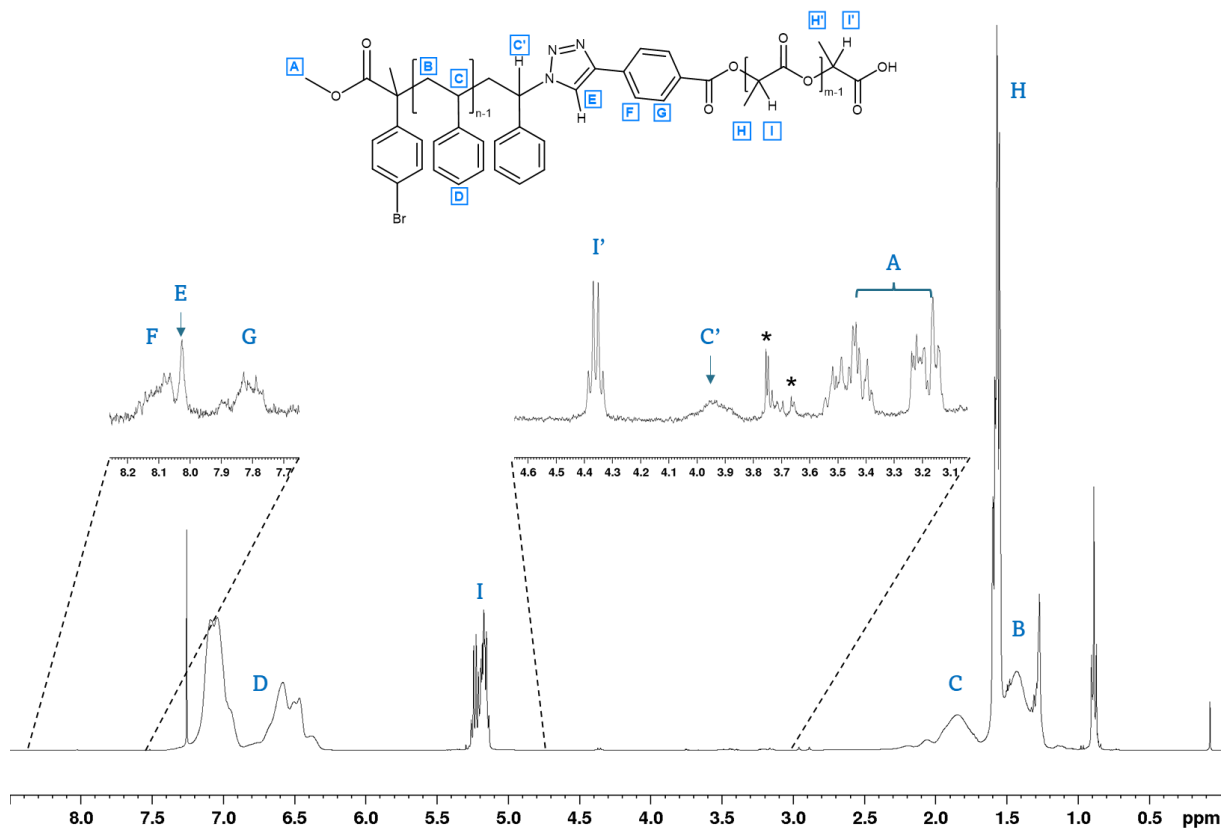
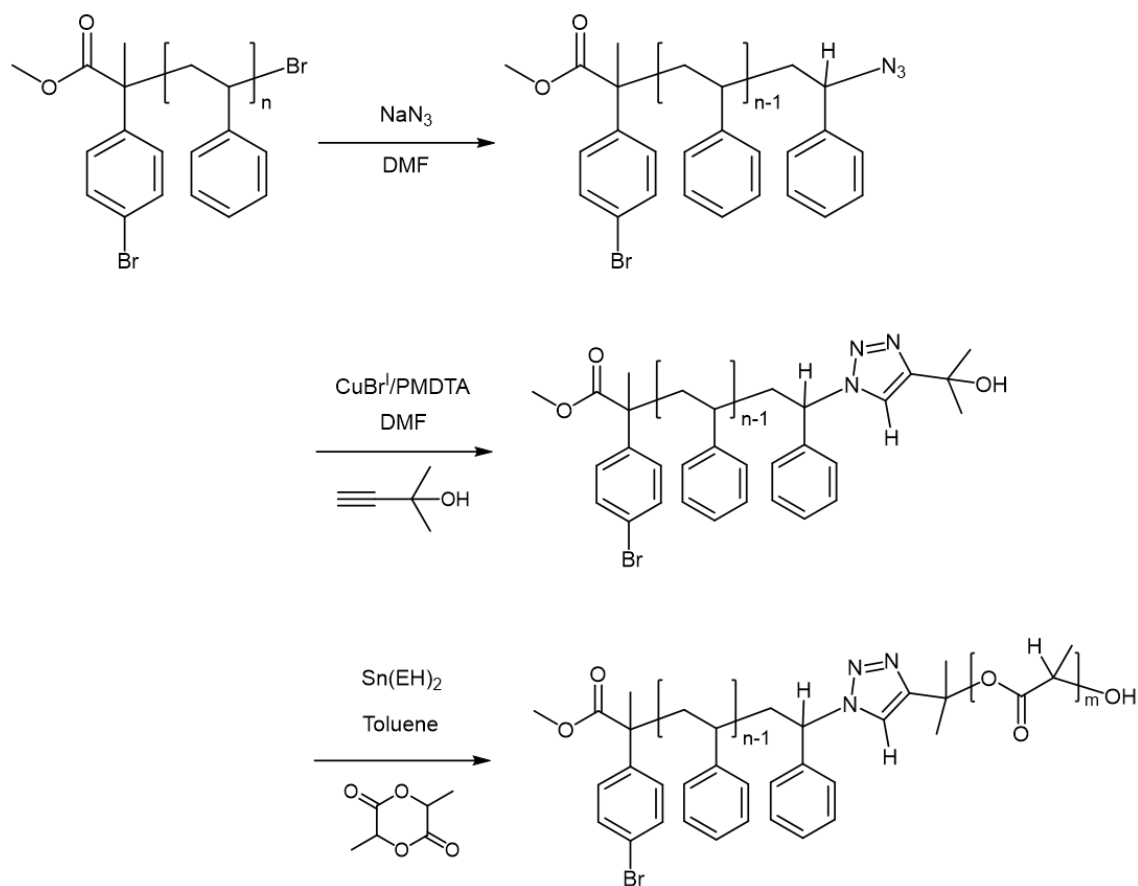


Figure 6.12 ¹H NMR spectrum of PS₁₁₇-b-PLA₁₃₀ (C1-15) copolymer (400 MHz, r.t., CDCl₃).

Considering these results, we assume that the obtained copolymers are adequate candidates to undergo microphase segregation. Physicochemical properties of PS-PLA-based copolymers will enable microphase segregation regardless of the functionalization present in their structure. Although, with the triazole junction in the synthesized copolymers we expect that functionality will not interfere in the segregation process and can still be present on the final PS-porous matrix.

6.4.2 Route 2: ROP of a PS-OH macroinitiator.

This route consisted in the functionalization of the chain end groups of the adduct PS–Br by performing a substitution of the terminal bromide for an azide group to isolate PS–N₃. Subsequently, this product was reacted with an acetylene to form a triazol-alcohol group at the end (PS–OH).^{36,79} The hydroxy terminal group of PS–OH would act as an initiator to synthesize the PLA block. This route is displayed in the Scheme 6.12.



Scheme 6.12 Route 2 synthetic pathway to obtain PS-*b*-PLA copolymer.

The assignment of the –CH terminal proton on the PS chain is important to ensure that the terminal group is transforming according to each step on the

synthesis pathway. Hence this signal was identified by the ^1H NMR spectrum at each step. Figure 6.13 shows a comparative ^1H NMR of the products involved in the proposed synthetic route. It is worth to note that the synthesis was performed in a sequential manner, meaning that each step was carried out using the corresponding precursor. Represented by the blue series is product PS–Br, a broad signal at $\delta = 4.57 - 4.32$ ppm was assigned to $-\text{CHBr}$; the pink series represents PS- N_3 product, the corresponding end proton, $-\text{CHN}_3$ was assigned at $\delta = 4.05 - 3.84$ ppm. The last step in the end functionalization is the click reaction which results in product PS–OH represented by the green line, $-\text{CH}$ -triazole terminal proton shifted towards $\delta = 5.19 - 5.93$ ppm.

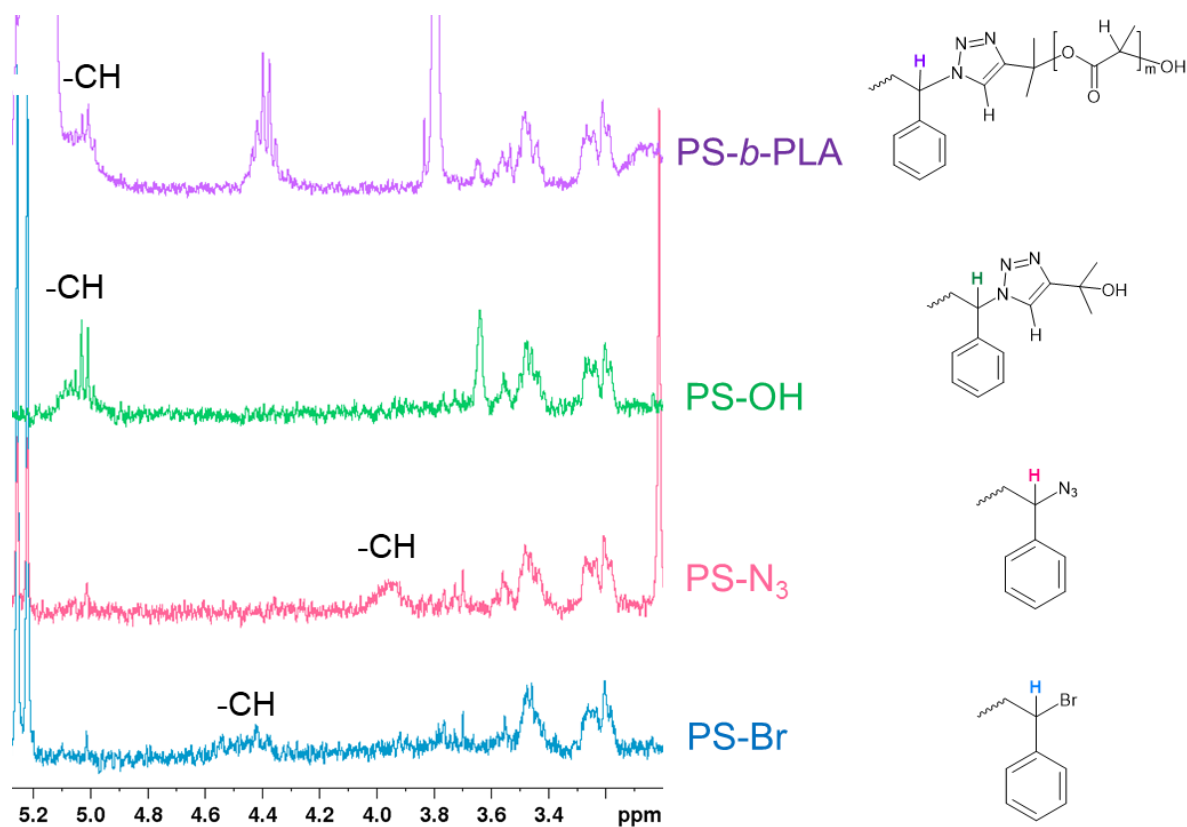


Figure 6.13 Comparative ^1H NMR spectra of PS-Br, A1-11 (blue), PS-N3, A2-7 (pink), PS-OH, A3-1 (green) and PS-b-PLA, C2-4 (purple). (Zoom into chemical shift $\delta = 5.2 - 3.0$ ppm)

The chemical shift in each case is clearly visible and it is also consistent with the chemical vicinity of the observed proton at each step. A similar behavior was reported by Anastasaki⁷¹ and colleagues where the -CH-triazole terminal proton exhibited a chemical shift of $\delta = 5.37 - 5.29$ ppm, similar to the obtained in this work.

The following synthesis step involved the copolymerization of the PLA block by employing the PS–OH adduct as a macroinitiator to initiate the ring opening of a lactide. Hence, this reaction was executed as described (5.4.5). as a result of this reaction, it was possible to isolate the formed PS-*b*-PLA copolymer as evidenced in the spectra represented in the purple series of the figure. By observing the PS end proton, a broad signal was assigned to correspond to a chemical shift at $\delta = 5.10 - 4.95$ ppm. It is evident that this signal is overlapped with the corresponding to the repetitive unit of the PLA block, –CH $\delta = 5.34 - 5.08$ ppm, nonetheless both of these signals can be identified on the spectra.

As mentioned before, f_{PLA} is an important parameter to obtain a certain morphology of the final materials. Therefore, similar to route 1, this variable was calculated by ¹H NMR of the copolymers obtained employing route 2. Table 6.8 summarizes the molecular data of the synthesized copolymers.

Table 6.8 Summarized data of PS_{*n*}-*b*-PLA_{*m*} copolymer synthesis with route 2.

ID	PS _{<i>n</i>} - <i>b</i> -PLA _{<i>m</i>} ^a	M _n PS (Kg·mol ⁻¹) ^a	$f_{\text{PLA T}}$	$f_{\text{PLA exp}}^{\text{a}}$	M _n PS- <i>b</i> -PLA (Kg·mol ⁻¹) ^a	Yield (%) ^c
C2-1	PS ₅₂ - <i>b</i> -PLA ₁₆	5.7	0.21	0.14	7.0	57.0
C2-2	PS ₁₆₂ - <i>b</i> -PLA ₁₀	17.2	0.16	0.03	18.0	55.0
C2-3	PS ₃₁ - <i>b</i> -PLA ₈	3.5	0.13	0.11	4.2	62.0
C2-4	PS ₁₀₉ - <i>b</i> -PLA ₁₅	11.7	0.23	0.09	12.8	43.0

^a *n*, *m*: number-average polymerization degree and number-average molar mass, M_n, determined by ¹H NMR (CDCl₃, R.T., 300 MHz).

$f_{\text{PLA}} = M_{\text{n PLA}}/\rho_{\text{PLA}} / (M_{\text{n PLA}}/\rho_{\text{PLA}} + M_{\text{n PS}}/\rho_{\text{PS}})$, assuming densities of 1.02 and 1.25 g·mL⁻¹, for PS and PLA, respectively.

^c Yield estimated by gravimetry.

As gathered from the data, the molar ratio between PS and PLA block is lower than expected, the integral value on the PLA repetitive unit is low in most cases. The overall quantity of PLA on the copolymer is important to reach a proper segregation of the phases during the self-assembly. Hence, by observing the estimated f_{PLA} values it can be concluded that the values are insufficient to promote a cylindrical morphology. The methodology employed with route 2 enabled the synthesis of PS-*b*-PLA copolymers by employing a PS–OH macroinitiator. However, the f_{PLA} of the copolymers was not in accordance with the theoretical value, necessary to promote the segregation on latter steps.

The synthesis of the PS_{*n*}-*b*-PLA_{*m*} copolymers was explored by evaluating two different routes and according to the results it can be concluded that the click coupling (indicated as route 1) of the PS–N₃ and PLA–Ac homopolymers through the azide-alkyne cycloaddition yielded better results. According to the ¹H NMR analysis, PLA volume fraction of the obtained copolymers ($f_{\text{PLA}} \sim 0.35$) was closer to expected with synthetic route 1. Thus, the selected examples were chosen to undergo self-assembly on thin films as discussed in the following section

Part B – Self-assembly of PS-*b*-PLA copolymers on thin films

The synthetic pathway allowed to obtain triazole-embedded PS-*b*-PLA copolymers as thoroughly described in Part A, this can influence the copolymer self-assembly behavior to some extent. Part B addresses the results obtained from the preparation of thin films based on the previously synthesized copolymers. The included experimentation and results focused on techniques solvent vapor annealing (SVA) and thermal annealing (TA) of the copolymer films

6.5 Annealing experiments of PS-*b*-PLA thin films

To begin with the self-assembly study of the synthesized copolymers, product **C1-5** was chosen as a template due to the f_{PLA} and M_n of the copolymer. As it has been stated before, PS-*b*-PLA copolymers are eligible materials to pattern different morphologies at a meso scale.⁹¹ Therefore, the assembly of these copolymers was monitored by observing the morphology of the prepared thin films via Scanning Electron Microscopy (SEM). For this purpose, a copolymer solution was made by dissolving the copolymer **C1-5** in THF to yield a concentration of 2.0% wt. This solute-solvent system was chosen after comparing a first set of as-spun substrates employing THF, toluene, CH₂Cl₂ and dioxane copolymer solutions at the same concentration. SEM of the as-spun samples dissolved in THF exhibited a better periodicity of the domains on the surface compared to the samples dissolved in toluene, CH₂Cl₂ or dioxane. (See Appendix, Figure 9.3) In addition, samples that were dissolved in THF also appeared to promote the phase segregation simply by spin coating on the silicon wafer. Hence, it was decided to continue the analysis with THF-based copolymer solutions.

6.5.1 SVA experiments

Regarding the annealing experiments solvent, *o*-xylene was chosen as annealing solvent due to the polar affinity with the PS phase, which could selectively

contribute to the self-assembly process on the thin film surface. On that account, several pieces of wafers were spin coated and annealed at various times. For this purpose, a 5-mL vial was filled with *o*-xylene and placed inside a closed glass chamber. Next to the vial, the substrates were carefully placed and taken out at various times. After SVA, the substrates were air-dried inside a fume hood and analyzed by SEM.

SEM images of the as-spun substrate, shown in Figure 6.14-A, exhibited a two-phased surface in which circle-like structures are homogeneously distributed across a continuous phase. It was expected to obtain a cylindrical morphology of PLA domains homogeneously distributed across a PS matrix. Therefore, it is assumed that the circular structures (0.5 – 1 μm) correspond to a segregated phase of PLA, given that it is the minority block of the BCP system. Hence, the continuous phase might correspond to a PS matrix.¹⁰⁸ After 15-minute of SVA (Figure 6.14-B), these structures did not exhibit a major change as compared to the morphology observed in the as-spun substrate. After 45 minutes of annealing with *o*-xylene (Figure 6.14-C), the surface of the substrates exhibited a hollowed structure considering the difference in contrast between the continuous phase and the circle-like structures. At this point, the PLA minority phase seems to be etched from the surface. Nonetheless, no attempts of removing the PLA phase were made at this stage. Thus, it is hypothesized that the PLA domains formed an interphase between the PS and the silicon substrate, which may be attributed to the chemical affinity between the PLA and the silicon wafer surface. This effect was further investigated via Atomic Force Microscopy (AFM) on the same substrate. In this additional characterization, the holes (PLA domains), formed after 45-minute of SVA, seemed to interact with the substrate at approximately 100 nm below the continuous phase (PS) (Appendix, Figure 9.4-D). As evidenced from the 3D image, the difference from the highest to the lowest point of the film is around 100 nm, hence it is assumed that the PLA domains may be interacting with the surface of the wafer.

According to a size analysis of the pore-like structures on the SEM image of Figure 6.14-C, the diameter of the formed cylinders has a mean size of 125 nm after 45 minutes of SVA with *o*-xylene.

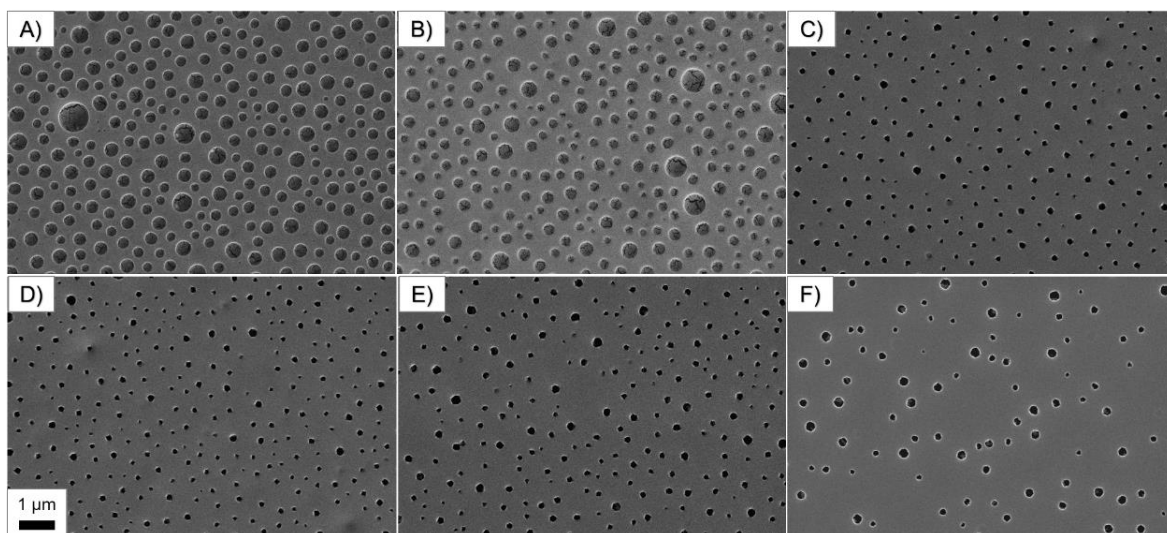


Figure 6.14 SEM images of the as-spun and annealed substrates at various times: A) as-spun, B) 15 min, C) 45 min, D) 1 h 30 min, E) 3 h, and F) 6 h.

Longer annealing times were performed on the rest of the spun substrates and the corresponding SEM images are shown in Figure 6.14D – F. In these images, a similar pattern to that of Figure 6.14C (45-min of SVA) can be observed. Although, after 6 h (Figure 6.14F), the pore homogeneity on surface of the film starts vanishing as compared to shorter annealing times. This suggests that for longer SVA times, the solvent may begin to dissolve the film. The size analysis of the pore diameter for images *D* to *F* yielded similar values within a range from 121 to 139 nm.

After the annealing step, it is desirable to selectively remove the PLA minority phase to obtain a hollowed PS-matrix. In this regard, an attempt to remove the PLA was made by immersing the substrates in an alkaline solution (NaOH 0.5 M). However, delamination of the entire film was observed after a couple of minutes of

being immerse in the alkaline medium. This effect has also been observed for analogous systems where the substrate surface is not compatible enough with the continuous phase, which leads to delamination of the film.^{109,110}

Consequently, a pre-treatment of the substrates was carried out to avoid delamination of the film. Pre-treatment of the substrates consisted in the formation of an interlayer between the BCP film and the silicon-wafer surface. It is hypothesized that this interlayer might promote compatibility between the substrate surface and the copolymer film. As described in the experimental section, the surface of the silicon wafer was etched with a piranha solution. Afterwards, a silylation of the surface was conducted by dipping the wafer into a hexamethyldisilazane (HMDS)-toluene solution. As a result, a solvophobic interlayer was formed between polymer film and substrate.²⁰ Thereafter, substrates were pre-treated as indicated above and, subsequently, spin coated using the same conditions to those applied to the untreated substrates. Previous results suggested that 45-minute of SVA with *o*-xylene (untreated substrates) would form cylindrical cavities and, therefore, we attempted to replicate this procedure on pre-treated substrates.

Figure 6.15 displays a comparison between a spin-coated sample on an untreated surface (Figure 6.15-A) and a spin-coated sample on a pretreated surface (Figure 6.15-B) after 45-min of SVA. The previously tested annealing conditions were not reproducible for the HMDS-treated surfaces. A noticeable difference can be observed on the pretreated surface of the substrates, where large 'islands' (1 – 3 μm) were formed across the surface of the film as well as some smaller pore-like structures that surround those larger structures. Thereafter, the pores and the pattern regularity of the film could not be reached after 45-minute annealing, as opposed to the untreated samples. Thus, it was hypothesized that longer SVA times would allow the phases to reach an equilibrium into a more ordered state.

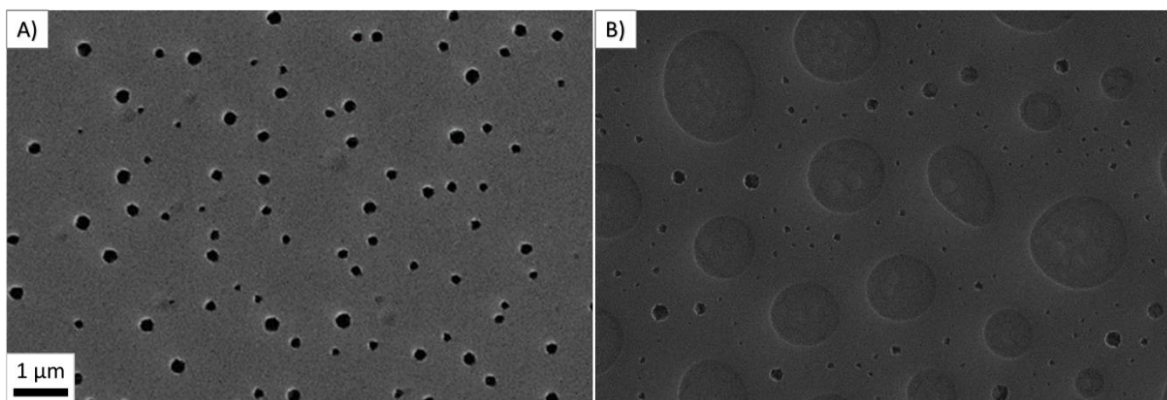


Figure 6.15 SEM images of the untreated A) and the silylated substrate B) after 45-min SVA with o-xylene.

Considering this, an additional SVA experiment was performed at considerably longer annealing times: 2, 4, 8 and 16 h. Unexpectedly, longer SVA times did not promote phase segregation and the formation of morphology on the film. Based on this SEM analysis of the samples, we theorized that at longer annealing times ($t > 45$ minutes) the films seem to be prone to dewett from the surface leading to their damage. (See Figure 9.5 for more details) The interlayer formation derived from the HMDS pretreatment had a significant influence on the self-assembly process of the investigated BCP system on the surface. Thus, in this case, the utilized annealing solvent and conditions did not promote the cylindrical morphology observed on the untreated substrates.

Despite the aforementioned, it should not be discarded that as-spun substrates on untreated substrates exhibited a homogeneous pattern. In this regard, we considered that the morphology of the as-spun films is comparable to those observed in previous reports with analogues systems.⁴⁰ Therefore, we decided to further investigate and exploit the characteristics of as-spun films on untreated substrates and without SVA, which is discussed later on in Section 5.5.3. Considering these results, we explored other alternative methods to obtain ordered-porous structures as discussed next.

6.5.2 TA experiments

Thermal transitions of BCPs have also been used to anneal microphases to access certain morphologies. To further investigate the microphase segregation behavior of the copolymer **C1-5**, Thermal Annealing (TA) experiments of thin films were additionally performed. In this regard, the thermal transitions of the synthesized BCPs were previously evaluated using Differential Scanning Calorimetry (DSC) and Thermogravimetric Analysis (TGA) (Table 6.6).

Regarding DSC investigations, the glass transition temperature (T_g) of each block allowed to determine a range of values where the copolymer is in a disordered state. Furthermore, based on TGA measurements it was determined at which temperature the copolymer begins to decompose (T_D). By analyzing these two parameters a range of temperature values was proposed in which the copolymer transitions may drive the system from a fluid disordered state into an ordered state. Hence, the order-disorder transition (T_{ODT}) can be found above the values of the T_g 's of both individual blocks and below the T_D . According to DSC and TGA measurements of the synthesized BCPs, the proposed temperature range is from 110 to 210 °C. Previous investigations with analogue systems report a $T_{ODT} = 138$ °C.¹⁰⁶

As discussed for previous annealing experiments, we observed delamination of the films deposited on the untreated substrates. In an attempt to prevent this effect, a silylation treatment on the wafers was also performed for the thermal annealing experiments. Considering the thermal profile of the investigated BCP system, a thermal annealing experiment was carried out using the same procedure for the preparation of thin films as described above for the SVA experiments. Figure 6.16-A and B displays SEM images of thin films annealed at 120 and 150°C for 10 min, respectively. Figure 6.16-A displays an irregular distribution of PLA domains suggesting that the system did not reach an equilibrium leading to a cylindrical phase segregation at the investigated conditions. Two size populations of the pore-like

structures are visible in this image, where the smaller pores seem to merge with each other to form the larger structures. Although, at this point, this latter statement is only a hypothesis of what may be occurring.

At 150°C (Figure 6.16-B) the SEM image presents a noticeable difference between the size populations of PLA domains. It has been reported that higher temperatures promote the formation of more uniform patterns in PS-PLA based thin films; nonetheless, this can also conduct to the PLA decomposition if annealing times are extended.²⁰ However, this was not the case for the observed films as there is a greater gap between the sizes population of the formed structure and, somewhat, a more irregular pattern after increasing temperature to 150°C.

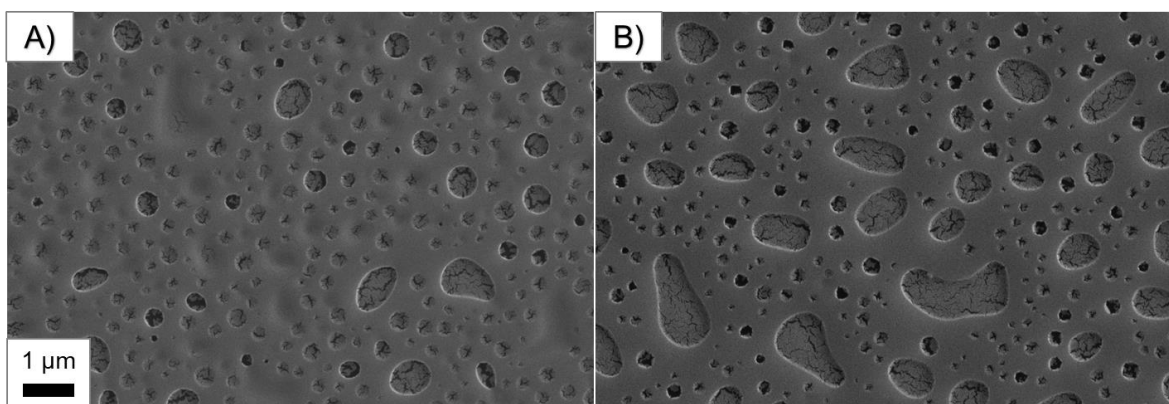


Figure 6.16 SEM images of the thermally annealed thin films at 120°C A), and 150°C, B) in a 10-minute TA.

The thermally annealed films exhibited a different morphology pattern as compared to that obtained with the SVA method on treated substrates. At a first glance, TA might seem to promote a better arrangement of the domains regarding the size of the pore like structures opposed to the observed with SVA, where the difference between size of 'islands' and pores is larger (Figure 6.15-B). However, the pore like structures in the thermally annealed films yielded two size populations,

which might lead to irregularities in the resulting film once the PLA phase is selectively removed.

Thermal annealing of the thin films may represent an alternative to promote orientation of the PS-PLA domains by varying parameters such as time, temperature and/or inert conditions during the annealing.²⁰

6.5.3 Hydrolysis of the as-spun films

At this stage, it is worth to outline some of the findings: *a)* SVA of untreated surfaces yielded an acceptable homogeneity on the film surface, however, it lead to delamination when attempting to selectively remove the PLA domains; *b)* SVA of the pretreated substrates did not exhibit the same homogeneity and regularity on the morphology of the film as it did for untreated substrates; *c)* TA of the pretreated substrates at the experimental conditions did not promote the formation of the desired morphology of the film, *d)* spin coating of the substrates seemed to promote the segregation of the phases and a cylindric morphology (Figure 6.17-A.) Henceforth, this section addresses this last premise and explores the possibility of hydrolyzing the PLA of as-spun films, meaning that no annealing was performed for this substrates prior to the hydrolysis. As well, it is worth to note that these experiments were carried out on pre-treated substrates to avoid delamination of the film.

Following the same spin-coating process used for prior samples, an as-spun film was dipped into an alkaline solution (NaOH 0.5 M) to selectively remove the PLA domains and obtain a PS-porous film matrix. Figure 6.17-B displays a SEM image of the hydrolyzed as-spun pretreated substrate where a difference in contrast between the formed pores and the PS continuous phase can be distinguished. By comparing the as-spun film (Figure 6.17-A) and the corresponding hydrolyzed film (Figure 6.17-B), it can be concluded that the PLA was removed. The difference in the topology of the film can be better appreciated with the aid of the SE detector (utilized in this SEM

measurement). The regularity and the condition of the film seem to be unaffected by the hydrolysis procedure suggesting that the silylation pretreatment on the substrates contributed to the stability of the supported film.

The diameter of the formed pores of Figure 6.17-B was analyzed using the software *Image J*, resulting in a mean size of 245 nm. The estimated diameter value decreased after the hydrolysis of the film; prior to this treatment, the mean diameter of the cylinders was calculated around 322 nm. As mentioned before, in this case the as-spun films were not subjected to any further treatment. Nonetheless, it is observed that the morphology on this film suggests a suitable phase segregation. At this point, it is hypothesized that THF may have contributed to this effect due to the polar affinity between this solvent and the PLA phase.⁹³

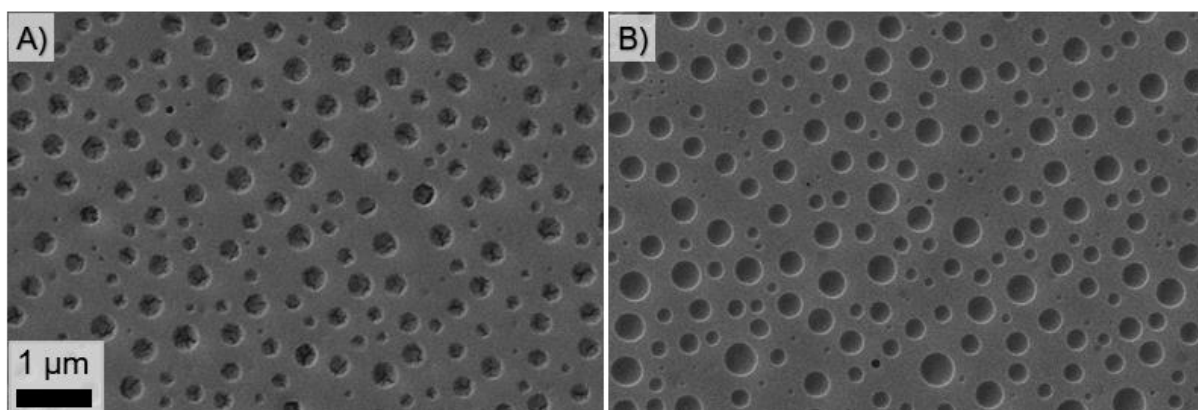


Figure 6.17 SEM images of the as-spun A) and the hydrolyzed film B).

To further confirm the change in the topography of the film, AFM measurements of both films were performed. Figure 6.18-A displays an AFM image of the as-spun film, a 3D image, and a topographic profile of the film; the corresponding is also observed for the hydrolyzed film on Figure 6.18-B. From the 3D images of the films, a difference in the density of the pores can be observed. This was validated by the morphology profile extracted from this image. After hydrolysis,

the valleys of the pores become more defined (Figure 6.18-B), whereas prior to hydrolysis, the valleys seem to be broader suggesting that PLA domains are present at the interphase.

All in all, the hydrolysis of the as-spun films based on the synthesized PS-*b*-PLA copolymers may represent an attractive alternative to obtain porous films considering the rather simple preparation steps.

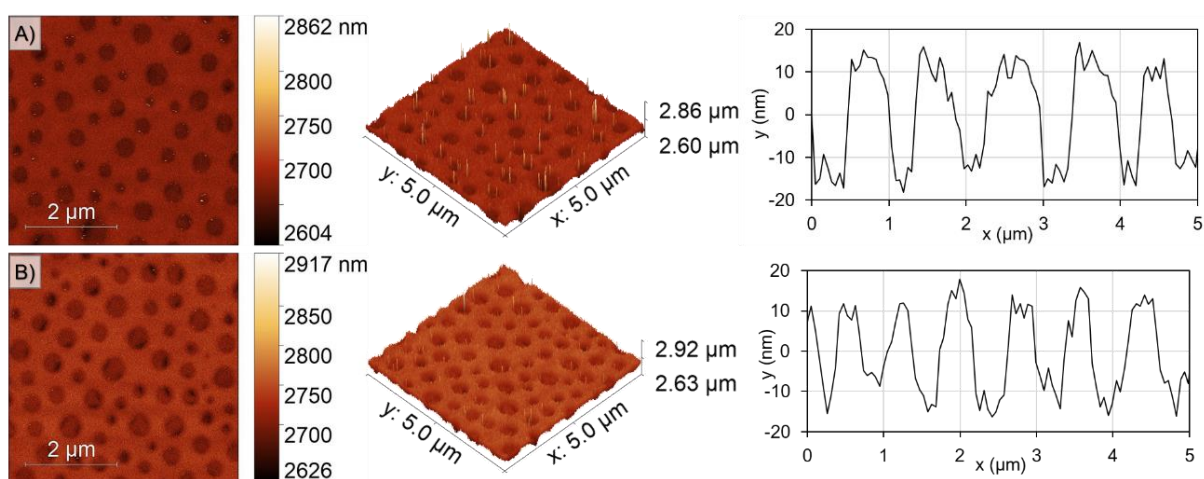


Figure 6.18 AFM images and profiles on the morphology of the as-spun, A), and the hydrolyzed film, B), on pre-treated substrates.

6.6 Binding tests of metal salts using hydrolyzed films

After PLA hydrolysis of the as-spun substrates, it was decided to analyze the metal cation capacity of the obtained films. At this stage, it is speculated that the generated porous thin films bear in their structure triazole groups available at the surface of the pores. These functional groups are capable of binding to metal cations through a coordination bond.⁸⁵ Hence, the metal cation capacity of the functional porous PS film was tested with a metal. The experiments were conducted by dipping

the hydrolyzed film into a CuCl_2 solution. The metal cation was studied with Cu^{2+} due to its affinity to imidazole and triazole derivatives.¹¹¹

After thoroughly rinsing and drying the used substrates were analyzed via Scanning Electron Microscopy – Energy Dispersive X-ray spectroscopy, SEM-EDX, to survey the presence of Cu^{2+} moieties that may have remained attached to the porous matrix.

For this experiment, copolymer **C1-5** was subjected to the described spin coating and subsequent PLA hydrolysis procedures (Figure 6.17-B). The utilized substrate for this experiment was pre-treated with the silylation process to avoid delamination of the film as discussed above.

Figure 6.19-A shows a SEM image of the film after being in contact with a CuCl_2 solution. It is evident that after a thorough rinsing, some large pieces of the metallic salt remain attached onto the surface of the film. Figure 6.19-B displays the Cu-mapping of the same substrate, Cu moieties on the film are clearly observed. However, a minimum portion of Cu salt is distributed on the film as it can be observed from the little dotting pattern. At this point, it is unclear whether these micro-moieties are coordinated to the triazole groups on the PS-film or whether the Cu salt is physically attached onto the surface.

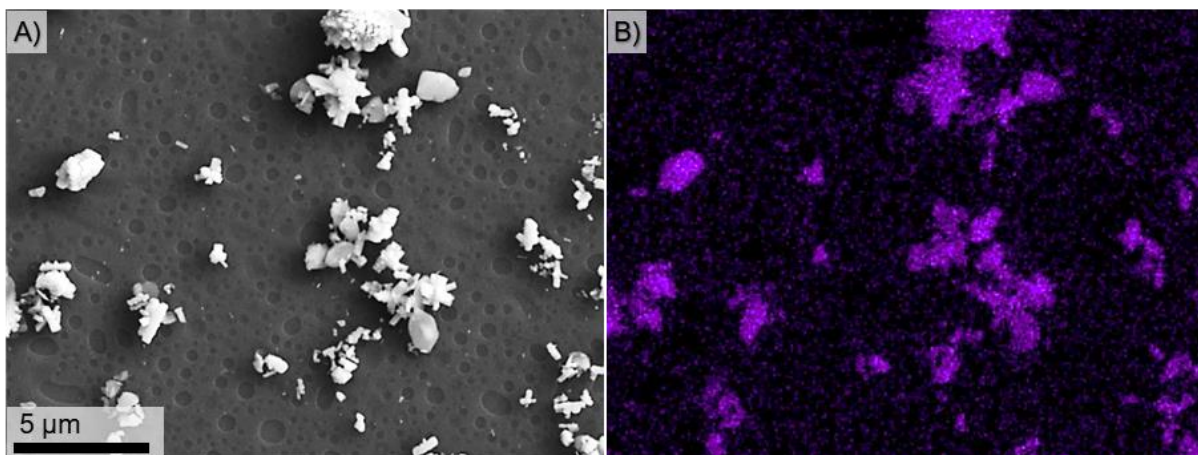


Figure 6.19 SEM-EDX image of the metal-treated PS-film A) hydrolyzed sample w/ CuCl_2 , and B) Cu-mapping image of the same sample.

It is hypothesized that the PS-film possesses certain affinity towards the copper salts as it can be seen from the EDX images. A minimum quantity of the copper salt is attached to the film possibly by the interaction between the triazole groups and the metallic center.

6.7 PS-*b*-PLA semi-bulk and bulk samples as templates for porous membranes

Self-assembly and phase segregation of BCPs in thin films are governed by factors different to those applied for the preparation of bulk or semi-bulk samples. Complementary to the previous analysis, several experiments were conducted to prepare monoliths from the synthesized $\text{PS}_n\text{-}b\text{-PLA}_m$ copolymers. Following method 1 described in the experimental section, a concentrated solution ($C = 10.0$ wt. %) of copolymer **C1-9** in toluene was employed to execute these experiments. After complete dissolution of the copolymer a highly viscous solution was obtained. As mentioned in the experimental section, the solution was poured into an as-made Teflon mold (~ 60 mm²) at 50°C. A slight increase in the temperature of the solution allowed the material to become more fluid when casting it into the mold. Once the

solvent evaporated, the sample was annealed at 110°C for 1h and a thin copolymer film was recovered from the Teflon mold.

According to a SEM image of the material (Figure 6.20-A), the exhibited morphology on the surface evidences the formation of some pores. The distribution of these pores is less homogenous than that observed on the wafer-supported thin films. This may suggest that it is possible to modulate experimental conditions to obtain more homogeneous patterns on the samples prepared in semi-bulk aiming to replicate the behavior observed on supported thin films. However, the thickness (0.11 mm) and brittleness of the isolated film made it difficult to handle and to characterize by SEM. The stability and mechanical properties are also important to avoid disintegration of the film during the subsequent hydrolysis step. Therefore, the experiment was re-attempted to increase the thickness of the final monolith. This was achieved by pouring the copolymer solution into a Teflon mold of smaller dimensions (~ 20 mm²). In addition, a higher temperature (160° C) was employed in this experiment to further promote phase segregation. As a result, a thicker and more stable film was recovered from the mold (1.20 mm). Figure 6.20-B displays a micrograph of the monolith surface with a more defined pore formation as compared to that of Figure 6.20-A. Although the distribution of these pores may not be very homogeneous, this result suggests that a self-assembly process may occur as a result from the thermal annealing at semi-bulk conditions.

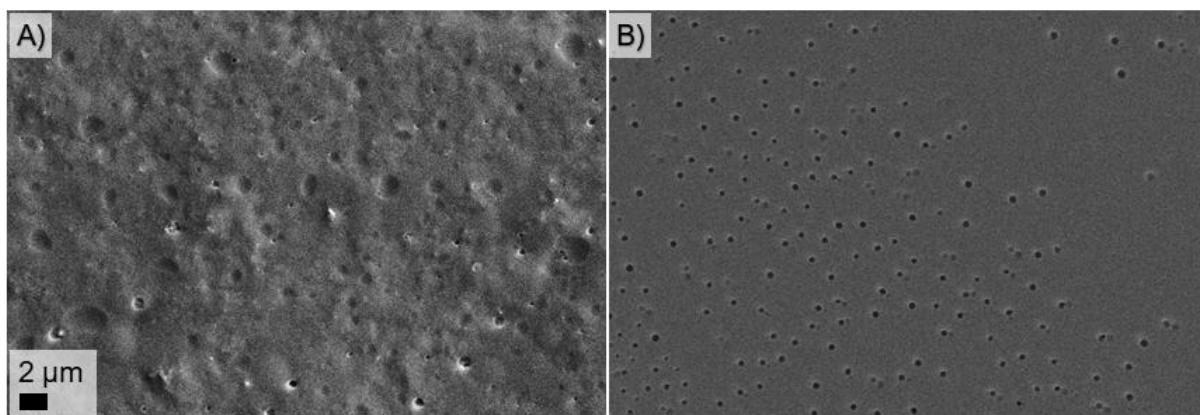


Figure 6.20 SEM images of copolymer C1-9 annealed at 110°C for 1h, A) and annealed at 160°C, B).

To continue with the established experimental scheme, a hydrolysis of the annealed sample, shown in Figure 6.20-A, was carried out as described in section 5.6.3 to form a PS-based porous matrix. The hydrolysis selectively removed the PLA from the as-made monoliths. As described in section 5.6.3, small pieces of the prepared monoliths were immersed in an excess of an alkaline solution to form a heterogeneous mixture. This reaction was monitored via ^1H NMR, specifically, by observing the change in the integral value of the signal of -CH proton corresponding to the repetitive unit of PLA ('E' signal in Figure 6.6) in relation to the PS aromatic signal. By following the analysis of the ^1H NMR spectra at different times and by monitoring the indicated signal shown in Figure 6.21, we determined that after 56 h, 97 % of PLA had been removed from the thin film derived from copolymer **C1-9** (Table 6.5).

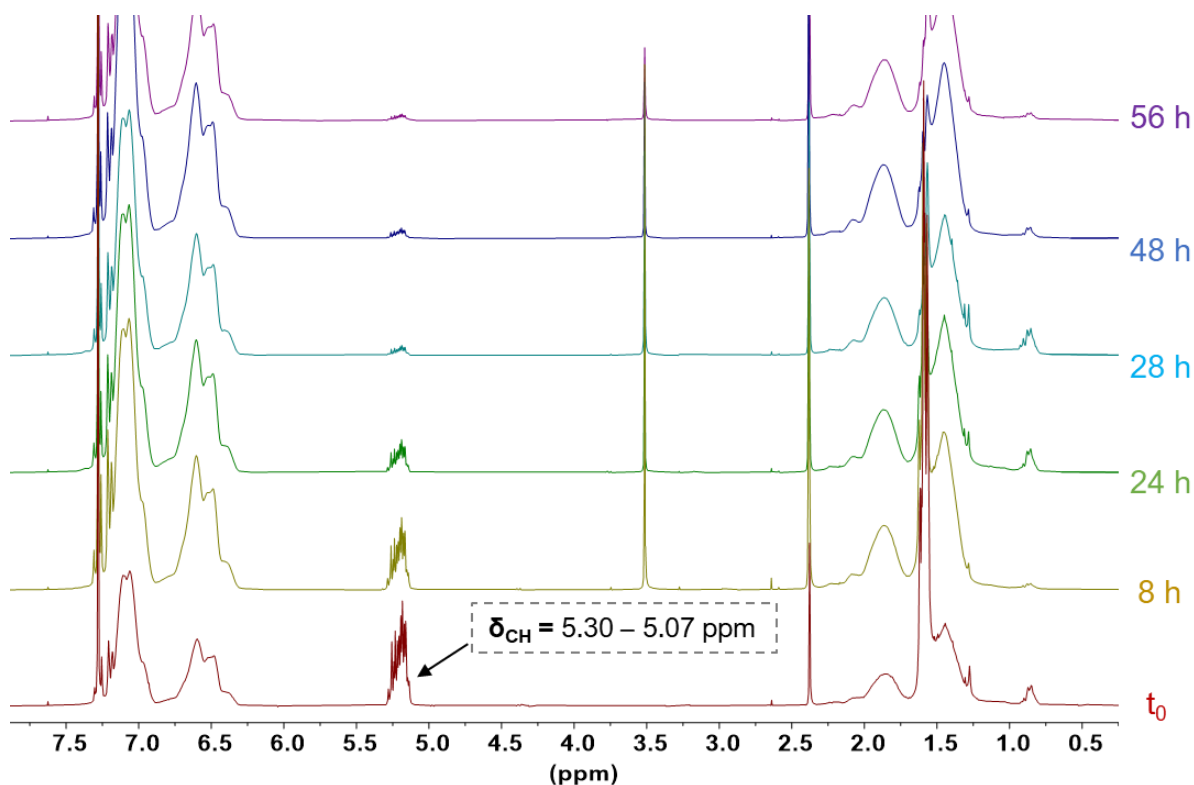


Figure 6.21 ^1H NMR spectra of the hydrolyzed samples at various times (C1-9, method 1).

A similar experiment was performed for the thicker sample (prepared with copolymer **C1-9** as well) displayed in Figure 6.20-B. In this case, a longer hydrolysis time was considered, after 77 hours, only 74 % of PLA was removed (See Figure 9.6 for details). Hence, a lower amount of PLA was removed when the bulk sample was thicker. This effect may be attributed to the diffusional effects related to the fact that a larger amount of mass was confined into a smaller mold ($\sim 20 \text{ mm}^2$) during the preparation of the thicker sample. Thus, PLA domains are more densely packed within the monolith. Nevertheless, it was possible to selectively remove and quantify the PLA phase from the bulk sample to form a PS porous matrix.

Furthermore, it was decided to employ a second method that could enhance phase segregation in the bulk. In method 2, a different mold was employed to prepare the monoliths, in which the added material was more constrained. In this manner, the

sample could be within a confined volume that forces the material to undergo an alignment of the domains in the bulk.³⁴

Hence, by following method 2, ~300 mg of copolymer **C1-13** were placed inside a PEEK mold at 160°C for 2 h to trigger self-assembly of the phases. The mold was further capped with a metallic piece once the material was in a fluid state, in theory, this would aid to the confinement of the material. After annealing, a monolith was recovered from the mold and characterized by SEM, at a glance, the morphology of the annealed sample did not exhibit the formation of cavities as compared to previous examples (Figure 6.20). In this case, only a few circular structures were unevenly distributed on the surface of the material, thus, the aimed morphology could not be reached at these experimental conditions. A subsequent hydrolysis (7 days) of the material did not allow to obtain an ordered-hollowed structure as expected. SEM images before and after hydrolysis of the monolith exhibited an uneven size, shape, and distribution of the phases (see Figure 9.7 in Appendix for more details).

The results obtained from method 2 could be attributed to the fact that there was no additional pressure applied onto the mold other than placing the metallic piece on top. In this regard, the metallic piece did not enhance the self-assembly to shift the phases in the material into a more ordered phase. The use of compression at a constant load on the mold could also trigger self-assembly of the phases, since it can provide a more confined space in which the domains are forced to be oriented.³⁴

Although method 1 exhibited better results for accessing the desired morphology, it is not conclusive that these conditions are suitable to ensure a self-assembly of the copolymer. It is important to further investigate the variables that rule dynamics of BCPs in bulk to promote the formation of ordered structures at a meso scale. In this manner, an improvement may be achieved by specifically evaluating the effects of such variables in order to obtain a functional porous matrix.

7 Conclusions

This investigation has presented the synthesis of a benzylic initiator by employing carboxymethylation and bromination of a styrene-based adduct. As a result, the corresponding product was isolated and characterized via ^1H NMR and GC-MS. This product was employed as an initiator in the polymerization of styrene. ATRP and ARGET-ATRP experiments were conducted, and the use of these techniques enabled the synthesis of PS-Br adducts using the synthesized initiator, the end-bromine functionality was transformed to introduce a triazol functional group on the polymeric chain. A subsequent substitution reaction of PS-Br allowed to isolate the adduct PS-N₃ under the stated conditions.

PS-N₃ products were used in two different synthetic routes to obtain PS-*b*-PLA copolymers. In route 1, PS_n-*b*-PLA_m copolymers were obtained by click coupling the azide and alkyne end groups of PS and PLA homopolymers, respectively. Two series of copolymers were synthesized containing an aliphatic and an aromatic triazole derivative as a junction. In route 2, it was possible to monitor the evolution of the end-group connectivity throughout the synthetic pathway, from end-bromine to end-triazole, via ^1H NMR characterization. From the analysis of the spectra at each step it was possible to determine the change in the chemical shift according to the chemical group vicinity. However, the estimated value of f_{PLA} was lower than estimated by following route 2, which led to conclude that the employed experimental conditions were not suitable for this system. Hence, route 1 was the one that exhibited the best results by observing the M_n , \bar{D} and f_{PLA} values of the isolated copolymers.

In summary, PS_n-*b*-PLA_m copolymers were successfully isolated and characterized by the spectroscopic and calorimetric techniques described. Selected copolymer samples were employed to observe their self-assembly behavior on the preparation of thin films. By ^1H NMR analysis it was determined the presence of triazole derivatives in the investigated BCPs located at the junction between PS and PLA blocks.

The self-assembly behavior of one of the synthesized copolymers was studied via SVA and TA techniques, by preparing thin films onto untreated and pretreated silicon wafer substrates. SVA of the untreated substrates yielded a cylindrical morphology with a mean diameter of 125 nm after 45-minute of SVA using *o*-xylene as an annealing solvent. The observed morphology agreed with the predicted by theory and presented an acceptable homogeneity of the cylinders as observed by SEM analysis. However, the incompatibility between substrate and film led to delamination of the film when trying to hydrolyze the PLA. A silylation pre-treatment of the substrates was performed to avoid delamination of the films. As a result, this pre-treatment allowed to selectively remove the PLA without destruction of the film. Though the SVA of the pre-treated substrates did not yield the expected morphology at the experimental conditions. Based on the thermal analysis of the synthesized copolymers we established the annealing temperatures to perform TA on the pre-treated substrates. These experiments did not allow to access the expected morphology at the investigated conditions (120 and 150°C, 10 min).

Regardless, the segregation of the phases was evidenced on the morphology of the spin-coated substrates (as-spun samples), since homogeneously distributed pore-like structures were observed without an annealing treatment. Subsequent hydrolysis of PLA on the as-spun films evidenced the formation of pores on the surface as proved by SEM and AFM. The obtained PS-porous film exhibited some affinity to metallic centers after being in contact with a Cu salt solution as revealed by SEM-EDX investigations. It is concluded that triazole-functionalized porous PS are suitable candidates to further study its metal-capture properties.

Semi-bulk and bulk experiments were performed to obtain monoliths based on the synthesized copolymers. As evidenced with SEM, the thermally annealed samples prepared in semi-bulk, exhibited an uneven distribution of pores at the working conditions (110 and 160°C, 1 h). Further investigations of these copolymers in the bulk need to address the variables that rule this process to ensure a self-assembly of the copolymer.

Overall, this contribution widens the fact that functional block copolymers remain as macromolecules with a vast potential due to the practically endless possibilities that arise from combining well-known RDRP processes and functionalization reactions. In addition, self-assembly studies of these polymers may be improved by varying annealing and/or spin-coating variables when preparing thin films by monitoring the morphology. Further investigations on this topic may also consider experiments to quantify the amount of metal bonded to the porous matrix employing techniques such as chelate titration or atomic absorption spectrometry.

8 References

- (1) Cychoz, K. A.; Guillet-Nicolas, R.; García-Martínez, J.; Thommes, M. Recent Advances in the Textural Characterization of Hierarchically Structured Nanoporous Materials. *Chem. Soc. Rev.* **2017**, *46* (2), 389–414. <https://doi.org/10.1039/C6CS00391E>.
- (2) Werber, J. R.; Osuji, C. O.; Elimelech, M. Materials for Next-Generation Desalination and Water Purification Membranes. *Nat. Rev. Mater.* **2016**, *1* (5), 16018. <https://doi.org/10.1038/natrevmats.2016.18>.
- (3) Paul, M.; Jons, S. D. Chemistry and Fabrication of Polymeric Nanofiltration Membranes: A Review. *Polymer (Guildf)*. **2016**, *103*, 417–456. <https://doi.org/10.1016/j.polymer.2016.07.085>.
- (4) Calvo, C. Novel Membrane Materials for Reverse Osmosis Desalination. *J. Waste Water Treat. Anal.* **2014**, *5* (2), 1–7. <https://doi.org/10.4172/2157-7587.1000167>.
- (5) Perreault, F.; Fonseca de Faria, A.; Elimelech, M. Environmental Applications of Graphene-Based Nanomaterials. *Chem. Soc. Rev.* **2015**, *44* (16), 5861–5896. <https://doi.org/10.1039/C5CS00021A>.
- (6) Gin, D. L.; Lu, X.; Nemade, P. R.; Pecinovsky, C. S.; Xu, Y.; Zhou, M. Recent Advances in the Design of Polymerizable Lyotropic Liquid-Crystal Assemblies for Heterogeneous Catalysis and Selective Separations. *Adv. Funct. Mater.* **2006**, *16* (7), 865–878. <https://doi.org/10.1002/adfm.200500280>.
- (7) Jackson, E. A.; Hillmyer, M. A. Nanoporous Membranes Derived from Block Copolymers: From Drug Delivery to Water Filtration. *ACS Nano*. 2010, pp 3548–3553. <https://doi.org/10.1021/nn1014006>.
- (8) Ariga, K.; Vinu, A.; Yamauchi, Y.; Ji, Q.; Hill, J. P. Nanoarchitectonics for Mesoporous Materials. *Bull. Chem. Soc. Jpn.* **2012**, *85* (1), 1–32. <https://doi.org/10.1246/bcsj.20110162>.

- (9) Li, Y.; Shi, J. Hollow-Structured Mesoporous Materials: Chemical Synthesis, Functionalization and Applications. *Adv. Mater.* **2014**, *26* (20), 3176–3205. <https://doi.org/10.1002/adma.201305319>.
- (10) Liang, C.; Li, Z.; Dai, S. Mesoporous Carbon Materials: Synthesis and Modification. *Angew. Chemie Int. Ed.* **2008**, *47* (20), 3696–3717. <https://doi.org/10.1002/anie.200702046>.
- (11) Deng, Y.; Wei, J.; Sun, Z.; Zhao, D. Large-Pore Ordered Mesoporous Materials Templated from Non-Pluronic Amphiphilic Block Copolymers. *Chem. Soc. Rev.* **2013**, *42* (9), 4054–4070. <https://doi.org/10.1039/C2CS35426H>.
- (12) Grande, D.; Penelle, J.; Davidson, P.; Beurroies, I.; Denoyel, R. Functionalized Ordered Nanoporous Polymeric Materials: From the Synthesis of Diblock Copolymers to Their Nanostructuration and Their Selective Degradation. *Microporous Mesoporous Mater.* **2011**, *140* (1–3), 34–39. <https://doi.org/10.1016/j.micromeso.2010.10.007>.
- (13) Lin, Y.-C.; Kuo, S.-W. Hierarchical Self-Assembly Structures of POSS-Containing Polypeptide Block Copolymers Synthesized Using a Combination of ATRP, ROP and Click Chemistry. *Polym. Chem.* **2012**, *3* (4), 882. <https://doi.org/10.1039/c2py00574c>.
- (14) Park, M.; Harrison, C.; Chaikin, P. M.; Register, R. A.; Adamson, D. H. *Block Copolymer Lithography: Periodic Arrays of ~10 11 Holes in 1 Square Centimeter*; Academic Press, 1990; Vol. 91.
- (15) Sageshima, Y.; Arai, S.; Noro, A.; Matsushita, Y. Fabrication and Modification of Ordered Nanoporous Structures from Nanophase-Separated Block Copolymer/Metal Salt Hybrids. *Langmuir* **2012**, *28* (50), 17524–17529. <https://doi.org/10.1021/la3042023>.
- (16) Lo, T. Y.; Dehghan, A.; Georgopoulos, P.; Avgeropoulos, A.; Shi, A. C.; Ho, R. M. Orienting Block Copolymer Thin Films via Entropy. *Macromolecules* **2016**, *49* (2), 624–633. <https://doi.org/10.1021/acs.macromol.5b02685>.

- (17) Zhang, X.; He, Q.; Chen, Q.; Nealey, P. F.; Ji, S. Directed Self-Assembly of High Poly(Styrene- b-(Lactic Acid- Alt-Glycolic Acid)) Block Copolymers on Chemical Patterns via Thermal Annealing. *ACS Macro Lett.* **2018**, *7* (6), 751–756. <https://doi.org/10.1021/acsmacrolett.8b00293>.
- (18) Rzayev, J.; Hillmyer, M. A. Nanochannel Array Plastics with Tailored Surface Chemistry. *J. Am. Chem. Soc.* **2005**, *127* (38), 13373–13379. <https://doi.org/10.1021/ja053731d>.
- (19) Arredondo, J.; Elizalde, L. E.; Le Droumaguet, B.; Grande, D. A New Route toward Imidazoline-Functionalized Porous Polymeric Materials from Corresponding Polystyrene-Poly lactide Diblock Copolymers. *React. Funct. Polym.* **2016**, *104*, 62–70. <https://doi.org/10.1016/j.reactfunctpolym.2016.05.003>.
- (20) Olayo-Valles, R.; Guo, S.; Lund, M. S.; Leighton, C.; Hillmyer, M. A. Perpendicular Domain Orientation in Thin Films of Polystyrene-Poly lactide Diblock Copolymers. *Macromolecules* **2005**, *38* (24), 10101–10108. <https://doi.org/10.1021/ma0509006>.
- (21) Gamys, C. G.; Schumers, J. M.; Mugemana, C.; Fustin, C. A.; Gohy, J. F. Pore-Functionalized Nanoporous Materials Derived from Block Copolymers. *Macromol. Rapid Commun.* **2013**, *34* (12), 962–982. <https://doi.org/10.1002/marc.201300214>.
- (22) Bates, F. S. Polymer-Polymer Phase Behavior. *Science* (80-.). **1991**, *251* (4996), 898–905. <https://doi.org/10.1126/science.251.4996.898>.
- (23) Sunday, D. F.; Maher, M. J.; Hannon, A. F.; Liman, C. D.; Tein, S.; Blachut, G.; Asano, Y.; Ellison, C. J.; Willson, C. G.; Kline, R. J.; Willson, C. G.; Kline, R. J.; Willson, C. G.; Kline, R. J. Characterizing the Interface Scaling of High χ Block Copolymers near the Order-Disorder Transition. *Macromolecules* **2018**, *51* (1), 173–180. <https://doi.org/10.1021/acs.macromol.7b01982>.
- (24) Swann, J. M. G.; Topham, P. D. Design and Application of Nanoscale Actuators

- Using Block-Copolymers. *Polymers (Basel)*. **2010**, *2* (4), 454–469. <https://doi.org/10.3390/polym2040454>.
- (25) Leibler, L. Theory of Microphase Separation in Block Copolymers. *Macromolecules* **1980**, *13* (6), 1602–1617. <https://doi.org/10.1021/ma60078a047>.
- (26) Bates, F. S.; Fredrickson, G. H. Block Copolymer Thermodynamics: Theory and Experiment. *Annu. Rev. Phys. Chem.* **1990**, *41* (1), 525–557. <https://doi.org/10.1146/annurev.pc.41.100190.002521>.
- (27) Sinturel, C.; Bates, F. S.; Hillmyer, M. A. High χ –Low N Block Polymers: How Far Can We Go? *ACS Macro Lett.* **2015**, *4* (9), 1044–1050. <https://doi.org/10.1021/acsmacrolett.5b00472>.
- (28) Wang, H. F.; Yu, L. H.; Wang, X. B.; Ho, R. M. A Facile Method to Fabricate Double Gyroid as a Polymer Template for Nanohybrids. *Macromolecules* **2014**, *47* (22), 7993–8001. <https://doi.org/10.1021/ma501957b>.
- (29) Zalusky, A. S.; Olayo-Valles, R.; Wolf, J. H.; Hillmyer, M. A. Ordered Nanoporous Polymers from Polystyrene-Polylactide Block Copolymers. *J. Am. Chem. Soc.* **2002**, *124* (43), 12761–12773. <https://doi.org/10.1021/ja0278584>.
- (30) Saldívar-Guerra, E.; Vivaldo-Lima, E. *Handbook of Polymer Synthesis, Characterization, and Processing*.
- (31) Higuchi, T.; Motoyoshi, K.; Sugimori, H.; Jinnai, H.; Yabu, H.; Shimomura, M. Phase Transition and Phase Transformation in Block Copolymer Nanoparticles. *Macromol. Rapid Commun.* **2010**, *31* (20), 1773–1778. <https://doi.org/10.1002/marc.201000299>.
- (32) Olson, D. A.; Chen, L.; Hillmyer, M. A. Templating Nanoporous Polymers with Ordered Block Copolymers. *Chem. Mater.* **2008**, *20* (3), 869–890. <https://doi.org/10.1021/cm702239k>.
- (33) Drzal, P. L.; Barnes, J. D.; Kofinas, P. Path Dependent Microstructure

- Orientation during Strain Compression of Semicrystalline Block Copolymers. *Polymer (Guildf)*. **2001**, *42* (13), 5633–5642. [https://doi.org/10.1016/S0032-3861\(00\)00864-8](https://doi.org/10.1016/S0032-3861(00)00864-8).
- (34) Majdoub, R.; Antoun, T.; Droumaguet, B. Le; Benzina, M.; Grande, D. Original Route to Polylactide-Polystyrene Diblock Copolymers Containing a Sulfonyl Group at the Junction between Both Blocks as Precursors to Functional Nanoporous Materials. *React. Funct. Polym.* **2012**, *72* (8), 495–502. <https://doi.org/10.1016/j.reactfunctpolym.2012.04.012>.
- (35) Bennet, H. *Concise Chemical and Technical Dictionary*, 3rd Editio.
- (36) Poupart, R.; Benlahoues, A.; Le Droumaguet, B.; Grande, D. Porous Gold Nanoparticle-Decorated Nanoreactors Prepared from Smartly Designed Functional Polystyrene- Block -Poly(d , l -Lactide) Diblock Copolymers: Toward Efficient Systems for Catalytic Cascade Reaction Processes. *ACS Appl. Mater. Interfaces* **2017**, *9* (37), 31279–31290. <https://doi.org/10.1021/acsami.6b16157>.
- (37) Jin, C.; Olsen, B. C.; Lubber, E. J.; Buriak, J. M. Nanopatterning via Solvent Vapor Annealing of Block Copolymer Thin Films. *Chem. Mater.* **2017**, *29* (1), 176–188. <https://doi.org/10.1021/acs.chemmater.6b02967>.
- (38) Ho, R. M.; Tseng, W. H.; Fan, H. W.; Chiang, Y. W.; Lin, C. C.; Ko, B. T.; Huang, B. H. Solvent-Induced Microdomain Orientation in Polystyrene-b-Poly(l-Lactide) Diblock Copolymer Thin Films for Nanopatterning. *Polymer (Guildf)*. **2005**, *46* (22), 9362–9377. <https://doi.org/10.1016/j.polymer.2005.07.069>.
- (39) Li, M.; Douki, K.; Goto, K.; Li, X.; Coenjarts, C.; Smilgies, D. M.; Ober, C. K. Spatially Controlled Fabrication of Nanoporous Block Copolymers. *Chem. Mater.* **2004**, *16* (20), 3800–3808. <https://doi.org/10.1021/cm0493445>.
- (40) Vayer, M.; Hillmyer, M. A.; Dirany, M.; Thevenin, G.; Erre, R.; Sinturel, C. Perpendicular Orientation of Cylindrical Domains upon Solvent Annealing Thin Films of Polystyrene-b-Polylactide. *Thin Solid Films* **2010**, *518* (14), 3710–

3715. <https://doi.org/10.1016/j.tsf.2009.10.015>.
- (41) Mao, H.; Hillmyer, M. A. Macroscopic Samples of Polystyrene with Ordered Three-Dimensional Nanochannels. *Soft Matter* **2006**, *2* (1), 57–59. <https://doi.org/10.1039/B513958A>.
- (42) Brunauer, S.; Emmett, P. H.; Teller, E. ADSORPTION OF GASES IN MULTIMOLECULAR LAYERS. *J. Am. Chem. Soc.* **1938**, *60*, 309–319. <https://doi.org/citeulike-article-id:4074706>.
- (43) Li, C.; Li, Q.; Kaneti, Y. V.; Hou, D.; Yamauchi, Y.; Mai, Y. Self-Assembly of Block Copolymers towards Mesoporous Materials for Energy Storage and Conversion Systems. *Chem. Soc. Rev.* **2020**, *49* (14), 4681–4736. <https://doi.org/10.1039/D0CS00021C>.
- (44) Tang, J.; Liu, J.; Li, C.; Li, Y.; Tade, M. O.; Dai, S.; Yamauchi, Y. Synthesis of Nitrogen-Doped Mesoporous Carbon Spheres with Extra-Large Pores through Assembly of Diblock Copolymer Micelles. *Angew. Chemie Int. Ed.* **2014**, *54* (2), n/a-n/a. <https://doi.org/10.1002/anie.201407629>.
- (45) Phillip, W. A.; O’neill, B.; Rodwogin, M.; Hillmyer, M. A.; Cussler, E. L. Self-Assembled Block Copolymer Thin Films as Water Filtration Membranes. *ACS Appl. Mater. Interfaces* **2010**, *2* (3), 847–853. <https://doi.org/10.1021/am900882t>.
- (46) Chouyyok, W.; Shin, Y.; Davidson, J.; Samuels, W. D.; Lafemina, N. H.; Rutledge, R. D.; Fryxell, G. E.; Sangvanich, T.; Yantasee, W. Selective Removal of Copper(II) from Natural Waters by Nanoporous Sorbents Functionalized with Chelating Diamines. *Environ. Sci. Technol.* **2010**, *44* (16), 6390–6395. <https://doi.org/10.1021/es101165c>.
- (47) Mitragotri, S.; Anderson, D. G.; Chen, X.; Chow, E. K.; Ho, D.; Kabanov, A. V.; Karp, J. M.; Kataoka, K.; Mirkin, C. A.; Petrosko, S. H.; Shi, J.; Stevens, M. M.; Sun, S.; Teoh, S.; Venkatraman, S. S.; Xia, Y.; Wang, S.; Gu, Z.; Xu, C. Accelerating the Translation of Nanomaterials in Biomedicine. *ACS Nano*

- 2015**, 9 (7), 6644–6654. <https://doi.org/10.1021/acsnano.5b03569>.
- (48) Howe, D. H.; Hart, J. L.; McDaniel, R. M.; Taheri, M. L.; Magenau, A. J. D. Functionalization-Induced Self-Assembly of Block Copolymers for Nanoparticle Synthesis. *ACS Macro Lett.* **2018**, 7 (12), 1503–1508. <https://doi.org/10.1021/acsmacrolett.8b00815>.
- (49) Feng, H.; Lu, X.; Wang, W.; Kang, N.-G. G.; Mays, J. W. Block Copolymers: Synthesis, Self-Assembly, and Applications. *Polymers (Basel)*. **2017**, 9 (10), 494. <https://doi.org/10.3390/polym9100494>.
- (50) Matyjaszewski, K. Atom Transfer Radical Polymerization (ATRP): Current Status and Future Perspectives. *Macromolecules* **2012**, 45 (10), 4015–4039. <https://doi.org/10.1021/ma3001719>.
- (51) Pan, X.; Fantin, M.; Yuan, F.; Matyjaszewski, K. Externally Controlled Atom Transfer Radical Polymerization. *Chem. Soc. Rev.* **2018**, 47 (14), 5457–5490. <https://doi.org/10.1039/c8cs00259b>.
- (52) Matyjaszewski, K.; Xia, J. Atom Transfer Radical Polymerization. *Chem. Rev.* **2001**, 101 (9), 2921–2990. <https://doi.org/10.1021/cr940534g>.
- (53) Kwak, Y.; Matyjaszewski, K. ARGET ATRP of Methyl Methacrylate in the Presence of Nitrogen-Based Ligands as Reducing Agents. *Polym. Int.* **2009**, 58 (3), 242–247. <https://doi.org/10.1002/pi.2530>.
- (54) Jakubowski, W.; Min, K.; Matyjaszewski, K. Activators Regenerated by Electron Transfer for Atom Transfer Radical Polymerization of Styrene. *Macromolecules* **2006**, 39 (1), 39–45. <https://doi.org/10.1021/ma0522716>.
- (55) Altintas, O.; Speros, J. C.; Bates, F. S.; Hillmyer, M. A. Straightforward Synthesis of Model Polystyrene-: Block -Poly(Vinyl Alcohol) Diblock Polymers. *Polym. Chem.* **2018**, 9 (31), 4243–4250. <https://doi.org/10.1039/c8py00937f>.
- (56) Konkolewicz, D.; Wang, Y.; Krys, P.; Zhong, M.; Isse, A. A.; Gennaro, A.; Matyjaszewski, K. SARA ATRP or SET-LRP. End of Controversy? *Polym.*

- Chem.* **2014**, *5* (15), 4409. <https://doi.org/10.1039/c4py00149d>.
- (57) Endo, T. General Mechanisms in Ring-Opening Polymerization. In *Handbook of Ring-Opening Polymerization*; 2009; pp 53–63.
- (58) Kamber, N. E.; Jeong, W.; Waymouth, R. M.; Pratt, R. C.; Lohmeijer, B. G. G.; Hedrick, J. L. Organocatalytic Ring-Opening Polymerization. *Chem. Rev.* **2007**, *107* (12), 5813–5840. <https://doi.org/10.1021/cr068415b>.
- (59) Ghalia, M. A.; Dahman, Y. Biodegradable Poly(Lactic Acid)-Based Scaffolds: Synthesis and Biomedical Applications. *J. Polym. Res.* **2017**, *24* (5), 74. <https://doi.org/10.1007/s10965-017-1227-2>.
- (60) Czełuśniak, I.; Szymańska-Buzar, T. Synthesis and Characterization of Polylactide Functionalized Polyacetylenes. *Eur. Polym. J.* **2011**, *47* (11), 2111–2119. <https://doi.org/10.1016/j.eurpolymj.2011.07.014>.
- (61) Mezzasalma, L.; Harrisson, S.; Saba, S.; Loyer, P.; Coulembier, O.; Taton, D. Bulk Organocatalytic Synthetic Access to Statistical Copolyesters from L - Lactide and ϵ -Caprolactone Using Benzoic Acid. *Biomacromolecules* **2019**, *20* (5), 1965–1974. <https://doi.org/10.1021/acs.biomac.9b00190>.
- (62) Keen, I.; Yu, A.; Cheng, H.-H.; Jack, K. S.; Nicholson, T. M.; Whittaker, A. K.; Blakey, I. Control of the Orientation of Symmetric Poly(Styrene)- Block -Poly(d , l -Lactide) Block Copolymers Using Statistical Copolymers of Dissimilar Composition. *Langmuir* **2012**, *28* (45), 15876–15888. <https://doi.org/10.1021/la304141m>.
- (63) Trejo-Maldonado, M.; Elizalde, L. E.; Le Droumaguet, B.; Grande, D. Synthesis of Triazole-Functionalized Diblock Copolymers as Templates for Porous Materials. *React. Funct. Polym.* **2021**, *164* (January), 104919. <https://doi.org/10.1016/j.reactfunctpolym.2021.104919>.
- (64) Yu, C.; Wang, L.; Xu, Z.; Teng, W.; Wu, Z.; Xiong, D. Smart Micelles Self-Assembled from Four-Arm Star Polymers as Potential Drug Carriers for PH-

- Triggered DOX Release. *J. Polym. Res.* **2020**, *27* (5), 2–11. <https://doi.org/10.1007/s10965-020-02108-2>.
- (65) Wolf, F. F.; Friedemann, N.; Frey, H. Poly(Lactide)-Block-Poly(HEMA) Block Copolymers: An Orthogonal One-Pot Combination of ROP and ATRP, Using a Bifunctional Initiator. *Macromolecules* **2009**, *42* (15), 5622–5628. <https://doi.org/10.1021/ma900894d>.
- (66) Pennequin, P.; Fontaine, M.; Castanet, Y.; Mortreux, A.; Petit, F. Palladium Catalyzed Oxidative Carbonylation of Alkenes by Methyl Formate. *Appl. Catal. A Gen.* **1996**, *135* (2), 329–339. [https://doi.org/10.1016/0926-860X\(95\)00244-8](https://doi.org/10.1016/0926-860X(95)00244-8).
- (67) Whitfield, R.; Anastasaki, A.; Nikolaou, V.; Jones, G. R.; Engelis, N. G.; Discekici, E. H.; Fleischmann, C.; Willenbacher, J.; Hawker, C. J.; Haddleton, D. M. Universal Conditions for the Controlled Polymerization of Acrylates, Methacrylates, and Styrene via Cu(0)-RDRP. *J. Am. Chem. Soc.* **2017**, *139* (2), 1003–1010. <https://doi.org/10.1021/jacs.6b11783>.
- (68) Haddleton, D. M.; Waterson, C. Phenolic Ester-Based Initiators for Transition Metal Mediated Living Polymerization. *Macromolecules* **1999**, *32* (26), 8732–8739. <https://doi.org/10.1021/ma991323m>.
- (69) He, T.; Li, D.; Sheng, X.; Zhao, B. Synthesis of ABC 3-Miktoarm Star Terpolymers from a Trifunctional Initiator by Combining Ring-Opening Polymerization, Atom Transfer Radical Polymerization, and Nitroxide-Mediated Radical Polymerization. *Macromolecules* **2004**, *37* (9), 3128–3135. <https://doi.org/10.1021/ma036010c>.
- (70) Kolb, H. C.; Finn, M. G.; Sharpless, K. B. Click Chemistry: Diverse Chemical Function from a Few Good Reactions. *Angew. Chemie Int. Ed.* **2001**, *40* (11), 2004–2021. [https://doi.org/10.1002/1521-3773\(20010601\)40:11<2004::AID-ANIE2004>3.0.CO;2-5](https://doi.org/10.1002/1521-3773(20010601)40:11<2004::AID-ANIE2004>3.0.CO;2-5).
- (71) Anastasaki, A.; Willenbacher, J.; Fleischmann, C.; Gutekunst, W. R.; Hawker,

- C. J. End Group Modification of Poly(Acrylates) Obtained: Via ATRP: A User Guide. *Polym. Chem.* **2017**, *8* (4), 689–697. <https://doi.org/10.1039/c6py01993e>.
- (72) Kempe, K.; Krieg, A.; Becer, C. R.; Schubert, U. S. “Clicking” on/with Polymers: A Rapidly Expanding Field for the Straightforward Preparation of Novel Macromolecular Architectures. *Chem. Soc. Rev.* **2012**, *41* (1), 176–191. <https://doi.org/10.1039/c1cs15107j>.
- (73) Durmaz, H.; Sanyal, A.; Hizal, G.; Tunca, U. Double Click Reaction Strategies for Polymer Conjugation and Post-Functionalization of Polymers. *Polym. Chem.* **2012**, *3* (4), 825–835. <https://doi.org/10.1039/c1py00471a>.
- (74) Lutz, J. F.; Schlaad, H. Modular Chemical Tools for Advanced Macromolecular Engineering. *Polymer (Guildf)*. **2008**, *49* (4), 817–824. <https://doi.org/10.1016/j.polymer.2007.10.045>.
- (75) Lutz, J.-F.; Börner, H. G.; Weichenhan, K. Combining Atom Transfer Radical Polymerization and Click Chemistry: A Versatile Method for the Preparation of End-Functional Polymers. *Macromol. Rapid Commun.* **2005**, *26* (7), 514–518. <https://doi.org/10.1002/marc.200500002>.
- (76) Yilmaz, G. Combination of Photoinduced ATRP and Click Processes for the Synthesis of Triblock Copolymers. *J. Turkish Chem. Soc. Sect. A Chem.* **2018**, *5* (2), 727–736. <https://doi.org/10.18596/jotcsa.414060>.
- (77) Elupula, R.; Oh, J.; Haque, F. M.; Chang, T.; Grayson, S. M. Determining the Origins of Impurities during Azide–Alkyne Click Cyclization of Polystyrene. *Macromolecules* **2016**, *49* (11), 4369–4372. <https://doi.org/10.1021/acs.macromol.6b00968>.
- (78) Juriek, M.; Kouwer, P. H. J.; Rowan, A. E. Triazole: A Unique Building Block for the Construction of Functional Materials. *Chem. Commun.* **2011**, *47* (31), 8740–8749. <https://doi.org/10.1039/c1cc10685f>.

- (79) Okcu, S. S.; Durmaz, Y. Y.; Yagci, Y. Synthesis and Characterization of Telechelic Block Co-Polymers by Combination of Atom Transfer Radical Polymerization and Click Chemistry Processes. *Des. Monomers Polym.* **2010**, *13* (5), 459–472. <https://doi.org/10.1163/138577210X521350>.
- (80) Huang, D.; Liu, Y.; Qin, A.; Tang, B. Z. Recent Advances in Alkyne-Based Click Polymerizations. *Polym. Chem.* **2018**, *9* (21), 2853–2867. <https://doi.org/10.1039/c7py02047c>.
- (81) Kim, J.; Jung, H. Y.; Park, M. J. End-Group Chemistry and Junction Chemistry in Polymer Science: Past, Present, and Future. *Macromolecules* **2020**, *53* (3), 746–763. <https://doi.org/10.1021/acs.macromol.9b02293>.
- (82) Ouerghui, A.; Elamari, H.; Ghammouri, S.; Slimi, R.; Meganem, F.; Girard, C. Polystyrene-Supported Triazoles for Metal Ions Extraction: Synthesis and Evaluation. *React. Funct. Polym.* **2014**, *74* (1), 37–45. <https://doi.org/10.1016/j.reactfunctpolym.2013.10.007>.
- (83) Song, S.; Ko, Y.-G.; Lee, H.; Wi, D.; Ree, B. J.; Li, Y.; Michinobu, T.; Ree, M. High-Performance Triazole-Containing Brush Polymers via Azide–Alkyne Click Chemistry: A New Functional Polymer Platform for Electrical Memory Devices. *NPG Asia Mater.* **2015**, *7* (12), e228–e228. <https://doi.org/10.1038/am.2015.130>.
- (84) Zhu, J.; Wu, L.; Bu, Z.; Jie, S.; Li, B. G. Synthesis and CO₂ Capture Behavior of Porous Cross-Linked Polymers Containing Pendant Triazole Groups. *Ind. Eng. Chem. Res.* **2017**, *56* (36), 10155–10163. <https://doi.org/10.1021/acs.iecr.7b01961>.
- (85) Andersson Trojer, M.; Movahedi, A.; Blanck, H.; Nydén, M. Imidazole and Triazole Coordination Chemistry for Antifouling Coatings. *J. Chem.* **2013**, *2013*, 1–23. <https://doi.org/10.1155/2013/946739>.
- (86) Armarego, W. L. F.; Chai, C. *Purification of Inorganic and Metal-Organic Chemicals*; Elsevier, 2013. <https://doi.org/10.1016/b978-0-12-382161->

4.00005-4.

- (87) Dauben, H. J.; McCoy, L. L. N-Bromosuccinimide. I. Allylic Bromination, a General Survey of Reaction Variables. *J. Am. Chem. Soc.* **1959**, *81* (18), 4863–4873. <https://doi.org/10.1021/ja01527a027>.
- (88) Pennequin, P.; Fontaine, M.; Castanet, Y.; Mortreux, A.; Petit, F. Palladium Catalyzed Oxidative Carbonylation of Alkenes by Methyl Formate. *Appl. Catal. A Gen.* **1996**, *135* (2), 329–339. [https://doi.org/10.1016/0926-860X\(95\)00244-8](https://doi.org/10.1016/0926-860X(95)00244-8).
- (89) Knör, S.; Modlinger, A.; Poethko, T.; Schottelius, M.; Wester, H. J.; Kessler, H. Synthesis of Novel 1,4,7,10-Tetraazacyclodecane-1,4,7,10-Tetraacetic Acid (DOTA) Derivatives for Chemoselective Attachment to Unprotected Polyfunctionalized Compounds. *Chem. - A Eur. J.* **2007**, *13* (21), 6082–6089. <https://doi.org/10.1002/chem.200700231>.
- (90) Tang, Y.; Xue, Y.; Li, Z.; Yan, T.; Zhou, R.; Zhang, Z. Heterogeneous Synthesis of Glycerol Carbonate from Glycerol and Dimethyl Carbonate Catalyzed by LiCl/CaO. *J. Saudi Chem. Soc.* **2019**, *23* (4), 494–502. <https://doi.org/10.1016/j.jscs.2018.11.003>.
- (91) Cummins, C.; Mokarian-Tabari, P.; Andreatza, P.; Sinturel, C.; Morris, M. A. Solvothermal Vapor Annealing of Lamellar Poly(Styrene)-Block-Poly(D,L-Lactide) Block Copolymer Thin Films for Directed Self-Assembly Application. *ACS Appl. Mater. Interfaces* **2016**, *8* (12), 8295–8304. <https://doi.org/10.1021/acsami.6b00765>.
- (92) Wang, Y.; Narita, C.; Xu, X.; Honma, H.; Himeda, Y.; Yamada, K. Controlling the Ordered Transition of PS-*b*-P4VP Block Copolymer Ultrathin Films by Solvent Annealing. *Mater. Chem. Phys.* **2020**, *239*, 122072. <https://doi.org/10.1016/j.matchemphys.2019.122072>.
- (93) Vayer, M.; Vital, A.; Sinturel, C. New Insights into Polymer-Solvent Affinity in Thin Films. *Eur. Polym. J.* **2017**, *93* (December 2016), 132–139.

- <https://doi.org/10.1016/j.eurpolymj.2017.05.035>.
- (94) Li, Y.; Pionteck, J.; Pötschke, P.; Voit, B. Thermal Annealing to Influence the Vapor Sensing Behavior of Co-Continuous Poly(Lactic Acid)/Polystyrene/Multiwalled Carbon Nanotube Composites. *Mater. Des.* **2020**, *187*, 108383. <https://doi.org/10.1016/j.matdes.2019.108383>.
- (95) Sarkar, A.; Stefik, M. Robust Porous Polymers Enabled by a Fast Trifluoroacetic Acid Etch with Improved Selectivity for Polylactide. *Mater. Chem. Front.* **2017**, *1* (8), 1526–1533. <https://doi.org/10.1039/c6qm00266h>.
- (96) Muller, P. Glossary of Terms Used in Physical Organic Chemistry (IUPAC Recommendations 1994). *Pure Appl. Chem.* **1994**, *66* (5), 1077–1184. <https://doi.org/doi:10.1351/pac199466051077>.
- (97) Tang, W.; Kwak, Y.; Braunecker, W.; Tsarevsky, N. V.; Coote, M. L.; Matyjaszewski, K. Understanding Atom Transfer Radical Polymerization: Effect of Ligand and Initiator Structures on the Equilibrium Constants. *J. Am. Chem. Soc.* **2008**, *130* (32), 10702–10713. <https://doi.org/10.1021/ja802290a>.
- (98) Haddleton, D. M.; Waterson, C. Phenolic Ester-Based Initiators for Transition Metal Mediated Living Polymerization. *Macromolecules* **1999**, *32* (26), 8732–8739. <https://doi.org/10.1021/ma991323m>.
- (99) Tsarevsky, N. V.; Sumerlin, B. S.; Matyjaszewski, K. Step-Growth “Click” Coupling of Telechelic Polymers Prepared by Atom Transfer Radical Polymerization. *Macromolecules* **2005**, *38* (9), 3558–3561. <https://doi.org/10.1021/ma050370d>.
- (100) Tang, W.; Matyjaszewski, K. Effects of Initiator Structure on Activation Rate Constants in ATRP. *Macromolecules* **2007**, *40* (6), 1858–1863. <https://doi.org/10.1021/ma062897b>.
- (101) Dirany, M.; Lacroix-Desmazes, P.; Vayer, M.; Erre, R.; Boutevin, B.; Sinturel, C. Polystyrene-Block-Polylactide Obtained by the Combination of Atom Transfer

- Radical Polymerization and Ring-Opening Polymerization with a Commercial Dual Initiator. *J. Appl. Polym. Sci.* **2011**, *122* (5), 2944–2951. <https://doi.org/10.1002/app.34101>.
- (102) Albert, J. N. L. L.; Epps, T. H. Self-Assembly of Block Copolymer Thin Films. *Mater. Today* **2010**, *13* (6), 24–33. [https://doi.org/10.1016/S1369-7021\(10\)70106-1](https://doi.org/10.1016/S1369-7021(10)70106-1).
- (103) Rieger, J. The Glass Transition Temperature of Polystyrene. *J. Therm. Anal.* **1996**, *46* (3–4), 965–972. <https://doi.org/10.1007/bf01983614>.
- (104) Suijkerbuijk, B. M. J. M.; Aerts, B. N. H.; Dijkstra, H. P.; Lutz, M.; Spek, A. L.; van Koten, G.; Klein Gebbink, R. J. M. “Click” 1,2,3-Triazoles as Tunable Ligands for Late Transition Metal Complexes. *Dalt. Trans.* **2007**, No. 13, 1273–1276. <https://doi.org/10.1039/B701978P>.
- (105) Philipps, K.; Junkers, T.; Michels, J. J. The Block Copolymer Shuffle in Size Exclusion Chromatography: The Intrinsic Problem with Using Elugrams to Determine Chain Extension Success. *Polym. Chem.* **2021**, *12* (17), 2522–2531. <https://doi.org/10.1039/d1py00210d>.
- (106) Shi, W.; Tateishi, Y.; Li, W.; Hawker, C. J.; Fredrickson, G. H.; Kramer, E. J. Producing Small Domain Features Using Miktoarm Block Copolymers with Large Interaction Parameters. *ACS Macro Lett.* **2015**, *4* (11), 1287–1292. <https://doi.org/10.1021/acsmacrolett.5b00712>.
- (107) Terzic, I.; Meereboer, N. L.; Loos, K. CuAAC Click Chemistry: A Versatile Approach towards PVDF-Based Block Copolymers. *Polym. Chem.* **2018**, *9* (27), 3714–3720. <https://doi.org/10.1039/c8py00742j>.
- (108) Lei, L.; Xia, Y.; Chen, X.; Shi, S. Long-Range-Ordered, Hexagonally Packed Nanoporous Membranes from Degradable-Block-Containing Diblock Copolymer Film Templates. *J. Appl. Polym. Sci.* **2014**, *131* (1), n/a-n/a. <https://doi.org/10.1002/app.39638>.

- (109) Baruth, A.; Seo, M.; Lin, C. H.; Walster, K.; Shankar, A.; Hillmyer, M. A.; Leighton, C. Optimization of Long-Range Order in Solvent Vapor Annealed Poly(Styrene)-Block-Poly(Lactide) Thin Films for Nanolithography. *ACS Appl. Mater. Interfaces* **2014**, *6* (16), 13770–13781. <https://doi.org/10.1021/am503199d>.
- (110) Cummins, C.; Mokarian-Tabari, P.; Holmes, J. D.; Morris, M. A. Selective Etching of Polylactic Acid in Poly(Styrene)-Block-Poly(d,L)Lactide Diblock Copolymer for Nanoscale Patterning. *J. Appl. Polym. Sci.* **2014**, *131* (18), n/a-n/a. <https://doi.org/10.1002/app.40798>.
- (111) Elliott, P. I. P. Chapter 1. Organometallic Complexes with 1,2,3-Triazole-Derived Ligands. In *Organometallic Chemistry*; Royal Society of Chemistry, 2014; Vol. 39, pp 1–25. <https://doi.org/10.1039/9781849737692-00001>.

9 Appendix

9.1 Additional characterization of MBBP (I-2a)

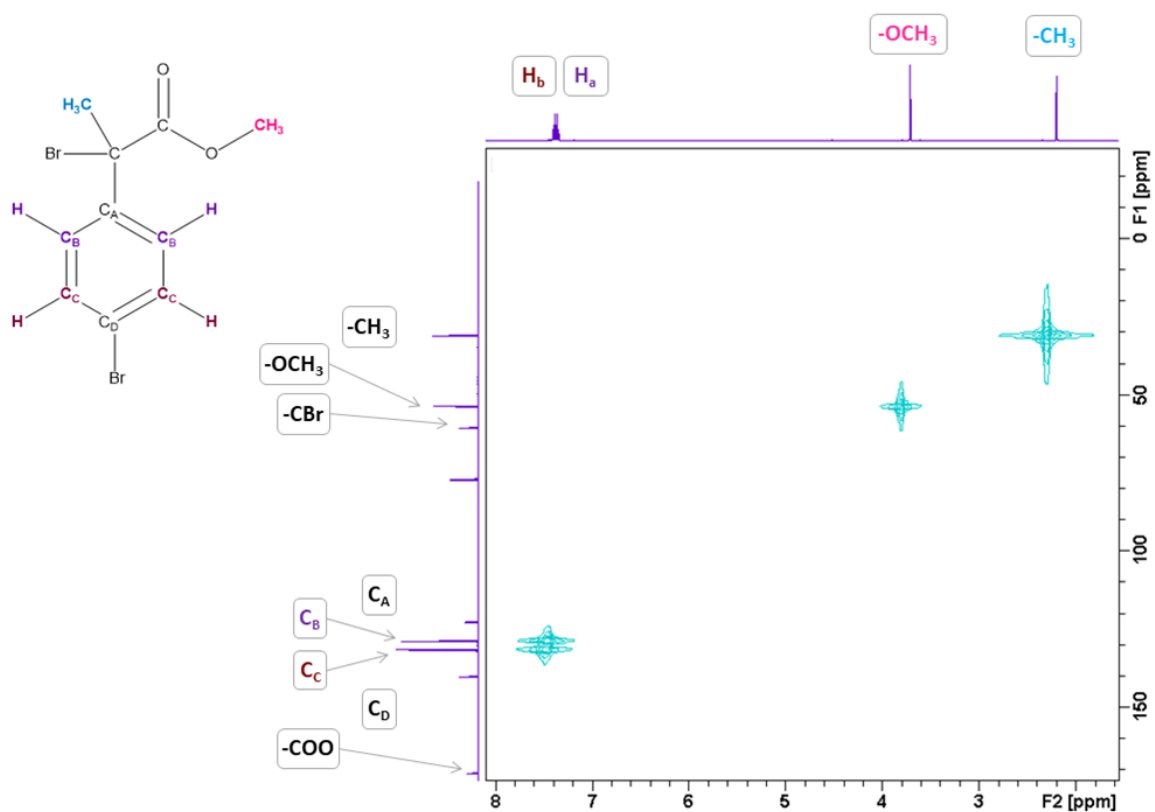
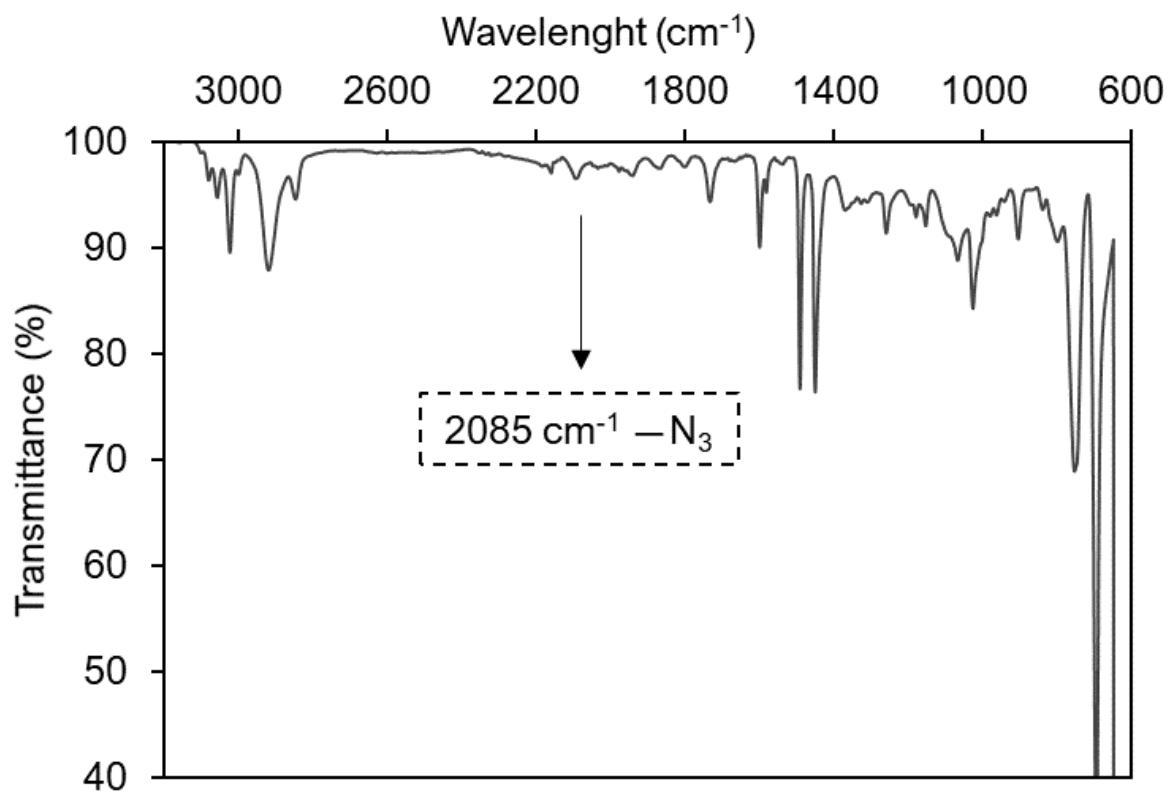


Figure 9.1 Heteronuclear Multiple Quantum Coherence (gHMQC) ^1H - ^{13}C of product I-2a.

9.2 FT-IR spectrum of PS-N₃Figure 9.2 FT-IR spectrum of PS-N₃.

9.3 Solvent selection for the polymer casting

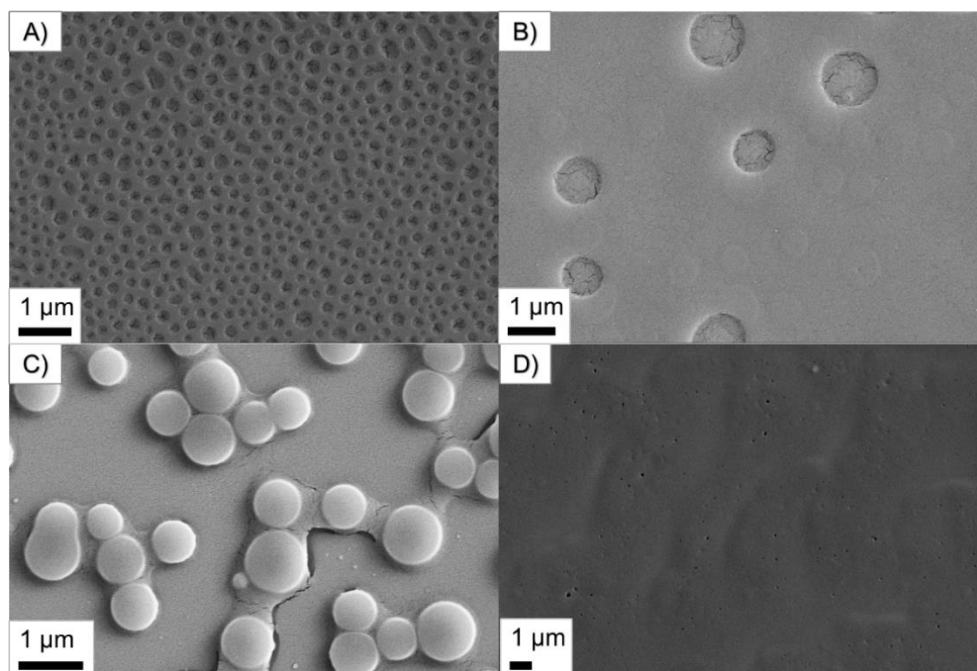


Figure 9.3 As-spun silicon wafers with a 2.0% wt. solution with different solvents: A) THF, B) CH_2Cl_2 , C) dioxane, and D) toluene.

9.4 Atomic Force Microscopy (AFM) of untreated and annealed substrates.

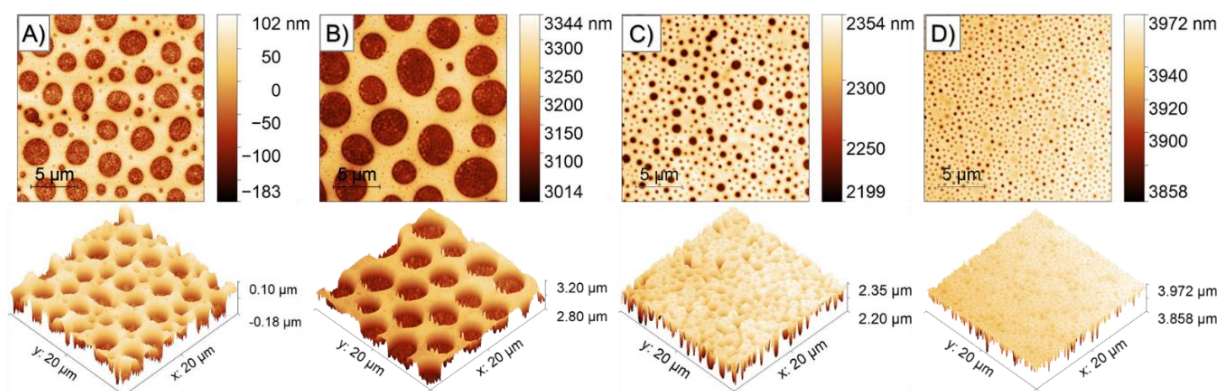


Figure 9.4 AFM of the untreated substrates at A) $t = 0$, B) 15 min, C) 30 min and D) 45 min of SVA.

9.5 Solvent vapor annealing (SVA) on silylated substrates.

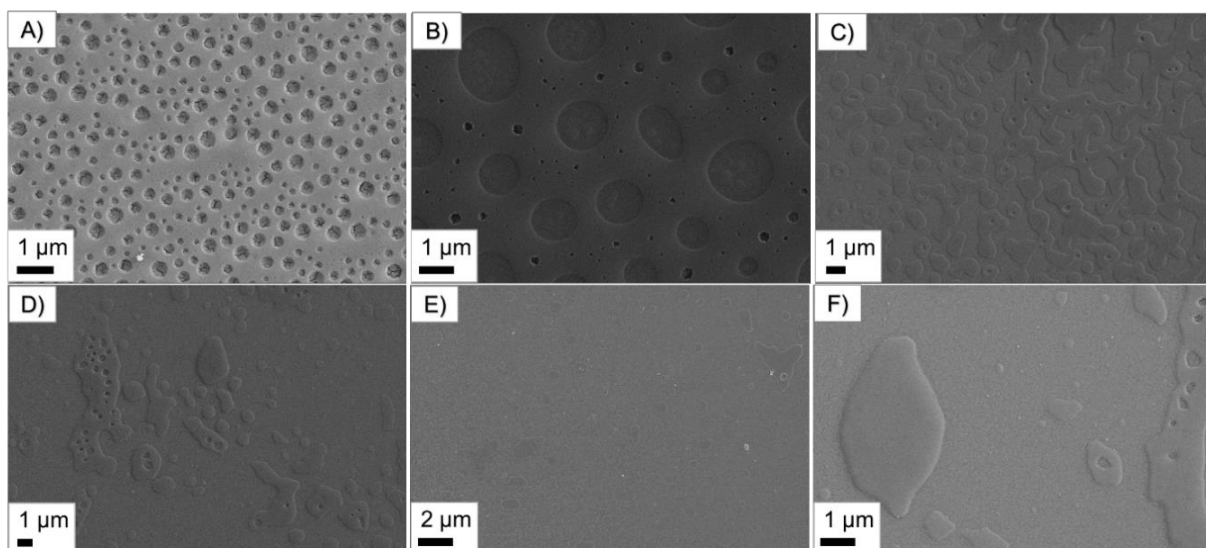


Figure 9.5 SVA of treated substrates at longer annealing times A) as-spun, B) 45 min, C) 2h, D) 4h, E) 8h, and F) 16 h.

9.6 PLA hydrolysis of C1-9 monolith (thicker sample)

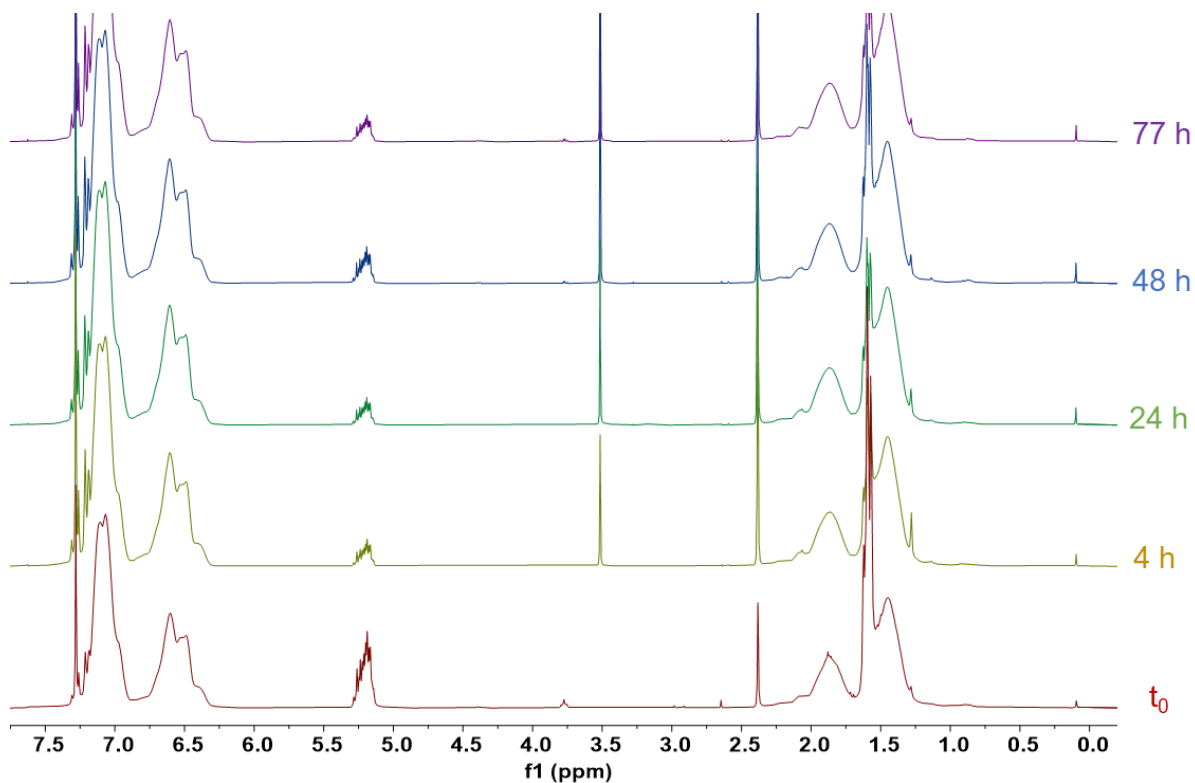


Figure 9.6 ^1H NMR spectra of the hydrolyzed samples at various times (C1-9, thick sample, method 1).

9.7 Before and after hydrolysis of C1-13 monolith

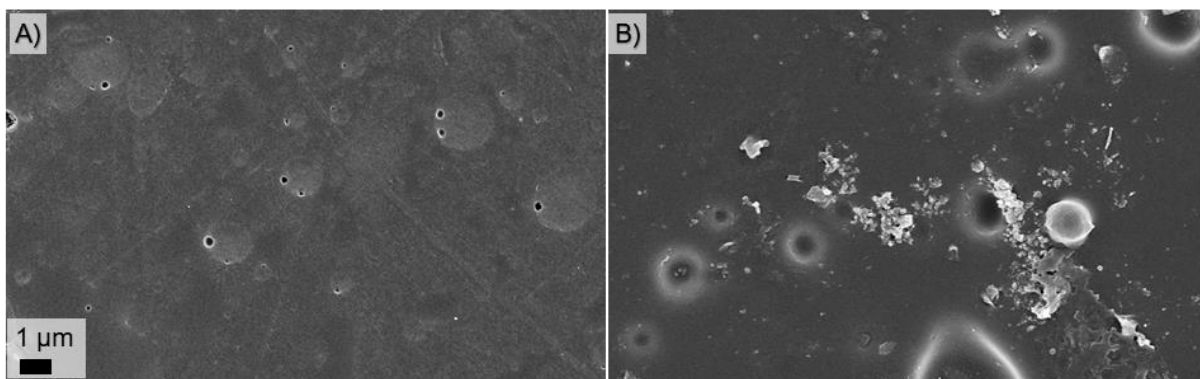


Figure 9.7 SEM images of C1-13 monolith A) before and B) after hydrolysis (method 2).